Molecular Characterization of Perineural Invasion in Pancreatic Ductal Adenocarcinoma: Proteomic Analysis and *In Vitro* Modelling

Wasfi Alrawashdeh

PhD Thesis

Centre for Molecular Oncology and Imaging

Barts Cancer Institute

Queen Mary Univeristy of London

London EC1M 6BQ

This thesis is dedicated to my mother and my late father

whose love, wisdom and sacrifices will forever live with me.

Declaration

I declare that the work presented in this thesis was performed by me, except where stated otherwise in the text, and that this work has not been submitted for any other degree or professional qualification. The work was performed between Oct 2009 and Sep 2013 in the Centre for Molecular Oncology and Imaging, Barts Cancer Institute, Queen Mary University of London.

Wasfi Alrawashdeh

Sep 2013

Acknowledgment

First and foremost, I wish to thank Allah, the lord, for all his blessings throughout my life. I wish to thank my principal supervisor Tatjana Crnogorac-Jurcevic for the support she gave me, in various shapes and forms, all through my time at the institute, and for providing the funds to complete this work. I would like to thank her particularly for welcoming, in her lab, a surgeon who had only the desire to pursue research in pancreatic cancer field and then supporting him through a project that was stretching faith, knowledge and resources at times. I would like also to thank my second supervisor, Pedro Cutillas for his guidance through what was a particularly enjoyable part of my project.

From within the Barts Cancer Institute and afar, there are so many people who made this project possible, sometimes without even realising it. A special thank you goes to Richard Jones (MSbioworks) who offered their state of the art MS platform to perform part of the proteomics work. I would also like to thank our collaborators, Ekin and Gurlap from Germany as well as Lesley Robson from the Blizzard Institute.

I also would like to thank my group members, past and present, Kate, Sayka, Nish, Hanna, and particularly Tomasz and Laurent, not only for their help and stimulating conversations but also for their everyday support.

I wish to thank all the members of Molecular Oncology particularly Constantia, Margot and Delphine. I must also thank Mohammed, George, William and Guglielmo from Pathology and Flow-cytometry core services.

A very special thank you goes to my friend Mohammed Ghallab, for his friendship and support, you made everything much easier than it would have been.

Last but not least, I would like to thank Geraldine for her unwavering patience, presence and support and my family for their boundless love and faith in me.

Abstract

Pancreatic ductal adenocarcinoma (PDAC) is the most common type of pancreatic cancer, and the 5th most common cause of cancer death in the UK. One of the peculiarities of this malignancy is its ability to invade nerves, a process called perineural invasion (PNI). PNI is found in almost 100% of PDAC, and is associated with poor prognosis, tumour recurrence and generation of pain. However, the molecular bases of PNI remain largely unknown.

We investigated the molecular alterations underlying the neuro-epithelial interactions in PNI using one and two dimensional liquid chromatography – mass spectrometry (1D and 2D LC-MS) of laser microdissected PNI and non-PNI cancer from formalin fixed, paraffin embedded PDAC tissues. We also performed 1D LC-MS analysis of invaded and non-invaded nerves from the same cases. In addition, we developed an *in vitro* model of PNI using a co-culture system comprising PC12 cells, a rat pheochromocytoma cell line, as the neuronal element and PDAC cell lines.

The overall proteomic profiles of PNI and non-PNI cancer appeared largely similar; of very few deregulated proteins, we have validated the up-regulation of antiapoptotic protein Olfactomedin 4 in PNI cancer using immunohistochemistry.

In contrast, nerve samples demonstrated widespread molecular alterations characteristic of neuronal plasticity upon invasion by cancer cells. Immunohistochemistry confirmed the up-regulation of VGF in nerves from PDAC and chronic pancreatitis (CP) specimens compared to normal pancreas, as well as in invaded compared to non-invaded nerves in PDAC tissues. Furthermore, VGF expression strongly correlated with pain in CP; similar analysis in PDAC cases is still pending. Using the *in vitro* co-culture model, several PDAC cell lines were able to induce PC12 cells neuronal plasticity including survival, neurite extension as well as VGF expression, recapitulating thus the changes observed in human tissues. PDAC-induced PC12 plasticity was not mediated via NGF, a neurotrophin acting upstream of VGF and thought to be involved in the neuro-epithelial interactions. The induction of VGF expression was shown not to be necessary for PC12 cell survival, however, it contributed to the neurite extension induced by PDAC cell lines.

In summary, based on proteomics analysis and *in vitro* modelling, we show the complex and intricate involvement and crosstalk of both tumoral and neural elements that are activated during perineural invasion in pancreatic cancer.

Glossary of abbreviations

1D	One Dimensional
2D	Two Dimensional
ACCHN	Adenoid Cystic carcinoma of the Head and Neck
BSA	Bovine Serum Albumin
cDNA	complementary DNA
CM	Complete Media
CnM	Conditioned Media
CP	Chronic Pancreatitis
DAPI	4',6-diamidino-2-phenylindole
DMEM	Dulbecco's Modified Eagle Media
DMSO	Dimethyl Sulfoxide
DRG	Dorsal Root Ganglion
DTT	Dithiothreitol
ECM	Extracellular Matrix
EDTA	Ethylenediamine Tetraacetate
FCS	Fetal Calf Serum
FDR	False Discovery Rate
FFPE	Formalin-Fixed, Paraffin-Embedded
GO	Gene Ontology
HPF	High Power Field
H&E	Hematoxylin and Eosin
ICC	Immunocytochemistry
IHC	Immunohistochemistry
IPA	Ingenuity Pathway Analysis
IPNI	Intrapancreatic PNI
kDa	Kilodalton
LC-MS	Liquid Chromatography-Mass Spectrometry
LMD	Laser Microdissection
LN	Lymph Node
Min	Minute
mRNA	Messenger RNA

Nex	Intrapancreatic Extratumoural PNI
NGF	Nerve Growth Factor
PBS	Phosphate Buffered Saline
PCR	Polymerase Chain Reaction
PDAC	Pancreatic Ductal Adenocarcinoma
PDAC	Pancreatic Ductal Adenocarcinoma
Plx	Plexus Invasion
PNI	Perineural Invasion
RNA	Ribonucleic Acid
RP	Reverse Phase
RPMI	Roswell Park Memorial Institute (media)
SCCHN	Squamous Cell Carcinoma of the Head and Neck
SCX	Strong Cation Exchange
SDS	Sodium Dodecyl Sulphate
Sec	Second
SF	Serum Free
SiRNA	Short Interfering RNA

Table of contents

Figures and tables

List of figures

List of Tables

Appendices

Chapter One: Introduction

1. Introduction

1.1. Pancreatic cancer

Pancreatic cancer is the 10th most common cancer and the 4th most common cause of cancer death in the USA. In 2010, there were an estimated 43,000 cases and 37,000 deaths [1]. Mortality rates have closely followed incidence emphasizing the deadly nature of this disease. Pancreatic ductal adenocarcinoma (PDAC) is the most common type of pancreatic cancer comprising around 90% of cases [2] and it is also the most lethal one [2, 3].

Pancreatic cancer patients present with predominantly nonspecific symptoms including abdominal/back pain, indigestion, jaundice and weight loss [4, 5]. Therefore, late diagnosis is common and most patients have either locally advanced or metastatic disease at presentation [1, 6]. Currently, surgery is the only potentially curative treatment available [7, 8], however due to advanced stage at presentation, only 10-20% of patients have a potentially resectable disease [9, 10]. PDAC has the worst prognosis of all cancers with an overall 5-year survival of less than 5% and a median survival of less than 6 months [11]. Even in the small proportion of patients who receive potentially curative surgery, the median survival is 11-20 months and the 5-year survival is only 7-25% [11], with most series reporting around 10% or less actual 5-year survival rates [12, 13]. Furthermore, long-term survival in pancreatic cancer is rare; 5-year survival in PDAC is not equivalent to cure as most of the 5-year survivors ultimately die of recurrent disease [11, 14, 15]. The improvement in surgical techniques and perioperative care over the last three decades has significantly reduced perioperative mortality and morbidity; however, the disease specific mortality remains largely unchanged [5, 16] (**Figure 1**).

PDAC is characterised by extensive local invasion and early metastases. Even in patients with small tumours (≤2cm), only 1/3 will have stage I disease and at least 50% will have locally advanced (stage III) or metastatic (stage IV) disease [17-19]. The biologically aggressive behaviour of PDAC is clearly evident by the much favourable prognosis of other malignancies within the same region of the pancreas (periampullary cancers) including bile duct, duodenal and ampullary cancers and pancreatic cancers other than PDAC [20, 21]. In view of this invasive behaviour and the favourable prognostic significance of resection margins that are microscopically free of tumour (R0) [22-24], extensive radical surgeries have been performed to

achieve locoregional control of the tumour. However, evidence suggest that more radical procedures do not improve survival [25]. In fact, even with radical surgeries, 20-80% of patients still have positive resection margins [26, 27]. It is thus widely accepted now that the biology of PDAC and not the exact type of surgical resection is the most important determinant of outcome [7, 19, 28].

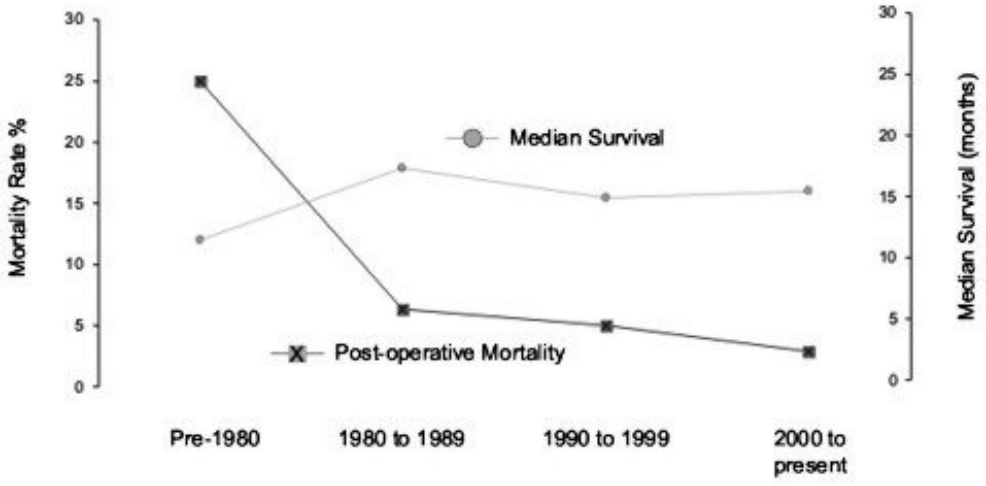

Figure 1. Postoperative mortality and median survival of PDAC patients following tumour resection over the last three decades. Adapted from [29].

The prognostic significance of several biological features of PDAC has been investigated. This is becoming more important as surgery has a limited role and new adjuvant and neoadjuvant approaches will benefit strongly from patient stratification based on pathological prognostic parameters and/or molecular biomarkers. Overall, tumour stage [14], degree of differentiation [24, 30-32], tumour size [30, 33] and lymph node (LN) metastases [23, 24, 28] appear to be strong prognostic factors.

The ability to invade nerves, perineural invasion (PNI), is another adverse biological feature of PDAC. It is a common and characteristic pathological finding in pancreatic cancer patients that has been associated with poor outcome. In the following sections, I will review the relevant neural anatomy and histological structure of nerves before discussing, in details, the published literature addressing PNI with specific focus on PDAC.

1.2. Perineural invasion

1.2.1. Pancreatic innervations and structure of peripheral nerves

Innervation of the pancreas

The pancreas is a retroperitoneal organ that lies in close proximity to the major abdominal vessels and neural ganglia, namely the superior mesenteric vessels, celiac axis, portal vein and the celiac and superior mesenteric ganglia and plexi.

Extrinsic sympathetic and parasympathetic nerves primarily from both celiac and superior mesenteric plexi richly innervate the pancreas via two pancreatic nerve plexi. Plexus pancreaticus capitalis I originates from the celiac plexus and arrives to the dorsal aspect of the head of the pancreas via the posterior hepatic plexus, whereas plexus pancreaticus capitalis II that is derived from the superior mesenteric plexus enters the lower part of the uncinate process of the pancreas along the inferior pancreaticodoudenal artery [34, 35] (**Figure 2**). In addition, the body and tail of the pancreas are innervated by the celiac plexus directly and via the splenic plexus [35]. Furthermore, the pancreas receives direct innervation from the enteric nervous system of the gut, mainly from the stomach and duodenum [36].

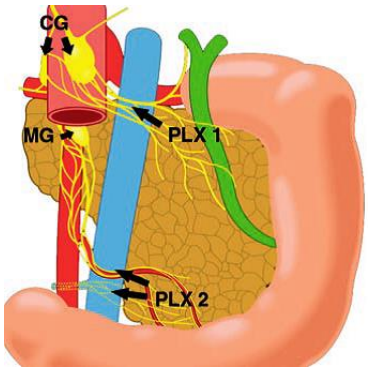

Figure 2. Schematic representation of the nerve supply to the head and neck of pancreas as depicted from a posterior view. CG: celiac ganglia; MG: mesenteric ganglion; PLX 1: plexus pancreaticus capitalis I; PLX 2: plexus pancreaticus capitalis II. Adapted from [34].

Within the pancreas, large number of ganglia is present, particularly in the head and neck region. These, along with the vast network of neural plexi around the ducts, acini, blood vessels and the islets, represent the intrinsic enteric nervous system of the pancreas [37, 38]. Complex interaction between the intrinsic and extrinsic systems as well as hormonal modulation control various physiological functions of

exocrine and endocrine pancreas, including secretion of enzymes and pancreatic juice, islet cell secretions and pancreatic blood flow [39]. These functions are mediated by an array of neurotransmitters such as acetylcholine (ACTH), norepinephrine (NE), nitric oxide (NO) and serotonin as well as neuropeptides, including gastrin releasing peptide (GRP), vasoactive intestinal polypeptide (VIP), calcitonin gene-related peptide (CGRP) and neuropeptide Y (NPY) [40]. In addition to their normal physiological functions, pancreatic nerves have been implicated in the regulation of regeneration and apoptosis in several pathological conditions such as pancreatitis and pancreatic cancer [37, 41]. Lastly, afferent nerves from the pancreas convey nociceptive and mechanoceptive pain signals either directly to the central nervous system via the vagus nerve or along the sympathetic nerves to the dorsal root ganglia of the spinal cord [39].

Structure of peripheral nerves

Peripheral nerves are composed of axons and Schwann cells surrounded by endoneurium and enclosed by the perineurium to form nerve fascicles. Groups of fascicles are enveloped in a fibrous sheath called the epineurium [42] (**Figure 3**).

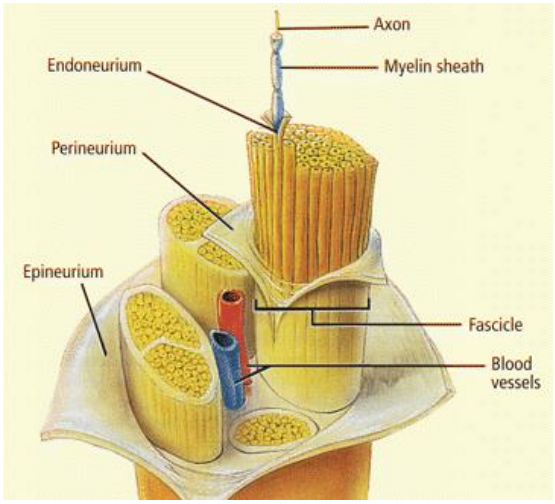

Figure 3. Structure of peripheral nerves, Adapted from *Human Anatomy and Physiology*, 7th ed., by Elaine N. Marieb and Katja Hoehn.

The epineurium is composed of an outer layer of areolar connective tissue containing vascular networks and an inner dense layer made of collagen (particularly type I and III), elastic fibres, fibronectin as well as fibroblasts [43-45].

The inner layer is closely associated with the perineurium. The epineurium is densely vascularised and blood vessels cross nerve sheaths to reach inner parts of the nerve [46].

The perineurium is a dense fibrous sheath comprising up to 15 concentric layers or laminae, each lamina is composed of flattened perineural cells with basement membrane on either side [42] (**Figure 4**). Collagen fibres, primarily type III and IV, in addition to laminin and fibronectin as well as fibroblasts are disposed between laminae [45, 47]. Within each lamina, tight junctions between perineural cells keep them firmly opposed and "dove-tailed" together [48]. The innermost layer of the epineurium is formed by tightly bound perineural cells separated from the endoneurium by the perineural space [47]. This is a potential space, the appearance of which in histological sections is a processing artefact [49, 50]. The perineurium, however, is defective at nerve endings, sites of entrance/exit of blood vessels as well as where it is penetrated by reticular fibres [47]. The primary functions of the perineurium are to provide mechanical support [42], maintain intrafascicular pressure [42] and provide, along with endoneural blood vessels, a diffusion barrier, the blood-nerve barrier, that maintains the endoneural hemostasis [47].

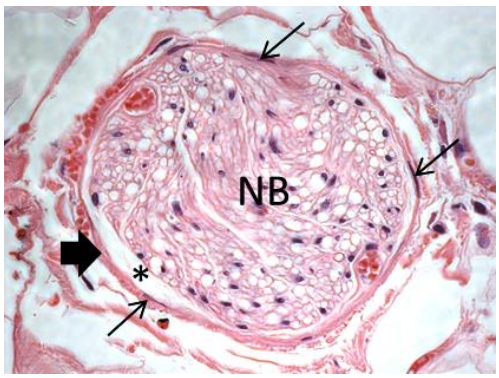

Figure 4. Histological structure of a pancreatic nerve using hematoxylin and eosin (H&E) staining showing nerve bundle (NB), perineurium (wide arrow) with perineural cells (narrow arrows) and the perineural space (*).

The endoneurium is made of collagen fibres (mainly type I and III, and to less extent IV) in addition to fibronectin and laminin as well as capillary endothelial cells, pericytes and small number of fibroblasts [45, 48]. Embedded within the endoneurium are the individual nerve fibres and associated Schwann cells.

1.2.2. Definition of PNI

The phenomenon of nerve invasion by cancer cells has been most commonly referred to as perineural invasion, less often as neural invasion and rarely perineur*ia*l invasion. A review of PNI in cutaneous malignancies advocated the diagnosis of PNI when cancer cells are observed in the perineural space whereas intraneural involvement and the circumferential presence of cancer cells around nerves are only supportive of the diagnosis of PNI in equivocal cases [50]. Another recent review suggested, however, that a widely accepted definition of perineural invasion is the invasion in, around, or through the nerves and proposed a definition that includes invasion of any of the three layers of the nerve sheaths or the presence of cancer cells around the nerve involving at least one third of its circumference [51]. However, the majority of studies that investigated PNI did not actually provide a definition to what they considered as PNI [17, 18, 26-28, 31, 52-64]. Moreover, in the studies that did provide a definition, the majority considered PNI only when cancer cells invaded the perineural space or the nerve bundle [65-78], and only few adhered to the wider definition as suggested above [33, 79] (**Figure 5**).

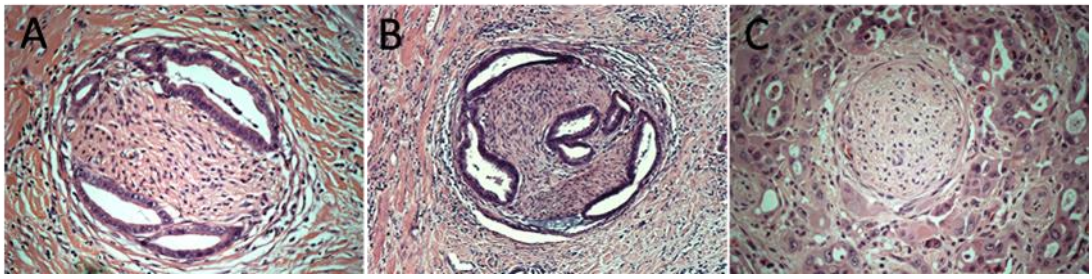

Figure 5. Histological patterns of perineural invasion. **A**: invasion of the perineural space; **B**: Invasion of the perineural space and nerve bundle; **C**: Nerve involvement where the nerve is surrounded by cancer but not invaded.

Further variation arises from the use of various classifications and grading systems for PNI. Whereas some groups used the term PNI without further specification, others differentiated between intrapancreatic perineural invasion (IPNI) and extrapancreatic neural plexus invasion (Plx) [27, 28, 33, 64]. Yet others subclassified IPNI into intratumoural and extratumoural PNI (Nex) [57]. Some authors also described the degree of PNI, usually on a scale of 0-3 according to the

frequency of PNI lesions in histological sections [28, 54, 57-59, 66] . However, the number of invaded nerves defining each grade varied between different studies. Furthermore, some studies considered nerve bundle invasion [69, 70] or PNI extending beyond the main tumour [75] as grade 3 regardless of the number of occurrences whereas others used the same grading (0-3) to denote the depth of invasion (nil, neurium, perineural, nerve bundle) rather than the frequency of PNI [63]. Other studies defined the degree of PNI by the number of invaded nerves relative to the total number of nerves observed [80]. In one study, the degree of PNI was calculated by multiplying the scores of the severity of PNI (the depth of invasion into the nerve) by the frequency of PNI lesions [81]. The assignment of higher grade of PNI to nerve bundle invasion suggests it is a more severe form of PNI that may have more impact on outcome, a finding that has been reported in rectal cancer [82]. However, one study that looked at the depth of PNI in pancreatic cancer found that nerve bundle invasion was not predictive of prognosis compared to perineural invasion or neural involvement [33]. Even after using the same scoring system (on a scale of 0-4) for PNI, some studies grouped grades 0 and 1 together and compared them with grades 2 & 3 [28, 33, 58, 64] while others compared grade 0 with the rest of the grades [54, 59].

While there are some arguments supporting each of these definitions and grading systems, none of them has been validated, making it difficult to standardize PNI parameters and subsequently compare outcomes from different studies. It is clear that while there is no consensus as to the definition of PNI, the most common definition used appears to be invasion of the perineurium and/or nerve bundles.

1.2.3. Pathology of PNI

Several studies examined the histological and ultrastructural features of PNI. Using electron microscopy analysis of oesophageal cancer sections, Takubo *et al* reported marked degeneration of perineurium in PNI along with loss of perineural cells and irregularities of basal laminae resulting in cancer cells lying in direct contact with the endoneurial elements [52]. Importantly, the authors also noticed the presence of cytoplasmic projections and lysosome-like structure at the invading front of cancer cells suggesting an active role of cancer cells in the degeneration of perineurium and gaining access into the perineural space. Similar findings were also reported in pancreatic cancer [83, 84].

Histologically, perineurally invasive cancer cells appeared well to moderately differentiated, forming glandular structures in most cases [33] and cancer cells in direct contact with the nerve appeared more flattened than those that are part of the same gland but not in direct contact with the nerve [83].

In a detailed histological analysis of serial sections of PDAC tissues, Kayahara *et al* concluded that PNI occurs through direct invasion and destruction of the perineurium and/or through perforating blood vessels. They also found that perineurally invasive cancer cells form an advancing tip and grow in continuous fashion, branching where the nerve branches [65] (**Figure 6**). Similar continuous pattern of growth as well as extensive branching of PNI following the neural branching was also noted in 3D reconstruction of serial PNI sections [85]. Although rarely, discontinuous growth along the perineural space has also been observed [59]. A varying degree of nerve damage is common in PNI and proximal and distal extension of the cancer for few centimetres could sometimes be seen [53].

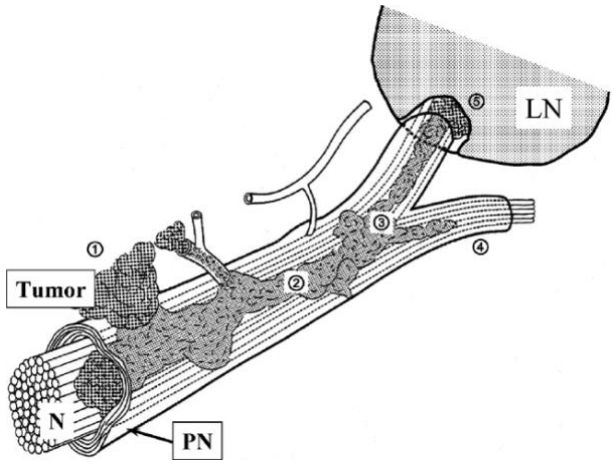

Figure 6. The pattern of invasion and spread of cancer cells along nerves in PNI. N: nerve; PN: perineurium; LN: lymph node; 1: direct invasion of perineurium; 2: continuous growth of cancer along the perineural space; 3: branching of cancer cells as the nerve branches; 4: advancing tip of cancer, 5: possible extension into LN via nerves. Adapted from [65].

From the primary tumour, PNI develops continuously along nerves to reach the superior mesenteric and celiac plexi and as the invasion advances, PDAC cells may spill out of the perineurium into adjacent fatty tissue [59, 86]. Significant association was found between intrapancreatic tumour invasion and extrapancreatic plexus

invasion lending support to the direct and continuous extension of cancer cells from the primary tumour along the nerve to reach the main neural plexi [54, 64, 66, 68].

The most commonly involved plexus in pancreatic cancer of the head and neck region is the plexus pancreaticus II, less frequently the plexus pancreaticus I, the nerve plexus of the hepatopancreatic ligament and the plexus around the mesenteric vessels [19, 66, 87]. In pancreatic body and tail tumours, the splenic plexus is the most commonly invaded, but the celiac or superior mesenteric plexi are also occasionally involved [27].

1.2.4. Incidence and clinical significance of PNI in PDAC

As alluded to previously, PNI is a characteristic feature that is frequently observed in PDAC. Most studies reported intrapancreatic PNI in 50-100% of cases while neural plexus invasion occurred in 35-70% (**Table 1**). The estimates vary widely secondary to differing definitions of PNI, the extent of surgical resection (in the case of plexus invasion), the extent to which tumour samples are evaluated [88] as well as the accuracy of reporting [79]. In addition, routine H&E staining may underestimate the incidence of PNI. In oral cavity squamous cell carcinoma, Kurtz *et al* showed that the incidence of PNI increased by 100% upon re-reviewing the original H&E slides and by almost 200% by IHC using antibodies against the neuronal marker S100B protein [78]. In this study, the mean number of PNI lesions identified using immunohistochemistry (IHC) was largest in the cases where PNI was identified in original reports and least in the cases in which PNI was only identified by IHC, suggesting that PNI can be missed when it is not frequent [78].

The enhanced detection of PNI using IHC has also been reported in other tumours including ampullary [89] and colorectal [90] cancer, suggesting that the rate of PNI could be much higher than currently thought. In pancreatic cancer, it has been suggested that PNI is present in 100% of cases if carefully looked for [91]. Furthermore, KRAS mutation analysis of nerve plexus revealed PNI that was not evident on routine histological sections suggesting widespread perineural microinvasion [88]. While the clinical significance of such finding is currently unknown, the high recurrence rate following apparently curative resection may suggest that these microinvasive lesions could be a source of recurrent disease. Finally, PNI has been commonly observed even in small tumours ≤20mm [17, 23].

This, along with the observation of PNI in minute tumours <2mm found at one autopsy study indicates that PNI is an early event in pancreatic cancer invasion [92].

Table 1. Incidence of PNI and its correlation with survival in PDAC. NA: not assessed; IPNI: intrapancreatic PNI; Plx: neural plexus invasion; Nex: intrapancreatic extra-tumoural PNI.

Study	**Incidence of PNI yes/total (%)**	**Correlation with survival**	**Notes**
Nagai H 1985 [60]	6/8 (75%)	NA	T1/T2 autopsy cases (≤2cm)
Nagakawa T 1991 [66]			
IPNI	33/34 (97%)	NA	
Plx	21/34 (62%)	NA	
Nagakawa T 1993 [26]			
IPNI	21/21 (100%)	NA	
Plx	17/21 (81%)	No	
Nakao A 1996 [54]			
IPNI	116/129 (90%)	Yes	
Plx	80/116 (69%)	Yes	
Sperti C 1996 [56]	71/113 (63%)	Yes (univariate)	
Furukawa H 1996 [17]	19/31 (61%)	NA	Small PDACs ≤2cm
Kayahara M 1996 [27]	14/20 (70%)	NA	
Plx			
Takahashi T 1997 [57]			
IPNI	88/90 (98%)	Yes	
Nex	47/90 (52%)	Yes	
Plx	47/90 (52%)	No	
Dang C 1998 [84]		NA	
IPNI	22/30 (73%)	NA	
Plx	20/30 (67%)		
Hermanek P 1998 [18]	187/219 (85%)	NA	
Ozaki H 1999 [55]	90/126 (76%)	Yes (for stage I & II)	
Meyer W 2000 [30]	42/93 (45%)	Yes (univariate)	
Okusaka T 2001 [62].	87/95 (92%)	NA	
Hirai I 2002 [59]	17/24 (71%)	Yes (multivariate)	
Cleary SP 2004 [31]	34/123 (28%)	No	
Tezel E 2004 [93]			
Plx	18/64 (28%)	Yes	
Shimada K 2006 [28]			
IPNI	82/88 (93%)	Yes (univariate)	
Plx	30/88 (34%)	No	
Shimada *et al* 2006 [23]			
IPNI	8/10 (80%)	NA	

Table1 continued…

Study	Incidence of PNI yes/total (%)	Correlation with survival	Notes
Plx	47/173 (27%)	Yes (univariate)	
Mitsunaga S 2005 [58]			
IPNI	95/101 (94%)	Yes (univariate)	
Plx	35/101 (35%)	Yes (multivariate)	
Dang C 2006 [70]	/56 (30%)	Yes (multivariate)	
Mitsunga S 2007 [33]			
Plx	49/75 (65%)	Yes (univariate)	
Garcea G 2007 [94]	19/27 (70%)	Yes	
Ma J 2008 [72]	34/51 (68%)	Yes	
Morris-stiff G 2009 [21]	134/144 (93%)	NA	
Wang W 2009 [69]	137/137 (100%)	NA	
Chen JWC 2009 [67]	31/60 (52%)	Yes (multivariate)	
Ceyhan GC 2009 [81]	115/149 (79%)	No	
Shimada K 2011 [64]			
IPNI	146/153 (95%)	Yes (multivariate)	
Plx	94/153 (61%)	Yes (univariate)	

The anatomical location of the pancreas in close proximity to the major abdominal neural plexuses and the rich innervation of the pancreas have been suggested as an explanation for the high incidence of PNI in PDAC. Evidence, however, suggests that this common occurrence of PNI is strongly related to the biology of PDAC. For instance, Kayahara *et al* found that the incidence of plexus invasion in pancreatic cancer (61%) was significantly higher than in bile duct (21%) and papilla of Vater (3%) tumours, all of which lie within the same anatomical position [87]. Several other studies corroborated these findings [19-21].

PNI has been associated with incomplete resection of PDAC [54, 95], tumour recurrence [58, 64, 96-98], generation of pain [99] as well as poor prognosis (**Table 1**). Nakao *et al* reported that PNI, particularly extrapancreatic plexus invasion, significantly correlated with survival; all patients who survived more than three years in their study showed no plexus invasion [54]. Similarly, in the study of Tezel *et al*, none of the patients with plexus invasion survived for three years compared to 18% 3-year survival in patients without plexus invasion [93]. Furthermore, Ozaki *et al* reported significant influence of intrapancreatic PNI on survival, particularly in early stage PDAC. They found that stage I and II (no LN metastases) patients without IPNI had significantly better 5-year survival (75%) compared to those with IPNI (29%) but there was no difference in survival in stage III and IV patients [55]. This may suggests a role of PNI in driving the local tumour spread, but once the tumour

is advanced PNI loses its prognostic significance. Mitsunaga *et al* found that plexus invasion distance of ≥2.5mm from pancreatic capsule correlated with poor prognosis on both univariate and multivariate analysis [33]. Furthermore, in a review of the Japanese experience of pancreatic cancer resections, Matsuno *et al* found that involvement of the neural plexi conferred poor prognosis whether it was resected or not, suggesting that the invasion of neural plexus reflects the malignant phenotype of PDAC [7]. It is generally accepted that periampullary cancers have better prognosis than PDAC [20, 21, 67]; a recent study suggested that this difference could be due to the more frequent occurrence of PNI in PDAC compared to the other cancers and that PNI was a stronger prognostic factor than the location of the tumour [100]. While most studies showed significant influence of PNI on survival, few failed to show such prognostic significance (**Table 1**). In a systematic review of prognostic factors in pancreatic cancer, Garcea *et al* found that PNI significantly correlated with median survival but not with overall 5-year survival [29]. It is worth mentioning however, that the review did not include some of the studies in **Table 1** and the heterogeneity of these studies in terms of patients' characteristics, definition of PNI and the anatomical location (IPNI vs plexus invasion) makes meta-analysis of such disparate studies difficult.

1.2.5. Pain and PNI in pancreatic cancer

In addition to recurrence and poor survival, PNI correlates closely with pain in pancreatic cancer patients [70, 81]. Abdominal pain is a common presenting feature and the degree of pain has been associated with advanced tumours, unresectability [98] and poor survival [62, 81, 101].

The mechanisms of pain in PDAC are not well understood. There is accumulating evidence which suggest that in pancreatic cancer, as well as in chronic pancreatitis, pain is of neuropathic origin as a result of direct damage to the nerves [81]. Pancreatic neuropathy could also be mediated through neuro-immune interactions as a result of perineural immune cells infiltrate, and/or from direct invasion of nerves by cancer cells [102]. In a recent study, Demir *et al* showed that pain in pancreatic cancer is associated with increased perineural mast cells infiltration [103]. Alterations in the pattern of autonomic innervations of the pancreas have also been demonstrated, whereby CP and PDAC patients with pancreatic neuritis, PNI or abdominal pain had decreased cholinergic and sympathetic innervations of the

pancreas [104]. In another study, an increase in sympathetic and CGRP expressing sensory neurons was demonstrated in a transgenic mouse model of pancreatic cancer [101].

Several neurotrophic factors, chemokines and neuropeptides have been associated with pain in pancreatic cancer, but experimental evidence for most of them is generally lacking. NGF and its receptor TrkA remain one of the best studied in this regard. In a transgenic mouse model of pancreatic cancer, it has been suggested that initial sprouting and sensitisation of nerve fibres induced by NGF from macrophages and subsequent damage to those nerves as the tumour advances may contribute to pain generation [101]. The vanilloid receptor TRPV1, a non-selective cation channel expressed in sensory nerve fibres has been shown to be over-expressed in pancreatic cancer and correlated with the intensity of pain [105]. Interestingly, NGF has been shown to modulate both the level and activity of TRPV1 in pancreatic sensory neurons in chronic pancreatitis [106]. Therefore, NGF signalling pathway has been tested as a potential therapeutic strategy for skeletal, inflammatory and neuropathic pain using monoclonal antibodies targeting NGF or its receptor TrkA [107-109].

1.2.6. PNI in other cancers

Although PNI has been most commonly seen in pancreatic cancer, it has also been described in several other cancers including cutaneous and non-cutaneous head and neck cancers [110, 111], prostate [112], colorectal [79] and gastric cancers [113].

In **prostate cancer**, the wide-spread use of Prostate Specific Antigen (PSA) as a screening tool resulted in increased detection rate. While many of these cancers are indolent and can be managed with a wait and watch approach, the greatest challenge is to identify the subset of patients who require more aggressive treatment including surgery and radiotherapy [114]. Radical prostatectomy, the standard surgical treatment for prostate cancer is not without risks, particularly in relation to nerve damage with resulting urinary incontinence and erectile dysfunction, and a nerve sparing variant could be performed in selected patients [115]. In this context of complex management options, PNI has been investigated as a possible indicator of a more malignant cancer phenotype that requires more immediate and aggressive treatments.

PNI has been reported in 19-34% of prostate biopsies [116-118] and in 42-79% in prostatectomy specimens [112, 119, 120]. PNI is associated with recognised aggressive features of prostate cancer such as advanced Gleason score, stage, positive resection margins as well as extraprostatic extension [112, 116, 119, 121]. The presence of PNI in prostate biopsies can also be a predictor of the final pathological stage following prostatectomy [122].

Several studies also showed that PNI is associated with biochemical recurrence, and reduced biochemical failure-free survival and overall survival in prostate cancer patients following both radiotherapy and surgery [116, 117, 121, 123]. Some studies, however, have failed to demonstrate prognostic significance for PNI [112, 119].

A recent systematic review by Cozzi *et al* found that patients with PNI on prostate biopsy specimens had a significantly higher risk of extraprostatic extension of tumour [124]. A separate systematic review of the prognostic significance of PNI in prostate cancer biopsies concluded that whilst the significance of PNI remains controversial, the weight of evidence suggests that the presence of PNI is a significant prognostic indicator and such patients should be offered treatment rather than watchful waiting [125].

More recently, the implications of PNI in **colorectal cancer** have been investigated. PNI has been reported in 18-34% of rectal cancers [82, 126, 127] and in 13-31% of colon cancers [126, 128]. PNI is also associated with advanced disease, incomplete resection, local recurrence as well as higher likelihood of metastasis [79, 82, 126, 129]. In addition, PNI is a strong and independent predictor of 5-year overall survival and disease-free survival [79, 82, 126, 130].

In their detailed study of PNI in rectal cancer, Ceyhan *et al* found that preoperative chemoradiotherapy significantly reduced PNI prevalence and severity compared to primary resection only and these patients had lower recurrence rate but no difference in survival [82]. In another study, stage II patients with PNI who received adjuvant chemotherapy had a significantly better disease-free survival compared to those not receiving chemotherapy whereas stage II patients without PNI showed no benefit, suggesting a role for PNI in stratification of colorectal cancer patients for adjuvant therapy [130]. This is particularly important in patients with stage II disease and those with node negative disease where there is no consensus on the role of adjuvant therapy. Santos *et al* found that PNI is a significant prognostic factor in stage II colon cancer patients [131] whereas Desolneux *et al* demonstrated the prognostic significance of PNI in node negative colorectal cancer [132].

Indeed, Liebig *et al* showed that the survival of patients with node negative colorectal cancer who have PNI is significantly worse than patients with nodal involvement and suggested PNI should be used for stratification for adjuvant therapy [79].

In **gastric cancer**, PNI occurs in 31-75% of cases [113, 133, 134]. Tianhang *et al* reported that PNI is associated with stage, poor differentiation and peritoneal metastasis and was an independent prognostic factor for overall 5-year survival [134]. Similar results were also reported by others [113, 135]. PNI was also shown to be a significant prognostic factor, along with tumour diameter and lymphatic/blood vessel invasion, that defines a high-risk subset of T2N0 gastric cancer patients who could potentially benefit from adjuvant therapy [136].

1.2.7. Mechanisms underlying PNI

Interactions between nerves and target tissues are part of normal physiology. In addition to functional control, the nervous system regulates structural development, maintenance and regeneration of various tissues and organs [37, 137-139].

In cancer, neuro-neoplastic interaction is a mutual relationship in which not only nerves can modify the biology of tumour cells but also, as recent studies suggest, and akin to neoangiogenesis and lymphangiogenesis, tumours are able to promote neoneurogenesis. This view has been supported by increased neurite growth in dorsal root ganglia (DRGs) co-cultured with several cancer cell lines [140-142], increased neural density in a mouse model of pancreatic cancer [101] as well as by the demonstration of neurogenesis and its negative impact on disease progression and prognosis in several human cancers such as colorectal [141] and prostate cancer [142].

PNI represents an environment in which the cancer cells and nerves are physically and functionally intertwined. By virtue of the obvious spatial proximity, PNI has been recognised since the 19th century but our understanding of its significance and exact nature has only started to evolve over the past three decades [51]. Initially, PNI was thought to be a form of lymphatic space invasion, however, later studies confirmed that the perineural space is not a lymphatic space, it does not connect with lymphatic channels and there are no lymphatic channels within nerves [49, 143]. Subsequently, two theories attempted to explain this specific route of cancer spread. The first theory suggested a physical explanation of PNI and proposed that cancer cells are spreading across a path of least resistance [49, 143]. Whilst the perineural space may be considered as a low resistance and accommodating path for cancer cells, arriving into that space is far from least resistance considering the structure of nerves and their sheaths. In addition, electron microscopy studies suggested active destruction of the perineurium by cancer cells during the process of PNI as discussed earlier. Furthermore, several recent studies have shown that neuro-neoplastic interaction appears to be more than just histological proximity and nerves seem to provide more than a defined anatomical path for cancer spread, supporting the second theory, neurotropism, as an explanation for PNI. The microenvironment created by this interaction appears to provide a suitable milieu for tumour growth resulting in enhanced proliferation and inhibition of apoptosis of cancer cells as well as increased neurite outgrowth [140, 144-147]. Moreover, in an *in vitro* co-culture model of DRGs and prostate cancer, the presence of stromal cells appears to

further increase the cancer cell and neurite growth [148]. Interestingly, a similar *in vitro* model of PNI using PDAC cells and DRGs or myenteric plexus cells demonstrated that morphological changes in cancer cells including flattening and elongation occurred at the migration front of cancer cells before direct contact with the neural element was established [149]. This mutual interaction was explored in several studies that investigated the role of various proteins in the process of PNI, mostly focusing on neurotrophins and neurotrophic factors, neural adhesion molecules as well as other neuronal proteins that have previously been implicated in cancer (**Figure 7**).

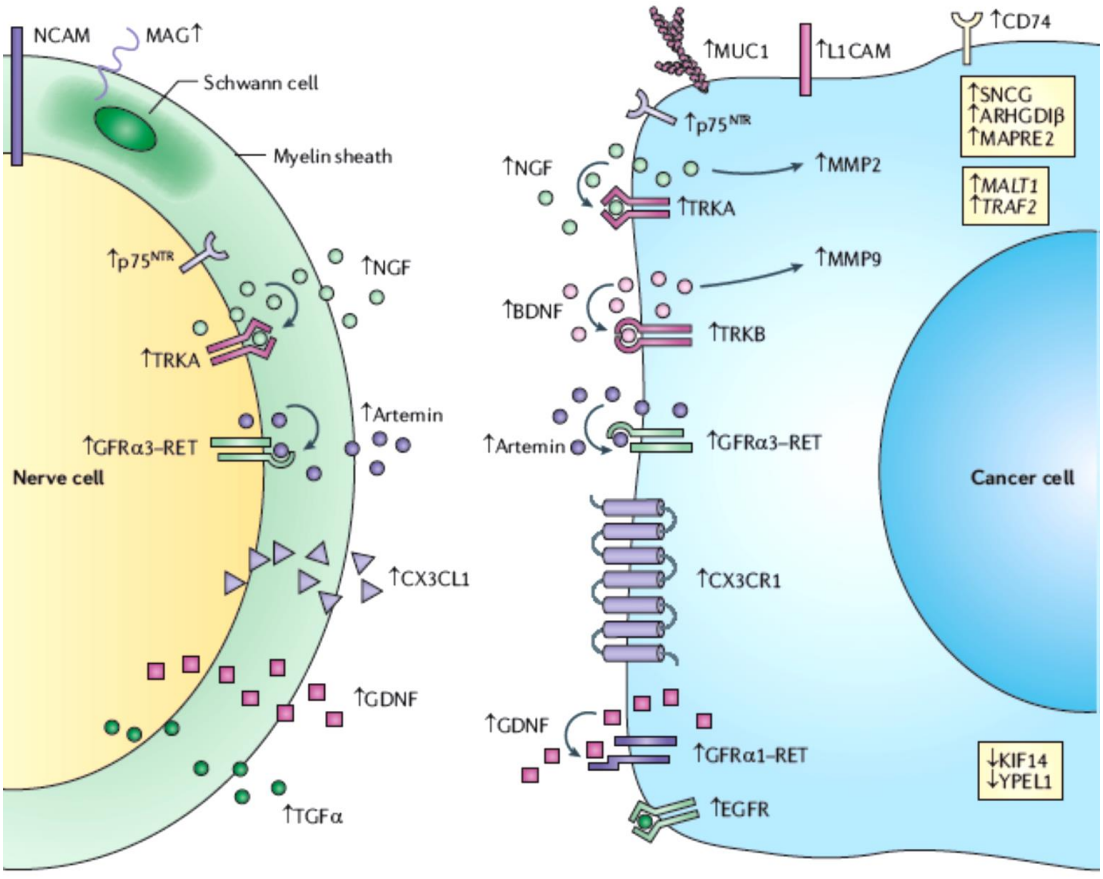

Figure 7. Schematic representation of the various signalling molecules thought to be involved in perineural invasion. Adapted from [150].

Neurotrophins

Neurotrophins are a group of structurally related growth factors including nerve growth factor (NGF), brain-derived neurotrophic factor (BDNF), neurotrophin-3 (NT-3) and neurotrophin-4 (NT-4). These factors bind to two types of unrelated receptors: Trk receptor tyrosine kinases A, B and C and the low affinity $p75^{NTR}$ receptor, a member of the tumour necrosis factor superfamily. All these neurotrophins bind to the $p75^{NTR}$ receptor but individual neurotrophins bind preferentially to one or more Trk receptors [151, 152]. The interaction between neurotrophins and their receptors is vital for neuronal development, maintenance and survival. In addition, neurotrophins have been shown to play important role in neuronal and non-neuronal cancer progression [151]. The biological actions however, are complex and may be paradoxical depending on the exact neurotrophin and receptors involved. The binding of neurotrophins to Trk receptors, which is modulated by the presence of $p75^{NTR}$ induces survival, whereas binding to $p75^{NTR}$ on its own induces apoptosis. To add to the complexity, pro-forms of neurotrophins can bind with higher affinity to the $p75^{NTR}$ receptor inducing apoptosis [153].

NGF and Trk receptors, particularly TrkA, have been shown to correlate with PNI, pain and poor prognosis in pancreatic cancer [70, 71, 154], while the expression of $p75^{NTR}$ negatively correlated with PNI and conferred better prognosis [70]. Other studies, however, showed positive correlation between $p75^{NTR}$ and PNI [69] and failed to show any correlation between NGF and TrkA and prognosis [72].

NGF has also been shown to increase proliferation and invasiveness of PDAC cell lines [155] and the invasion of prostate cancer cell lines [156]. For example, NGF appears to increase invasion of Panc1 PDAC cell line via stimulation of MMP-2 expression and activity through TrkA and subsequent activation of MAPK signalling pathway [157]. Yet in other studies, NGF has stimulatory, inhibitory or no effect on growth and invasion of various PDAC cell lines [158-160]. The actions of neurotrophins on cancer cells has been shown to be dose dependent and varies with cell types, and it has been suggested that the ratio of TrkA and $p75^{NTR}$ determines the outcome of NGF action on these cells [70, 159, 160]. Furthermore, studies that dissected the spatial distribution of neurotrophins and their receptors in tissue samples reported inconsistent results. While NGF was found to be highly expressed in both cancer and nerves in some studies [71, 72, 161], others reported low levels of expression in cancer but high levels in nerves within tumours [158] or absence of NGF in normal and cancer tissue [159]. On the other hand, Trk receptors

were reported to have higher expression in cancer compared to normal pancreas in one study [159], another found that Trk A was absent in cancer and highly expressed in the perineurium [71], whilst a third study reported that Trk A expression was weak in cancer and almost absent in the perineurium ([72]. A separate study described the absence of Trk B expression in PDAC [161]. $p75^{NTR}$ was probably the least controversial, as several studies reported high levels of expression in nerves but low or no expression in both normal and PDAC tissue, with lower levels of expression in PDAC [69, 159, 161].

The opposing actions of neurotrophins and the conflicting expression patterns reported by many authors has suggested that the biological actions of neurotrophins binding to their receptors do not rely only on expression levels but also the context, including cell type and ratio of expression of the two types of receptors, Trk and $p75^{NTR}$. However, despite their role in cancer invasion, the expression patterns of the mentioned neurotrophins and their receptors in pancreatic cancer do not point to particular mechanism in the development of PNI. These observations have prompted the suggestion of two different ways in which neurotrophins and their receptors could contribute to PNI, firstly, by promoting survival of neurons and axonal growth towards cancer cells and thus facilitating PNI and secondly, by promoting cancer growth and invasion and inhibiting apoptosis of cancer cells [71, 72].

Pleiotrophin (PTN) is another neurotrophic factor that has been linked to PNI in pancreatic cancer. It has been shown to be expressed in pancreatic cancer cells while its receptor N-syndecan was strongly expressed on the perineurium of nerves within the tumour mass and both correlated with PNI suggesting that this axis may promote neural growth into the cancer [77].

GDNF family

The glial-derived neurotrophic factor (GDNF) family is another family of neurotrophic factors that has been implicated in PNI. This family includes in addition to GDNF, artemin (ARTN), neurturin (NRTN) and persephin (PSPN). These neurotrophic factors exert their action by binding to a multicomponent receptor composed of GDNF family receptor-α (GFR-α1-4) as binding sites and the RET receptor tyrosine kinase as the signalling part of the receptor [162, 163]. These factors are involved in neuronal survival and differentiation, as well as neuronal and non-neuronal malignancies [163]. GDNF is the best studied factor in relation to pancreatic cancer and PNI. GDNF is expressed in intrapancreatic nerves as well as pancreatic cancer

and its expression is correlated to PNI [164-166], whereas RET is over-expressed in pancreatic cancer and its expression correlated with survival [165, 166]. In bile duct cancer, GDNF expression correlated with PNI but RET was not present in cancer cells [167]. Functionally, GDNF has been shown to increase the expression and activation of MMP-9 via MEK/ERK and PI3K pathways [168] and stimulate migration and invasion of PDAC cell lines via the same pathways [169]. In a recent study, Gil *et al* demonstrated that GDNF produced by DRGs induced directional migration of MiaPaca2 cells towards nerves in a dose dependent manner via the GDNF/GFRα1/RET signalling pathway [170]. Another study showed that endoneurial macrophages secret GDNF that increases the perineural invasive behaviour of PDAC cells in both *in vitro* and *in vivo* models again via activation of ERK [171].

ARTN as well as its receptor GFRα3/RET were reported to be highly expressed in both pancreatic cancer and nerves within cancer specimens and this protein also appears to increase invasiveness of PDAC cell lines [172], however, a direct link to PNI has not been established yet.

Cell adhesion molecules

Several studies suggested a role for the neural cell adhesion molecule (NCAM) in PNI as it was found to be associated with the extent of PNI in pancreatic cancer [173] and with the presence of PNI in squamous cell carcinoma of the head and neck (SCCHN) [174]. Furthermore, NCAM was found to be expressed in nerves in prostate cancer with significantly higher levels in nerve invaded by cancer compared to non-invaded nerves [175]. On the other hand, NCAM immunoreactivity was reported in nerve cells but not on the perineurium and endoneurium suggesting that NCAM may not be involved directly in the process of PNI [173]. Several other studies, however, failed to show any correlation between NCAM expression and PNI in PDAC [176], SCCHN [177] and adenoid cystic carcinoma of the head and neck (ACCHN) [178]. In a gene expression profiling study comparing matched laser capture microdissected perineurally invasive and non-perineurally invasive salivary adenoid cystic carcinoma cells (ACC) from human tissues, Melanoma Cell Adhesion Molecule (MCAM) was found to be over-expressed in perineurally invasive cancer [74]. Subsequently, the same group showed that silencing MCAM reduced proliferation and invasion of ACC cells *in vitro* [179].

Another adhesion molecule, L1-CAM reportedly correlated with the degree of PNI, pain and survival in PDAC patients [73].

Chemokines

The chemokine CXCL12 that is expressed in prostate cancer cells and nerves has also been suggested to act in a paracrine/autocrine manner to promote PNI in prostate cancer via its receptor CXCR4 that is expressed in cancer cells [180]. A recent study by Marchesi *et al* implicated another chemokine receptor, CX3CR1, in PNI [80]. In this study, PDAC cell lines expressing CX3CR1 had increased adhesiveness and chemotaxis towards CX3CL1 chemokine that is present in nerves. This was mediated via G protein-dependent signalling with activation of β1 integrin and FAK. The study also reported that CX3CR1 was expressed in most PDAC cases, correlated with PNI and independently predicted tumour recurrence [80].

Neurotransmitters

The role of neurotrasmitters in tumourogenesis and cancer progression is being increasingly investigated as epidemiological studies into the relationship of stress and cancer suggested a role for the autonomic nervous system in cancer [181]. A recent observational study has also shown that the use of β2-adrenergic blockers reduced breast cancer progression and mortality [182]. Experimental surgical or chemical sympathectomy was also able to inhibit prostate cancer xenograft growth [183].

Norepinephrine (NE), is a sympathetic neurotransmitter that has been shown to increase the invasiveness of MiaPaca2 pancreatic cancer cell lines and increase the levels of MMP-2, MMP-9 and VEGF, all of which could be inhibited by the β-adrenergic blocker Propranolol [184]. Guo *et al* also found that NE increases perineural invasive ability of PDAC cells lines through β-adrenergic/PKA/STAT3 signalling pathway in both *in vitro* and *in vivo* models of PNI [185]. Another recent study confirmed the expression of β-adrenoreceoptors in cancer cells in pancreatic cancer tissues whilst β2-receptor blockade in Panc1 pancreatic cancer cell line resulted in G1/S phase arrest and cell death [186]. Similarly, NE increased lymph node metastasis from PC-3 prostate cancer *in vivo* model and this was, again, blocked with propranolol [187].

Substance P (SP) is a neuropeptide released from sensory nerves and signals through its receptor NK-1R. SP has been shown to increase PDAC cells proliferation and invasion in addition to increasing neurite growth from DRGs in co-culture with PDAC cells [188]. These effects were blocked by NK-1R antagonists [188].

Altogether, evidence suggests a crucial role of several neurotrasmitters in modulating cancer cell biology into a more aggressive phenotype. The final influence could be dependent on the ability of cancer cells to respond to these cues and the degree of cancer innervation and neoneurogenesis, a phenomenon that is receiving more interest recently.

Other molecules

Using rat vagal nerve explants to establish highly neuroinvasive subclones of PDAC cell lines followed by gene expression profiling, Abiatari *et al* produced a catalogue of 680 transcripts that were differentially regulated between the less and the highly neuroinvasive clones [189]. Amongst these, they identified the kinesin-like protein KIF14 as an invasion-suppressing gene that was down-regulated in highly invasive clones *in vitro* as well as in perineurally invasive cancer cells compared to non-invasive cells in human PDAC tissues. Silencing of KIF-14 in T3M4 PDAC cell line resulted in increased invasiveness of these cells using both Transwell and vagus nerve invasion assays. In addition, the authors reported that the Rho-GDP dissociation inhibitor β (ARHGDIβ) was up-regulated in both highly neuroinvasive clones and perineurally invasive cancer cells in PDAC tissues. Silencing of ARHGDIβ did not affect transwell invasion but decreased invasion in vagus nerve neural invasion assays [189]. In a subsequent report, the same group suggested a role of the microtubule-associated protein MAPRE2, another protein that was up-regulated in the highly invasive clones, in PNI. However, there was no association between MAPRE2 expression and PNI in human tissue samples and apart from the over-expression in neuroinvasive cell lines, there was no evidence for its involvement [190].

MUC1 has also been suggested to contribute to PNI by enhancing adhesion to the nerves through interaction with the myelin-associated protein (MAG) on Schwann cells [191]. Others proposed that the basement membrane proteins laminin, fibronectin (FN) and collagen type IV, which are abundantly expressed in the basement membrane of perineurium may increase the migration of PDAC cell lines

(most notably undifferentiated ones) and contribute to PNI [192]. Specifically, the interaction between neuronal laminin and integrin α6β1 on malignant cells has been suggested to contribute to the neurotropism of prostate cancer [193]. Similarly, laminin γ2 (LAMC2) has been shown to increase the nerve invasion distance of PDAC cell lines in an *in vivo* sciatic nerve model of PNI possibly by enhancing the attachment of cancer cells to the neural tissue and/or increasing migration through interaction with integrin α6β4 on cancer cell surface [194].

Several other proteins have also been reported to be involved in PNI. Using a subcutaneous mouse model of pancreatic cancer, Koide *et al* reported that CD74 was up-regulated in PDAC cell lines with high propensity for PNI and its expression correlated with the degree of PNI in human PDAC samples [75]. In a subsequent study using the same model, they also found that synuclein-γ (SNGG) was over-expressed in neuroinvasive cell lines and its expression correlated with PNI, poor survival as well as other invasive parameters such as stage, LN metastases and tumour size, suggesting that SNGG over-expression results in a more aggressive and invasive malignancy and is not specifically related to PNI [76]. In another study, SNGG was found to be over-expressed in pancreatic cancer and significantly associated with LN metastases but correlation with PNI was not significant [61]. In addition, SNGG was not predictive of survival in this study although this could be related to the selection of patients as all of them were stage I and II [61]. In another study, Nestin (NES), an intermediate filament protein, has also been shown to correlate with PNI in pancreatic cancer using IHC [195].

In a genome-wide expression analysis of microRNA and mRNA of prostate cancers with and without PNI, Prueitti *et al* found 19 microRNAs that were over-expressed and 34 mRNA transcripts that were down-regulated in cases with PNI including genes involved in metabolism, negative regulation of cell death and interestingly neurogenesis [196].

Lastly, hyperglycemia has been reported to enhance neural alterations and increase PNI in pancreatic cancer. Patients with hyperglycemia showed increased neuronal density and hypertrophy as well as more frequent PNI [63]. Diabetic patients have also been shown to have more PNI and both diabetes and PNI predicted poor prognosis [197]. It has been hypothesized that hyperglycemia promotes PNI through both increasing proliferation of cancer cells as well inducing nerve damage as seen in diabetic neuropathy [198].

1.2.8. Neuronal plasticity in cancer

The presence and implication of alterations in the neuronal structure and/or function, neuronal plasticity, in the context of cancer is becoming increasingly recognised. Ceyhan *et al* showed that pancreatic cancer patients have increased neural density and hypertrophy and pancreatic neuritis that exceeded the one present in chronic pancreatitis, and neural density and hypertrophy significantly correlated with the degree of PNI [81]. In a separate study, the same group confirmed the neurotrophic effect of pancreatic cancer microenvironment by demonstrating increased neurite density in myenteric plexus cells treated with protein extract from pancreatic cancer tissues [199]. This effect was partially reversed by depletion of NGF and ARTN from the extract suggesting a role for those two proteins in addition to other unknown factors. In another report, protein extracts from PDAC and CP tissues increased neurite growth, branching complexity and neuronal cell size of both myenteric plexus and DRG neurons *in vitro* [200]. Similar results were obtained by treatment with conditioned media from several PDAC cell lines [200]. As pointed out earlier, alteration in the nature of autonomic and sensory pancreatic innervations has been observed both in human PDAC and in a transgenic mouse model of pancreatic cancer [101, 104].

In prostate cancer, Ayala *et al* presented the first evidence for active neurogenesis and axonogenesis in cancer [142]. They demonstrated increased neural density as well as number and size of neurons in prostate cancer samples compared to normal prostate, which was also evident in preneoplastic lesions. In another study, Magnon *et al* found higher autonomic neural density in high-risk compared to low-risk prostate cancer patients which was associated with poor clinical outcome [183].

In colorectal cancer, Albo *et al* showed that 66% of patients displayed some degree of neurogenesis which was an independent prognostic factor for overall and disease free 5-year survival [141]. In their study, colorectal cancer cells were also able to induce neurite growth in DRG neurons *in vitro*.

There is ample evidence to suggest that neuronal plasticity is a key feature of neuro-epithelial interactions, particularly in neurotropic cancers. The biological results of this in terms of influence on symptoms, aggressiveness of cancer cells and patients' survival are just starting to emerge.

1.2.9. Experimental models of PNI

In vitro models

In vitro models used primarily two types of neuronal cells or tissue explants co-cultured with cancer cells. DRG based models are the most widely used to investigate PNI. Initial models used DRGs excised from mice, and grown in a drop of extracellular matrix (ECM) next to another drop containing cancer cells [147]. Subsequent modifications used two drops of ECM on either side of cancer cells, only one containing DRG. ECM bridges were used to connect the cancer cells to the other two drops, thus the model provided the opportunity to measure unidirectional migration of cancer cells towards DRGs ([149].

Because DRGs are sensory nerve structures and the innervation of the pancreas is largely autonomic, a second model utilizing rat myenteric plexus cells from the enteric neuronal system was established, the results using these cells were largely consistent with those using DRGs [149].

An alternative in *vitro* model based on passaging cancer cells through a rat vagus nerve conduit has been used to establish progressively more neuroinvasive clones of PDAC cells [189]. The gene expression profiles of these cells were then compared to identify genes that are deregulated during this process. A potential disadvantage of this model is the lack of neuronal cells within the conduit as the neuronal cell bodies lie within the nucleus ambiguous in the brain and the conduit is mainly formed of nerve layers and degenerating axons.

In vivo models

In vivo models of PNI have only recently been described but remain limited in scope and technically demanding. In a subcutaneous mouse model of PNI, human PDAC cells that were injected subcutaneously formed tumours some of which, particularly the well differentiated ones showed high prevalence of subcutaneous nerves invasion [75]. More recently, an interesting *in vivo* model has been established by injecting cancer cells in the sciatic nerves of mice [194]. The animals are then followed up using various imaging and behavioural techniques to monitor tumour growth as well as sciatic nerve function. Tissues were also collected for downstream analysis. One caveat of this model is that the injection of cancer cells within the nerve bypasses the initial steps of the nerve invasion process. A recent modification

of the technique involved injecting cancer cells between the perineurium of the nerve and the adjacent muscle [201].

On the other hand, commonly used orthotopic pancreatic cancer mice models using nude mice do not show perineural invasion [202]. This could be, at least in part, due to the limited desmoplastic reaction in these models as the severity of dysmoplasia correlated with PNI in human PDAC tissues [81]. In a modification of such models, fragments of subcutaneously growing human PDAC cell lines in mice were transplanted into the pancreata of nude mice. Tumours were then resected at specific time points and animals were followed up. Although the authors did not report PNI in the resected primary pancreatic tumours, when animals were followed up and, subsequently killed, the recurrent tumours demonstrated invasion of peripancreatic tissue and nerves [203]. Despite the lack of PNI in the primary tumour, the pattern of recurrence following an apparently curative resection did resemble the human disease. One of the commonly used transgenic mouse models of pancreatic cancer, based on expression of oncogenic $KRAS^{G12D}$ has reportedly demonstrated PNI [204]. Intriguingly, we could not identify any PNI literature using this model.

In all these models, the neuronal part contains a mixture of neuronal cells, glia and other supporting cells, which reflects the structure of peripheral nerves including those of the pancreas. While this is more physiological, this makes understanding the roles that each of nerve component plays in the neuro-epithelial interaction difficult. Furthermore, the process of harvesting DRGs or myenteric plexus cells is laborious and requires the use of large numbers of animals.

1.3. Aim of the project

PDAC has a grave prognosis, largely due to the aggressive biological behaviour of this cancer, of which PNI is a cardinal feature. Whilst the involvement of nerves, along with other adverse biological features, appear to reflect the extremely malignant behaviour of this cancer, it also seems to provide further survival advantage to malignant cells and a potential nidus for recurrence following surgery. It is therefore imperative to understand the biology of PNI and the changes that occur to cancer cells and nerves during this process so that more effective therapeutic strategies can be designed.

Despite the increasing scientific interest, our knowledge of the neuro-epithelial interactions in cancer remains both limited and fragmented. We identified two key areas of deficiency that we could contribute to, namely, the lack of global molecular data on both cancer and nerves within PNI in human tissues and the need for a simple and easy to manipulate *in vitro* model of PNI.

Therefore, this project aims to uncover key molecular alterations underlying PNI and neuronal plasticity in PDAC, develop a simple *in vitro* model of PNI, and try to identify potential therapeutic targets for effective treatment strategies that could improve survival and alleviate pain in pancreatic cancer patients. Firstly, we will perform a detailed proteomic analysis of laser microdissected cancer and nerve samples from formalin-fixed, paraffin-embedded (FFPE) PDAC tissues followed by IHC validation of selected differentially expressed proteins. We will compare the expression profiles of matched perineurally invasive (PNI-cancer) and non-PNI cancer as well as invaded and non-invaded nerves. Secondly, we will develop an *in vitro* co-culture model of PNI based on PC12 rat pheochromocytoma cell line as the neuronal element. We will use this model to validate and further investigate the role(s) and regulation of putative candidates from our proteomic analysis.

Chapter Two: Materials and methods

2. Materials and methods

2.1. Tissues and cell lines

Human pancreas tissues (normal, CP and PDAC) were obtained from the Pathology departments of the Royal London hospital (London, UK), KBC Regional hospital (Osijek, Croatia) and the Department of Surgery, Technische Universität München (Munich, Germany). All tissues were obtained after full ethical approval and used in accordance with the Human Tissue Act 2004.

PDAC cell lines (MiaPaca2, BxPC3, Capan1 and Panc1) were obtained from Cancer Research UK Tissue Culture Service and routinely cultured in DMEM supplemented with 10% heat-inactivated fetal calf serum (FCS) and penicillin (100units/ml) /streptomycin (0.1mg/ml) at 37°C in an atmosphere of 5% CO_2. Cells were routinely passaged using Trypsin-EDTA solution when ~80% confluent. All cell lines used were verified by STR profiling.

PC12 cells, a rat pheochromocytoma cell line, were a kind gift from Dr Lesley Robson (Blizard Institute, London), and were routinely grown in poly lysine D coated plastic tissue culture flasks in RPMI media supplemented with 10% heat-inactivated donor horse serum, 5% heat-inactivated FCS and penicillin/streptomycin (concentrations as above) at 37°C in an atmosphere of 5% CO_2. Media was changed every 48 hours and cells were passaged when ~80% confluent.

2.2. Materials

All reagents were purchased from Sigma (Sigma Aldrich, UK) unless otherwise indicated. Acetonitrile (ACN), xylene and ethanol were purchased from Fischer Scientific (Fisher Scientific, UK). Hematoxylin and eosin (H&E) from Merck (Merck, Germany), MassPREP Enolase digest standard from Waters (Waters Corporation, USA), sequencing grade Trypsin from Promega (Promega, USA). Tissue culture media and reagents were from PAA (PAA, Austria) and plasticware and disposables from Corning (Corning Incorporated, NY, USA) unless otherwise specified.

2.3. Methods

2.3.1. Tissue section preparation and laser microdissection

Tissues resected at pancreatectomy were routinely fixed in formalin and embedded in paraffin. 5µm sections were cut and routinely stained with H&E. Details of five PDAC cases that contained significant PNI and were selected for subsequent laser microdissection are summarised below (**Table 2**). In addition, one case of normal pancreas was also used for preliminary optimisation of the proteomics workflow.

Table 2. Clinical details of PDAC cases used for laser microdissection and proteomic analysis. PD: pancreaticoduodenectomy; DP: distal pancreatectomy. TNM: tumour size, lymph node, distant metastases

	Sex	**Surgery/year**	**TNM (stage)**	**Grade**
PDAC1	F	PD/2006	T3N1M0 (IIB)	Moderate
PDAC2	M	PD/2009	T3N1M0 (IIB)	Poor
PDAC3	F	PD/2006	T2N1M0 (IIB)	Moderate
PDAC4	M	DP/2006	T4N1M0 (III)	Moderate
PDAC5	M	PD/2007	T3N1M0 (IIB)	Moderate

A special LMD slides comprising a glass slide covered with a PEN membrane (polyethylene naphthalate) (Zeiss, Germany) were used. PEN slides were baked in a UV box for 30min to enhance the adhesion of tissue sections to the membrane. 10µm sections were cut from PDAC blocks and mounted on the PEN membrane slides. For each case, approximately 60-80 sections were cut, stored at 4°C and used within two weeks. Every fifth section was cut at 5µm and mounted on standard glass slide for routine H&E staining and reviewed to determine areas for laser microdissection and estimate the number of cells that can be obtained. PEN slides with the mounted sections were then baked in an oven at 55°C for 45min. Sections were deparaffinised using xylene and rehydrated in graded ethanol (100%, 90%, 70%) followed by hematoxylin staining, dehydration through graded ethanol (70%, 90%, 100%) followed by five dips in xylene and air-drying for 5min. The staining procedure was completed in 15min.

Laser microdissection was performed using the PALM instrument (Zeiss, Germany). 10x and 20x objectives were used and energy and focus of laser were adjusted for each section to achieve narrowest possible cut. Areas of interest were dissected and catapulted into PCR tubes' caps containing double distilled water within two hours of staining. PNI cancer, non-PNI cancer, invaded nerves and non-invaded nerves were separately dissected from each of the five pancreatic cancer cases and stored at -20°C.

For initial evaluation of the proteomics approach, 10µm sections of normal pancreas FFPE block were also cut and mounted on glass slides. Slides were then prepared similar to PEN slides but without final dehydration step. Approximately 10mm^2 of sections were scrapped off the slides using the tip of 22G needle and placed in 20µl Liquid Tissue (LT) buffer (Expressionpathology, USA) for protein extraction.

2.3.2. Protein extraction for proteomics analysis

Bovine serum albumin (BSA) peptide digest as well as peptides extracted from MiaPaca2 cell line and normal pancreas FFPE tissue were used for the evaluation of HPLC fractionation.

150µg of BSA was suspended in 2% Rapigest (Waters Corporation, USA) in 50mM ammonium bicarbonate. Dithiothreitol (DTT) was added to a final concentration of 10mM and sample incubated at 60°C for 30min. Iodoacetamide (IAA) was then added to 15mM final concentration and sample incubated in the dark at room temperature for 30min. Sequencing grade trypsin was added at a ratio of 1:40 (w/w) and samples incubated at 37°C overnight. Formic acid (FA) was then added to a final concentration of 2% and samples incubated at 37°C for 30min followed by centrifugation at 16,000g for 10min. Supernatant was collected and divided into portions equivalent to 30µg BSA each, dried in SpeedVac and stored at -20°C until analysis.

MiaPaca2 cell pellets were resuspended in lysis buffer (8M urea in 20mM HEPES, pH 8.0). After sonication, samples were centrifuged at 16,000g for 10min at 5°C. Supernatant was transferred to fresh 1.5ml LoBind eppendorf tubes (Eppendorf, Hamburg, Germany) and protein concentration was measured using Bio-Rad assay (Bio-Rad, UK) according to manufacturer's protocol. DTT was added to 10mM final concentration and samples were incubated at room temperature for 15min, followed

by addition of IAA (15mM final concentration) and incubation at room temperature for 15min in the dark. Samples were diluted 1:4 with 20mM HEPES buffer, and sequencing grade trypsin was added at a ratio of 1:40 (w/w) followed by an overnight incubation in a water bath at 37°C . Next day, samples were acidified with trifluoroacetic acid (TFA) to a final concentration of 1%, centrifuged and supernatant transferred to a fresh eppendorf tube. Subsequently, samples were desalted using OASIS C18 cartridges (Waters Corporation, USA). After conditioning of the cartridges, samples were added followed by a wash with 2%ACN/0.1%TFA. Peptides were eluted with 70%ACN/0.1%TFA. The eluted samples were divided into aliquots equivalent to 100µg of protein each, dried in SpeedVac and stored at -20°C until used analysis.

Laser microdissected material from FFPE tissues was pooled according to the cell type for each case resulting in four samples per case (PNI and non-PNI cancer, invaded and non-invaded nerves) per case. Each sample was dried in SpeedVac, resuspended in LT buffer (approximately 20µl/30,000 cells) and protein extraction and digestion proceeded according to manufacturer's instructions. Briefly, samples were boiled for 90min at 95°C. After cooling on ice, sequencing grade trypsin was added (1µg/20µl buffer) for overnight digestion in a water bath at 37°C. Peptide concentration was measured with Micro BCA kit (Thermo Fisher Scientific, USA) according to manufacturer's instructions using 2µl of each sample and BSA standard in duplicates. 100mM DTT was added to each peptide sample to a final concentration of 10mM DTT and samples were boiled at 95°C for 5min before storing at -20°C until further analysis.

2.3.3. Capillary HPLC fractionation

Fractionation was performed on Agilent 1200 HPLC platform (Agilent Technologies, Berkshire, UK) after conversion to a capillary system as described previously [205]. Briefly, the conversion was accomplished using a flow splitting T-piece (Upchurch Scientific, USA) and restriction capillary. Following preliminary optimisation, the final flow from the pump was 380µl/min and flow through column was 5µl/min. Samples were injected manually using a Rheodyne manual injection valve (model 7125, Perkinelmer, USA) fitted with 20µl sample loop. Samples were injected with a 20µl HPLC syringe (Hamilton, USA) using under-fill technique. Samples were loaded on a NanoEase Xbridge BEH300 C18 capillary column (300µm ID x 100mm L, 3.5µm

particle size) (Waters Corporation, USA). Gradient was developed using buffer A: 10mM ammonium formate in water and buffer B: 10mM ammonium formate in 80% ACN, pH of both buffers was adjusted to 10 using 25% ammonium hydroxide. Separation was performed at ambient temperature and chromatograms were monitored at 214nm.

5µg of BSA digest resuspended in buffer A was manually loaded over 20min and peptides were then separated using a 2-42% B gradient over 40min. For MiaPaca2 and normal pancreas FFPE digests, 10µg samples suspended in buffer A were loaded over 20min and fractionated using a 2-50% B gradient over 60min followed by a final 10min isocratic step at 100%B. Flowthrough was collected followed by 12 fractions (one fraction every 5min) and a final fraction of the 100%B step (total 14 fractions). For PNI analysis, 7µg of peptides from each PNI cancer sample from three cases were pooled. A matching sample of non-PNI cancer was similarly pooled from the same cases. Pooled samples were dried in SpeedVac. Each pooled sample was resuspended in buffer A and fractionated in duplicate (10µg each replicate) as above. Fractions were collected every 5min (total 12 fractions). The flowthrough was added to the first fraction and the 100% B step fraction was added to the preceding one. Fractions were dried in SpeedVac and stored at -20°C until LC-MS analysis.

2.3.4. LC-MS analysis and data processing

LC-MS experiments for method validation were performed in the MS facility in Centre for Cell Signalling (Barts Cancer Institute) on a Nanoacuity LC system (Waters Corporation, USA) coupled to LTQ Orbitrap XL platform (Thermofisher, USA). Unfractionated (1µg) or dried fractions of peptide digests from MiaPaca2 cells and normal pancreas FFPE samples were suspended in 10µl 0.1% TFA containing 20 fmole/µl enolase standard digest. Buffer A was 0.1% FA in water, and buffer B was 0.1% FA in ACN. 4µl aliquots of the samples were first loaded on a Symmetry C18 trap column (180µm ID x 20mm L, 5µm particle size) (Waters Corporation, USA). Peptides were then eluted from Nanoacuity BEH130 C18 column (100µm ID x 100mm L, 1.7µm particle size) using 0-35% B gradient over 100min at 400nl/min flow rate. Total run time was 2 hours/sample. Data was acquired over mass range of 350-1800 in a data-dependent manner with 90s dynamic exclusion. Each full MS scan was followed by MS/MS of the five most abundant ions.

Peaks were searched using Mascot v2.2.2 (Matrixscience, USA) against the human SwissProt database (20100303, 20,326 entries) with the following critieria: fully tryptic peptides with maximum two missed cleavages allowed, carbamidomethylation of cysteine and oxidation of methionine as fixed and variable modifications respectively and a tolerance of 7ppm for parent ions and 0.6Da for fragments. Mascot data files were then analysed in Scaffold v 3-00-08 (Proteome Software, USA) to generate nonredundant protein identifications with ≥2 peptides/protein and minimum 90% and 95% confidence at peptide and protein level, respectively.

PNI proteomic profiling experiments were performed by Richard Jones (MSBioworks, USA) on a Nanoacuity LC system coupled to LTQ Orbitrap Velos platform (Thermofisher, USA). Unfractionated samples (1µg) or dried fractions were suspended in 0.1%FA. Buffer A was 0.1% FA in water, and buffer B was 0.1% FA in acetonitrile. 30µl samples were first loaded on an IntegraFrit trap column (75um x 30mm) packed with Jupiter Proteo C12 material with 5µm particle size (Thermofisher Scientfic, USA). Peptides were then eluted from a 75µm x 250mm, 4µm particle Jupiter Proteo C12 analytical column (Phenomex, CA, USA) at 350nl/min using 5-22%B over 70min then to 35%B over 20min and to 85%B over 15min. Total run time was 2 hours/sample. Data was acquired over mass range 300-1600 in a data-dependent manner. Each full MS scan was followed by MS/MS of the 15 most abundant ions, dynamic exclusion and repeat settings ensured each ion was selected only once and excluded for 30s thereafter.

The MS data were analyzed using MaxQuant version 1.4.0.1 [206]. The proteins were identified by searching MS and MS/MS data of peptides against the Swissprot human canonical database (20,556 entries) appended with common contaminants using the Andromeda search engine. Oxidation of methionine and protein N-terminal acetylation were chosen as variable modifications. The minimum peptide length was specified to be seven amino acids. The initial maximal mass tolerance in MS mode was set to 7 ppm, whereas fragment mass tolerance was set to 0.5 Da for fragmentation data. The maximum false protein and peptide discovery rate (FDR) was specified as 0.01 and determined using a decoy database. Proteins were identified with ≥2 peptides/protein.

2.3.5. Immunohistochemistry (IHC)

IHC validation was performed on 4µm sections cut from FFPE tissue blocks. For OLFM4, staining was performed in the Barts Cancer Institute core Pathology service using the automated Ventana Discovery System (Illkirch, France). Rabbit anti-OLFM4 primary antibody (Abcam) was used at 1/400 dilution. Staining intensity was semi-quantitatively assessed at 200x magnification as absent (0), background (1), weak (2), moderate (3) or strong (4) and the extent (percentage of cells displaying the maximum intensity) was assessed as 0-5% (0), 6-25% (1), 26-50% (2), 51-75% (3) or >75% (4). The final IHC score was calculated by adding the intensity and extent of immunoreactivity. Of note, all PNI lesions were assessed in each section. For non-PNI cancer, at least 10 HPF (high power fields, at 200x) were assessed for each section.

VGF IHC staining was performed manually in the following way: 4µm FFPE tissue sections were deparaffinized in xylene and rehydrated in graded ethanol as described before, followed by endogenous peroxidase block in 1.5%H_2O_2 in methanol. Following heat-induced antigen retrieval in citrate buffer (pH 6.0) and avidin and biotin block (Vector Labs, CA, USA), staining proceeded using Vectastain ABC kit (Vector Labs) according to the manufacturer's instructions. Protein blocking was followed by incubation with rabbit anti-VGF primary antibody (Abcam) at 1/400 dilution for 1 hour at room temperature. Sections were then washed three times with TBS-T 0.05% (Tris buffered saline, 0.05% Tween 20) and incubated with the biotinylated secondary antibody for 30min. Following another wash step, the sections were incubated with the ABC reagent for 30min, washed twice and 3-3' diaminobenzidine (DAB) kit (Vector Labs) was used for colour development. Slides were then counterstained with hematoxylin, dehydrated in graded ethanol and mounted. Staining intensity was semi-quantitatively assessed at 200x magnification as absent (0), weak (1), moderate (2) or strong (3). Assessment of immunoreactivity was done in a blinded manner to clinical details.

2.3.6. Grading of pain

For correlation of VGF protein expression and pain, tissue sections from clinically annotated CP and PDAC cases were provided by our collaborators at the Department of Surgery, Technische Universität München (Munich, Germany). Pain

data was collected prospectively from CP and PDAC patients as described previously [81]. Briefly, pain intensity was graded as no pain (0), mild pain (1), moderate pain (2) or severe pain (3). The frequency of pain was graded as daily (3), weekly (2) or monthly (1). The final pain severity score for each patient was calculated by multiplying pain intensity and frequency. Patients were then divided into three groups according to their pain severity score: No pain (0), mild pain (1-3) and moderate to severe pain (4-9).

2.3.7. PC12 co-culture experiments

Transwell (TW) co-culture:

$1.5x10^5$ PC12 cells were seeded in complete RPMI media in 6-well plates pre-coated with poly D lysine (PDL). $1.5x10^5$ PDAC cells lines or PC12 cells were also seeded in their respective media in 6-well plate inserts (1µm pore size, BD Biosciences, CA, USA) in separate plates. Next day, media was removed and cells in inserts and wells were washed three times with serum-free RPMI. Subsequently, inserts with PC12 or PDAC cells were combined with wells containing PC12 cells and serum-free RPMI was then added to wells (2ml) and inserts (1ml). 24 hours later, inserts were removed and phase-contrast photographs of PC12 cells in the wells were taken using an inverted Olympus CKX41 microscope (Olympus) at 200x magnification. PC12 cells were then harvested for RNA, protein extraction and flow-cytometry.

Contact co-culture:

$1.2x10^6$ PC12 cells were seeded in their complete RPMI media in T75 flasks pre-coated with PDL. Next day, media was removed and fresh media containing 2.5µM CellTracker Green CMFDA (Invitrogen) was added and cells incubated at 37˚ for 30min. Cells were then washed twice with serum-free RPMI media and $1.2x10^6$ PDAC or PC12 cells in complete RPMI media were added to the flasks. The added cells were then allowed to attach for 2 hours following which media was removed and the co-cultures were washed three times with serum-free RPMI. 24ml of fresh serum-free RPMI was then added. Co-culture was continued for further 22 hours, after which cells were harvested, and CMFDA positive cells (PC12 cells) were isolated for protein and RNA extraction using Fluorescence Activated Cell Sorting

(FACS). Sorted cells were always re-checked for purity using the same FACS settings. In addition, small aliquots of sorted cells were seeded on coverslips for subsequent immunocytochemical validation of their purity.

As noted, for both types of co-cultures, seeding density (~15,000 cells/1cm^2), ratio of PDAC to PC12 cells (1:1) and ratio of media to cells (1ml/1.0x10^5) were kept constant and both co-cultures were performed and analysed in parallel.

2.3.8. Immunocytochemistry (ICC)

ICC validation of the purity of the FACS sorted PC12 was performed using antibody against the epithelial-specific protein cytokeratin 19 (CK19). PC12 cells isolated from the contact co-culture were cultured in 12-well plates on PLD coated sterile coverslips in complete RPMI media. Separately, PDAC cells and PC12 cells alone were also similarly cultured and used as positive and negative controls for ICC staining, respectively. 24 hours later, media was removed and cells were washed with cold PBS and subsequently fixed in 4% paraformaldehyde (PFA) for 10min followed by three washes with cold PBS. All subsequent steps were performed at room temperature. Cells were permeabilised with 0.2% saponin in PBS followed by three washes with PBS and protein blocking using 6% BSA in PBS. Cells were then incubated with mouse ani-CK19 primary antibody (Dako, Cambridgeshire, UK) at 1/50 dilution in 6% BSA for 45min. Following 3 washes with PBS, the Alexa Fluor 568 cunjugated secondary antibody (Invitrogen, 1/1000 dilution) was added for 30min prior to further three washes with PBS. Coverslips were then mounted on glass slides using ProLong Gold mounting media (containing DAPI) (Invitrogen) and allowed to dry overnight in the dark. Imaging was performed using LSM 710 Zeiss confocal laser scanning system. For each post sort coverslip, a tiled 3x2 image was acquired using 40x objective and the number of cytokeratin positive cells were counted relative to the total number of cells.

2.3.9. Preparation of conditioned media

PDAC and PC12 cells ($4x10^6$) were seeded in T175 flasks in their respective complete media. Next day, cells were washed three times with serum-free RPMI, and fresh serum-free media was added for conditioning. 24 hours later, media was collected, centrifuged at 4,000g for 5min to remove cells and debris, filtered using 0.22µm filters (Millipore, Cork, Ireland) and immediately used to treat PC12 cells.

2.3.10. K252a treatment

K252a is a potent and selective inhibitor of Trk tyrosine protein kinases including A, B and C and has been shown to block the effects of NGF on PC12 cells [207]. K252a (Sigma Aldrich, UK) was dissolved in dimethyl sulfoxide (DMSO) to prepare a 100µM stock solution. Working solutions were prepared by diluting stock in serum-free RPMI just before use. PC12 cells were seeded in pre-coated 6-well plates as described previously. Next day, media was removed and cells washed three times with serum-free RPMI. 1ml serum-free media containing 10, 30 or 100nM K252a or DMSO was then added and cells incubated at 37˚C for 1 hour. Media was then removed and 2ml of serum-free media containing K252a or DMSO (at the same concentration as above) with recombinant human βNGF (R&D systems, Abingdon, UK) at 50ng/ml final concentration was added. In other experiments, 2ml of conditioned media containing K252a or DMSO was added. 24 hours later, photographs for neurite growth quantification were taken, as described previously, and cells were harvested for RNA, protein extraction and flow-cytometry.

2.3.11. SiRNA knock-down of VGF

$1.5x10^5$ PC12 cells were seeded in their complete RPMI media in 6-well plates pre-coated with PDL. Next day, media was removed and 1.5ml of fresh media was added. SiRNA knock-down was performed using Lipofectamine RNAiMAX (Invitrogen, Paisley, UK) according to the manufacturer's instructions. Following preliminary optimization, siRNA was used at 1nM final concentration. For each well, siRNA targeting VGF (On target plus pool) or non-targeting siRNA (Dharmacon, Fisher Scientific, UK) was mixed with 5µl of Lipofectamine RNAiMAX in 500µl Optimem media (Life Technologies, Paisley, UK). The mix was incubated at room

temperature for 15min before adding to the wells. Media was removed six hours later, cells were washed three times with serum-free RPMI media and PDAC or PC12 cells conditioned media was added for 24 hours.

2.3.12. Quantitation of PC12 neurite growth

Randomly selected HPF (three per well, at 200x magnification) of PC12 TW co-cultures or conditioned media treatment were analyzed for neurite growth in Image J (National Health Institute, http://rsb.info.nih.gov/ij/). The degree of neurite growth was estimated by counting the number of cells bearing neurites longer than the maximum diameter of the cell body [208]. At least 200 cells were counted in each well and results were expressed as percentage of total number of cells. Each condition was performed in duplicate in three independent experiments unless stated otherwise.

2.3.13. Annexin V/DAPI flow-cytometry assay

Both floating and attached PC12 cells from co-cultures and conditioned media treatment were harvested, centrifuged and washed once with ice cold PBS. Cells were pelleted and resuspended in 100µl Annexin binding buffer (10 mM HEPES, 140 mM NaCl, 2.5 mM $CaCl_2$, pH 7.4) containing 5µl of Annexin V Alexa Fluro 647 (Invitrogen, Paisley, UK). Following 15min incubation at room temperature in the dark, 400µl of the binding buffer containing 1µg/ml 4',6-diamidino-2-phenylindole (DAPI) was added to each sample. Cell suspensions were kept on ice and flow-cytometry was immediately performed using BD Fortessa cell analyzer (BD Biosciences, CA, USA). After doublets exclusion, initial gating was performed according to unstained samples. PC12 cells growing in their complete media or serum-free RPMI were included as negative and positive controls for apoptosis, respectively and used for fine-tuning of the gating. Cells that were negative for both Annexin V and DAPI were quantified as the surviving fraction and results were expressed relative to PC12 survival in complete growth media. Duplicate wells were analyzed within each experiment and experiments were repeated three times unless otherwise specified.

2.3.14. RNA extraction and cDNA synthesis

Total RNA was extracted using RNAqueous kit (Ambion, CA, USA) according to manufacturer's instructions. Briefly, tissue culture media was removed from the tissue culture wells and following a wash with ice cold PBS, 200µl lysis buffer was used to lyse cells. Lysate was collected and an equal volume of 64% ethanol was added and samples loaded onto the spin columns. Three washes and centrifugation steps were performed before eluting RNA in 40µl of elution buffer.

Quantitative and qualitative assessment of RNA was performed using NanoDrop ND-1000 spectrophotometer (NanoDrop Technologies, Rockland, USA) and gel electrophoresis using 1% agarose gel.

1µg of total RNA was used for reverse transcription using Quantitech reverse transcription kit (Qiagen, West Sussex, UK) according to the manufacturer's instructions. Briefly, RNase-free water was added to RNA to a total volume of 12µl. 2µl genomic DNA wipeout buffer was then added and samples were incubated at 42˚C for 9min. Following brief cooling on ice, 6µl mastermix solution containing 4µl RT buffer, 1µl Quantitech Reverse Transcriptase and 1µl of RT primers mix (both oligo-dT and random primers) was added to each sample and the RT reaction proceeded for 15min at 42˚C and terminated by incubation at 95˚C for 3min.

2.3.15. Quantitative real time PCR (qRT-PCR)

qRT-PCR reaction

qRT-PCR was performed using the SYBR green method. All primers were obtained from PrimerDesign (Southampton, UK). The VGF primers' sequences were (forward 5'-TGAGACTTTGACACCCTTATCC and reverse 5'-GGAACCGCCCAGGAATGA). Primerdesign, however, does not provide the sequences for their pre-validated housekeeping genes. Standard curves using serially diluted cDNA from PC12 cells was used to validate the specificity and linear amplification of each pair of primers. All primers had a standard curve with R^2 ≥0.99 and amplification efficiency of 90-110%.

Several genes were tested for their suitability as housekeeping genes. For this analysis, qRT-PCR reactions were run for five genes (GAPDH, B2M, RPL13, CANX,

UBC) using PC12 samples from seven experimental conditions (co-culture and NGF treatment). Results were analyzed using the geNorm algorithm [209] within qBase software (Biogazelle, Belgium) to determine genes with the most stable expression under our experimental conditions. B2M and RPL13 were the most stable and the geometric mean of their expression was used for normalization (data not shown).

qRT-PCR reactions were set up in 96-well optical reaction plates (Thermofisher Scientfic, USA). cDNA was diluted 10 times with RNase-free water, in each well, 5µl cDNA was added to 10µl SYBR green reagent (Qiagen, west Sussex, UK) and 2-3µl of specific primer pair for each gene (for an optimized final concentration of 600-900nM). Water was added to a total volume of 20µl. For each primer pair, wells without cDNA (water only) were included as a control for contamination. Following brief centrifugation (1000g x 30sec), the PCR reaction was performed on an ABI7500 cycler (Applied Biosystems, CA, USA). Run conditions were as follow: 50˚C for 2min, 95˚C for 15min followed by 40 cycles of 95˚C for 15sec, 60˚C for30 sec and 72˚C for 1min. A dissociation step was always performed to check the specificity of the amplification and the presence of contaminants or primer dimers. Duplicate wells were used for each sample and three independent experiments were performed.

Calculation of CT values and quantitative analysis:

Data was analyzed using AB17500 software (Applied Biosystems). Threshold was set in the exponential phase of the amplification. The cycle number at the point where each of the amplification curves crossed the threshold is the Ct value which was subsequently used for further analysis.

Data was analysed with the comparative quantification algorithm using the equation:

$$\text{Fold difference} = 2^{-\Delta\Delta Ct}$$

For all primers the Ct value was calculated by subtracting the geometric mean of the Ct values of the reference genes from the Ct value of the gene of interest in both the control and test samples. The ΔΔCt value was then calculated by subtracting the ΔCt value of the control samples from the ΔCt value of the test samples. Results are presented as fold change relative to control.

2.3.16. Protein extraction, measurement and gel electrophoresis

Cells lysates were prepared in NP40 lysis buffer (50mM Tris pH 7.4, 150mM NaCl, 1% NP40 and complete protease inhibitor tablets). Following 15min incubation on ice, samples were centrifuged at 16,000g for 15min and supernatant collected for analysis. Protein concentration was determined with BioRad assay (BioRad, Hertfordshire, UK) at 595nm using BSA standard curve. 15-30µg of protein was mixed with 5x Laemmli buffer (0.225M Tris pH6.8, 10% SDS, 50% glycerol, 0.25M DTT and 0.05% Bromophenol blue) and heated to 70˚C for 10min. Samples were then loaded onto 4-12% Bis-Tris NuPage gels (Invitrogen, Paisley, UK). SDS electrophoresis was performed at 130V for 90min. Rainbow marker (Amersham Biosciences, Sweden) was used for the estimation of molecular weight. Proteins were transferred onto PVFD Immobilin-P membranes (Millipore, Watford, UK) using a Trans Blot semi-dry transfer cell (BioRad, Hertfordshire, UK) at 20V for 50min.

2.3.17. Western blot

Following transfer, membranes were blocked in 5% milk in 0.05% TBS-T for 30min and then incubated with the primary antibody (**Table 3**) in blocking buffer at 4˚C overnight. Unbound antibody was then washed with TBS-T before incubating the membranes with the appropriate HRP conjugated secondary antibody (Santa Cruz Biotechnology) at 1/2,000 dilution in blocking buffer for 30min at room temperature. Membranes were then washed with TBS-T and signal from bound antibodies was visualised using ECL reagents (GE Healthcare, Buckinghamshire, UK) onto Hyperfilms (Amersham Biosciences, Sweden). The intensities of the obtained bands were quantified in Image J, and the intensity of each target protein band was divided by the intensity of the GAPDH in the same sample. Densitometry results of three independent experiments were then expressed as a fold change relative to the control samples.

Table 3. Details of the primary antibodies used for Western blot in this project.

Antibody	Source	Host species	Dilution
Anti-VGF	Santa Cruz	Goat	1/800
Anti-GAPDH	Santa Cruz	Mouse	1/20,000
Anti-GAP43	Abcam	Rabbit	1/20,000
Anti-Nestin	Abcam	Mouse	1/200
Anti-Caspase 3	Cell Signalling	Rabbit	1/400

2.3.18. Statistical analysis

Statistical analysis for differential expression of proteins was performed in Microsoft Excel. Student's t-test was performed using peak intensity values for label-free relative quantitative analysis of the 1D LC-MS data. For the 2D LC-MS dataset, spectral counting was used for relative label-free quantitative analysis. Spectral counts refer to the number of times spectra assigned to a particular protein have been observed [210]. This has been shown to correlate well with the relative abundance of proteins between samples [211, 212].

Because we had a limited number of replicates, we used the G test of likelihood ratio to assess differential expression [212, 213] according to the following equation:

$$G = 2[A_{sc} \ln(A_{sc}/E_{sc}) + B_{sc} \ln(B_{sc}/E_{sc})]$$

Where for each protein that has a spectral count A1 and B1 in samples A and B respectively, and the total spectral counts for all proteins in each sample is tA and tB, A_{sc} is A1+1, B_{sc} is (B1+1)(tA/tB) and E_{sc} is $(A_{sc}+B_{sc})/2$. A_{sc} and B_{sc} are spectral counts normalised to the total number of spectra in the respective sample and to which (1) was added to avoid (0) spectral counts. Subsequently, p values were calculated from G values based on Chi square probability using one degree of freedom. Proteins with $p<0.05$ (equates to G value of 3.81 at one degree of freedom) were deemed significantly differentially expressed.

For all other statistical analysis, GraphPad Prism 5.03 software was used. For continuous data, student's t-test was used to compare means of data and ANOVA with post-hoc correction for multiple comparisons was used when three or more samples were compared. For semiquantitative IHC data, Mann Whitney test was used to compare the means whereas Kruskal Wallis test with post-hoc correction for multiple comparisons was used when comparing more than two groups. Two-tailed p values were always calculated and results were plotted as mean ± standard error of mean. The significance level was set at $p<0.05$.

Chapter Three: Results

3. Results

3.1. Laser microdissection and protein extraction

Five cases of PDAC that had significant PNI were used for laser microdissection. On average, 60-80 sections were used from each case to dissect PNI cancer, non-PNI cancer, invaded and non-invaded nerves (**Figure 8**).

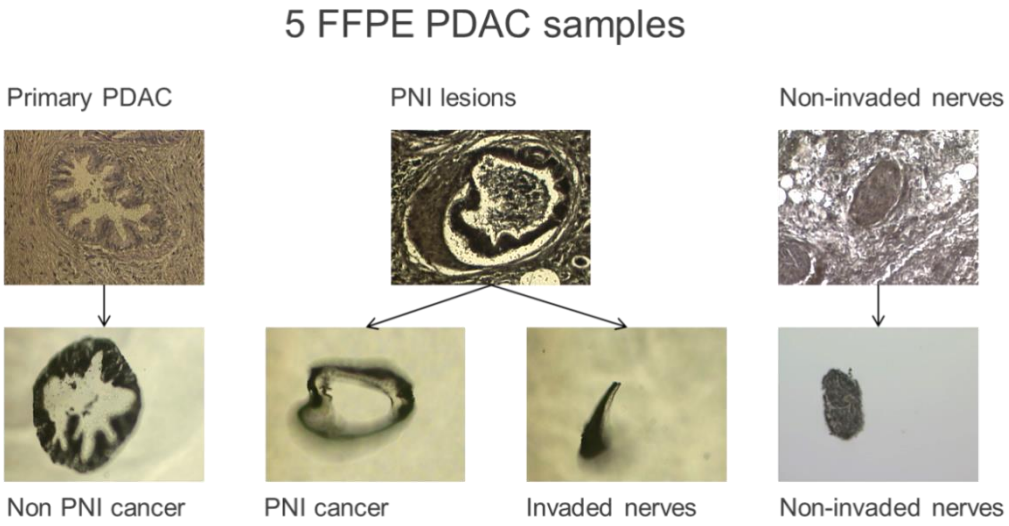

Figure 8. Samples collected by laser microdissection. Matched PNI cancer cells, non-PNI cancer cells, invaded nerves and non-invaded nerves were laser microdissected from each of five PDAC FFPE tissues. Top panel: before dissection, lower panel: verification of dissected material.

Protein extraction using Liquid Tissue buffer yielded satisfactory amounts of peptide digests for downstream analysis as shown in **Table 4** below. An average of 14.7µg, 15.6µg, 10.5µg and 12.8µg was extracted from 10mm^2 area of non-PNI cancer, PNI cancer, invaded nerves and non-invaded nerves, respectively. Approximately 25,000-55,000 cells were dissected from each of PNI or non-PNI cancer. Due to the nature of nerve structure, we did not estimate cell numbers and relied on dissected area.

Table 4. Area dissected and amount of peptide digest extracted from each sample.

	Amount of peptide digest extracted in µg (area dissected in mm^2)			
	Non-PNI cancer	**PNI Cancer**	**Invaded nerves**	**Non-invaded nerves**
PDAC1	26.5 (17.0)	26.5 (16.5)	12.2 (13.8)	11.3 (9.7)
PDAC2	10.6 (10.8)	14.0 (13.3)	11.1 (10.3)	13.6 (9.0)
PDAC3	17.3 (9.1)	14.3 (8.6)	10.8 (11.4)	11.7 (10.3)
PDAC4	12.9 (10.2)	13.9 (8.1)	9.8 (9.3)	10.9 (9.5)
PDAC5	9.9 (6.0)	9.9 (5.6)	8.1 (6.4)	9.1 (6.2)

3.2. HPLC conversion

3.2.1. HPLC conversion set up

The fractionation of the limited amounts of peptides typically extracted from laser microdissected lesions required the use of capillary columns and therefore low flow rates. Because the Agilent 1200 LC platform available to us is a standard analytical platform, we had to convert this to a capillary HPLC system using previously described method [205]. To achieve this, we used a restriction capillary and T-piece to split the flow from the pump. The conversion was completed by the exclusion of the autosampler, addition of a manual injection valve after the T-piece and replacing the standard UV cell within the detector with a nanoflow (80nl) cell. For tubing, small internal diameter (ID) capillaries with minimal length were used to minimise dead volume (**Figure 8**). The automated fraction collector was also excluded and fractions were collected manually.

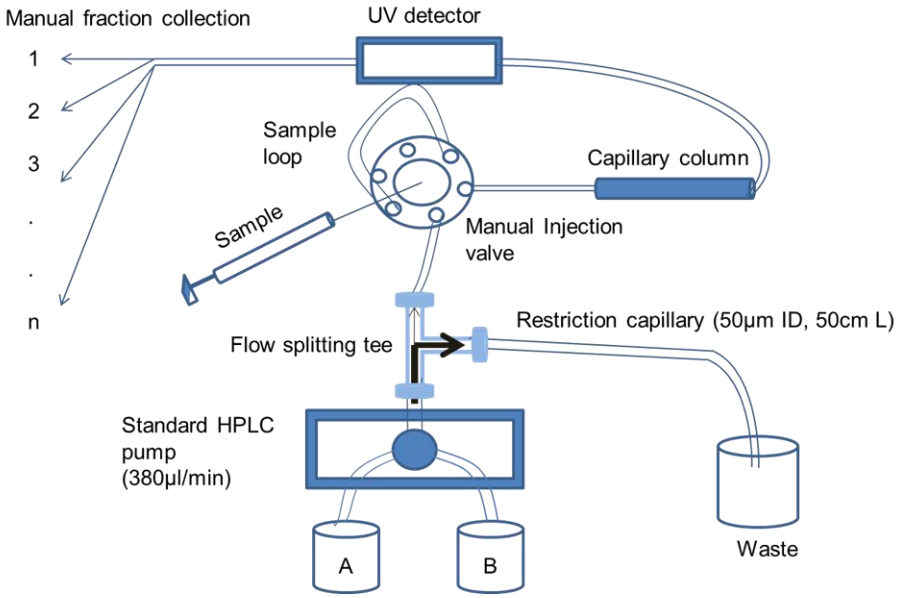

Figure 9. Schematic representation of the conversion of standard HPLC to capillary HPLC system. By using a flow splitting tee and a restriction capillary, most of the buffers (A,B) delivered by the pump were diverted to waste.

The minimum flow rate of our standard HPLC pump was 200µl/min, significantly larger than the flow rate appropriate for the capillary column we used (3-10µl/min). Preliminary tests were done to determine the appropriate length and diameter of the restriction capillary and the pump flow rate that will deliver the desired flow rate. Using the configuration in **Figure 9** we were able to achieve, throughout the gradient phase, a stable 5 µl/min flow rate through the column at 380 µl/min pre-split flow rate (**Figure 10**).

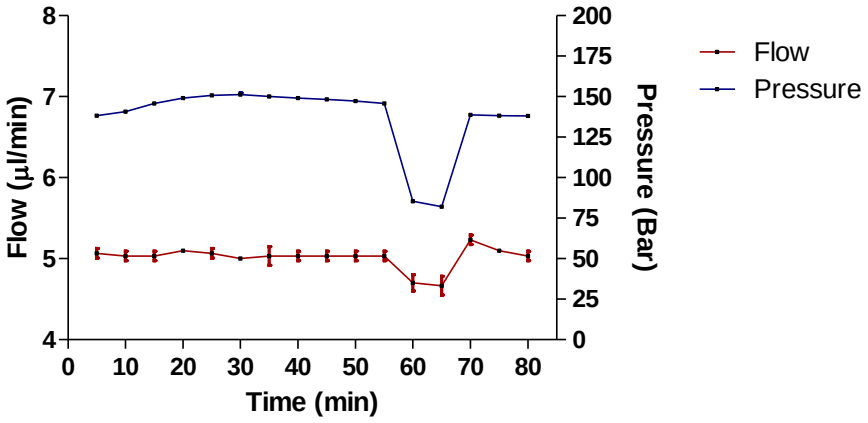

Figure 10. Post-split flow rate through the capillary column and the HPLC system pressure during three blank runs. Using buffers A & B, the run gradient was 2% B for 5min, 2-50% B over 50min, 100% B for 10min and then 2% B for 10min. Flow rate was measured by collecting flowthrough every 5min. Stable flow of 5µl/min is observed throughout the gradient (2-50%B).

To estimate the dead volume and determine the start time for the collection of the first fraction, we calculated the chromatographic gradient delay of the system. This is the time it takes the buffer to move between the pump and the detector and was calculated by running a 0-100%B over 20min followed by a hold at 100%B for another 20min. (A: 10mM ammonium formate, B: 0.5% acetone in 10mM ammonium formate) (**Figure 11**). The gradient delay (6.2min) was equivalent to 31µl dead volume within the system. In addition, the linear increase in absorbance indicated the absence of dead volume mixing.

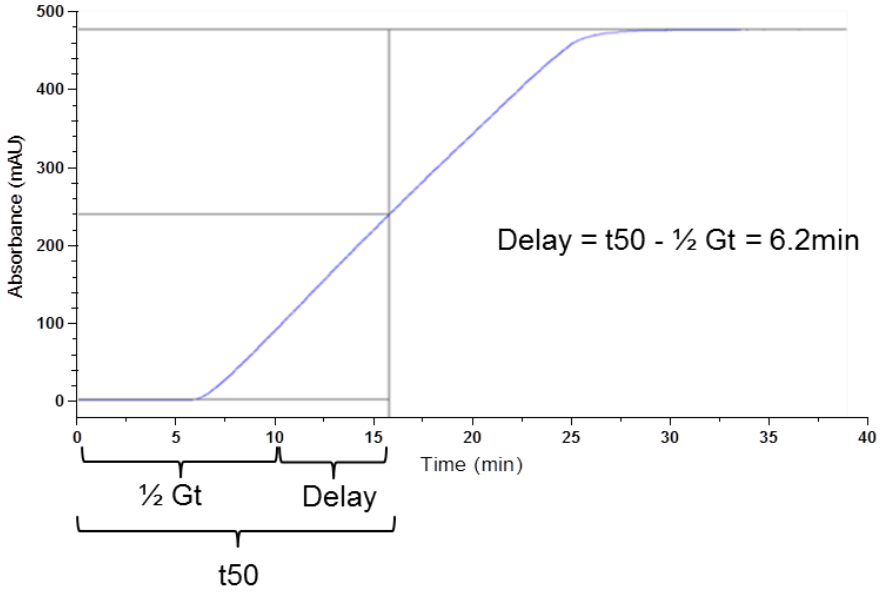

Figure 11. Chromatographic delay of the capillary HPLC system using 0.5% acetone as a UV marker. Absorbance was measured at 254nm. Gt: gradient time (20min). t50: the time corresponding to 50% of the maximum absorbance.

Therefore, the converted system demonstrated stable flow rates and minimal dead volume making it a suitable capillary system for further evaluation as the first dimension in the two dimensional LC-MS (2D LC-MS).

3.2.2. Validation of reproducibility of high pH RP HPLC fractionation

To assess the reproducibility of high pH fractionation using the converted HPLC system, we first used BSA as a simple peptide mixture. Intra-day variability was quantified using five consecutive replicate analyses of BSA digest on the same day (**Figure 12A**) and inter-day variability was assessed using three consecutive replicate analyses of BSA digest on each of three different days (**Figure 12B**).

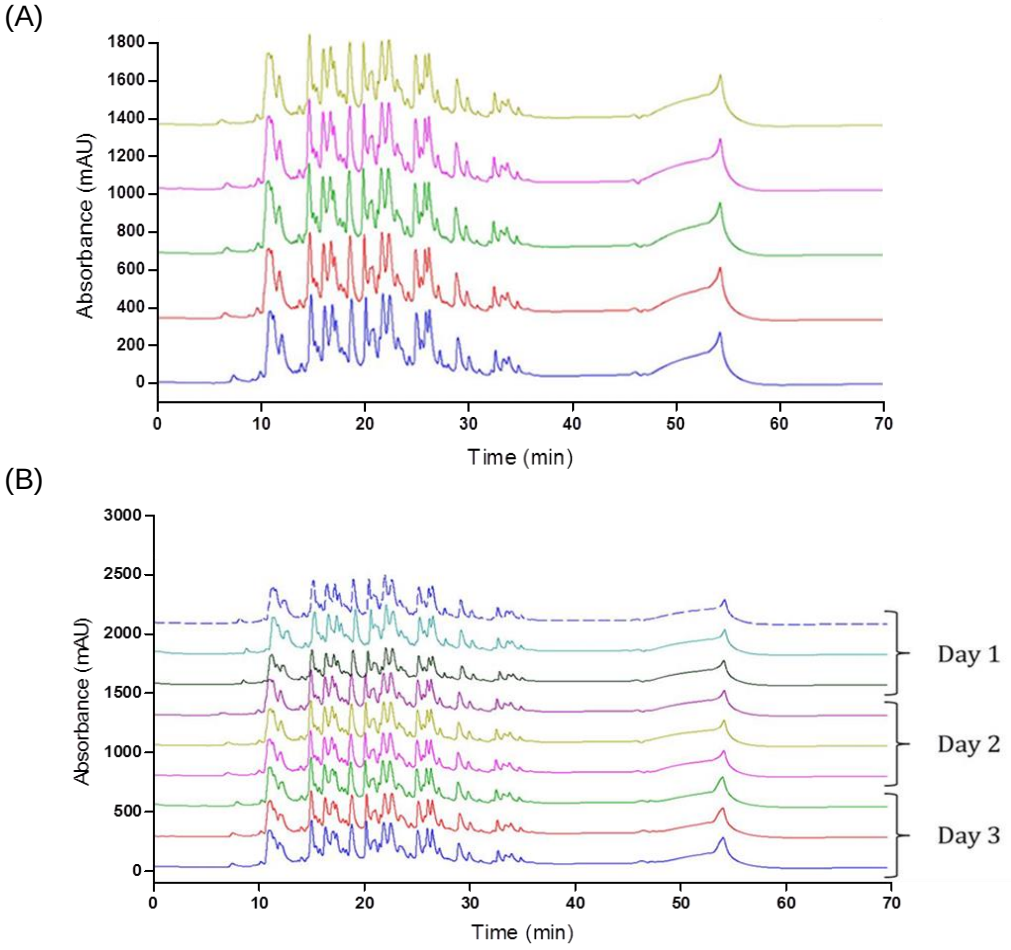

Figure 12. Chromatographic reproducibility of high pH fractionation of BSA tryptic digest. Intra-day variability using five consecutive runs (**A**) and inter-day variability using three consecutive runs on each of three different days (**B**).

Retention times, peak intensities and peak areas were quantified for selected peaks (**Figure 13A**). The chromatograms as well as CV values of retention times, intensity and peak area for the selected peaks demonstrated good reproducibility (**Figure 13B** and **C**).

(A)

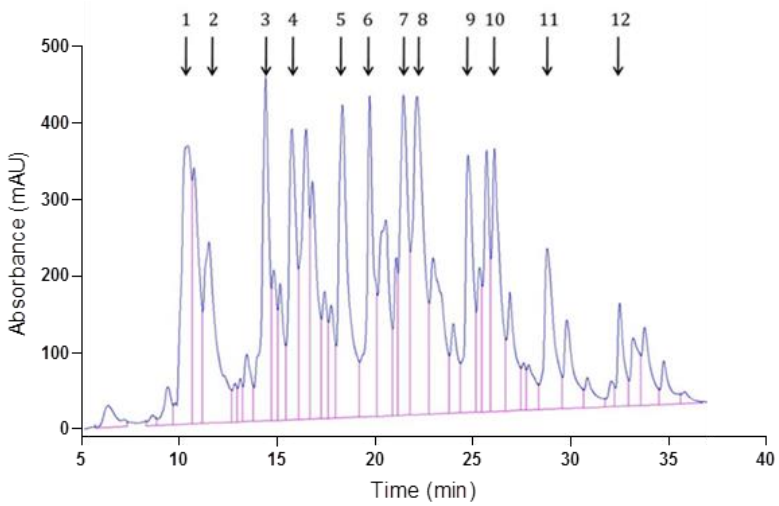

(B)

Peak	Retention time (min)			Intensity (mAU)			Peak area (mAU*s)		
	Mean	SD	CV (%)	Mean	SD	CV (%)	Mean	SD	CV (%)
1	11.14	0.08	0.74	360.14	6.61	1.83	11763.77	538.27	4.58
2	12.18	0.11	0.87	238.94	4.25	1.78	10256.12	252.84	2.47
3	15.03	0.08	0.53	444.38	9.34	2.10	11588.15	257.94	2.23
4	16.35	0.07	0.44	377.46	4.25	1.12	9954.61	141.24	1.42
5	18.89	0.09	0.45	409.37	1.91	0.47	13583.09	176.17	1.30
6	20.24	0.10	0.47	414.74	3.91	0.94	9903.33	315.23	3.18
7	21.93	0.06	0.26	421.95	10.19	2.41	11335.09	227.52	2.01
8	22.60	0.05	0.23	419.47	4.70	1.12	15844.95	152.18	0.96
9	25.15	0.05	0.21	334.98	2.41	0.72	9032.02	127.77	1.41
10	26.43	0.03	0.10	344.44	4.45	1.29	9985.60	434.42	4.35
11	29.14	0.08	0.26	208.56	2.76	1.32	7231.50	72.56	1.00
12	32.75	0.07	0.22	134.75	1.58	1.18	2951.62	25.19	0.85

(C)

Peak	Retention time (min)			Intensity (mAU)			Peak area (mAU*s)		
	Mean	SD	CV (%)	Mean	SD	CV (%)	Mean	SD	CV (%)
1	11.18	0.15	1.32	360.25	17.52	4.86	12381.08	864.73	6.98
2	12.25	0.21	1.68	229.17	15.12	6.60	10719.14	673.07	6.28
3	15.09	0.13	0.89	439.47	38.78	8.82	11338.30	1132.68	9.99
4	16.40	0.12	0.76	380.35	17.16	4.51	11115.65	992.45	8.93
5	18.93	0.14	0.73	411.70	8.58	2.08	13672.07	767.31	5.61
6	20.33	0.20	0.97	417.46	20.54	4.92	9059.77	1500.43	16.56
7	21.98	0.11	0.49	431.27	12.67	2.94	11461.15	580.98	5.07
8	22.65	0.10	0.44	415.88	17.71	4.26	16021.76	651.42	4.07
9	25.19	0.08	0.33	337.61	12.97	3.84	9348.41	354.06	3.79
10	26.50	0.08	0.30	343.13	14.47	4.22	10158.62	642.18	6.32
11	29.19	0.12	0.42	207.73	9.22	4.44	7219.54	343.26	4.75
12	32.81	0.10	0.31	132.79	8.49	6.39	2939.78	154.08	5.24

Figure 13. Quantitative analysis of selected peaks from BSA digest separation chromatogram (**A**) showing CV values of retention time, peak intensity and peak area of the selected peaks for evaluation of both intra-day (**B**) and inter-day (**C**) variability.

Next, we used MiaPaca2 peptide digest, a complex cellular proteome, to evaluate the reproducibility and the depth of proteomic coverage that can be achieved through high pH RP fractionation using the converted HPLC system. 10µg of MiaPaca2 peptide digest was fractionated, in duplicate, into 14 fractions that were subsequently analysed using LC-MS. Additionally, 1µg of unfractionated digest was also subjected to LC-MS analysis in duplicate. Visual inspection of the chromatograms of the two fractionated samples confirmed excellent reproducibility (**Figure 14**).

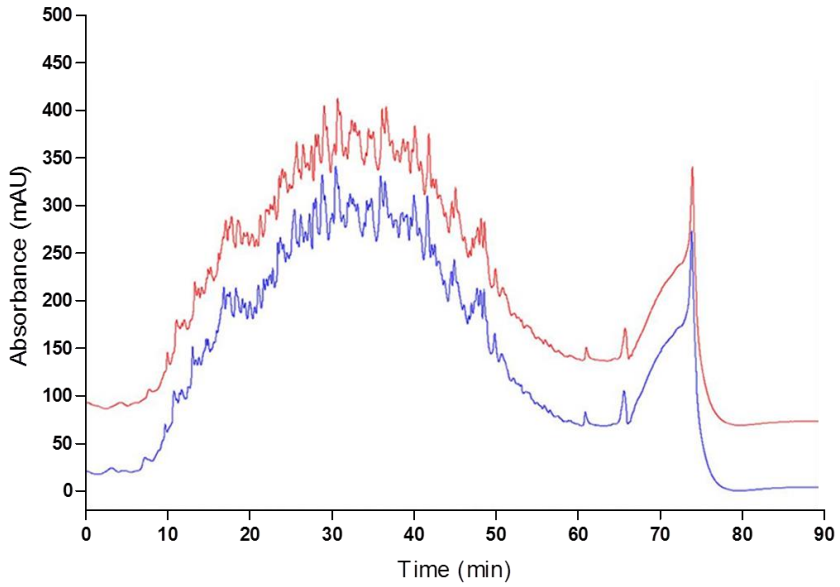

Figure 14. Chromatograms of duplicate runs of MiaPaca2 peptide digest fractionation using high pH RP HPLC showing excellent reproducibility. In each run, 10µg of peptide digest was fractionated over 70min. 14 fractions were manually collected.

The number of proteins identified from the two fractionated samples was 1602 compared to 340 from the two unfractionated samples representing approximately five-fold increase in the number of identified proteins (**Figure 15A**). All proteins that were identified in the unfractionated samples were also identified in the fractionated samples. The reproducibility of protein IDs between the two fractionated samples was 76%, which was only 7% lower than the technical reproducibility of the LC-MS itself for the technical replicates of unfractionated samples (83%). Furthermore, the abundance of proteins as determined by spectral counts was similar between the two fractionated replicates indicating good quantitative agreement (**Figure 15B**).

(A)

	Protein (peptide) identifications				
	1st replicate	2nd replicate	Common	Total	Reproducibility (Protein IDs)
Unfractionated MiaPaca2	304(1873)	318(1925)	282(1602)	340(2196)	83%
Fractionated MiaPaca2	1401(9965)	1423(9920)	1222(7330)	1602(12555)	76%

(B)

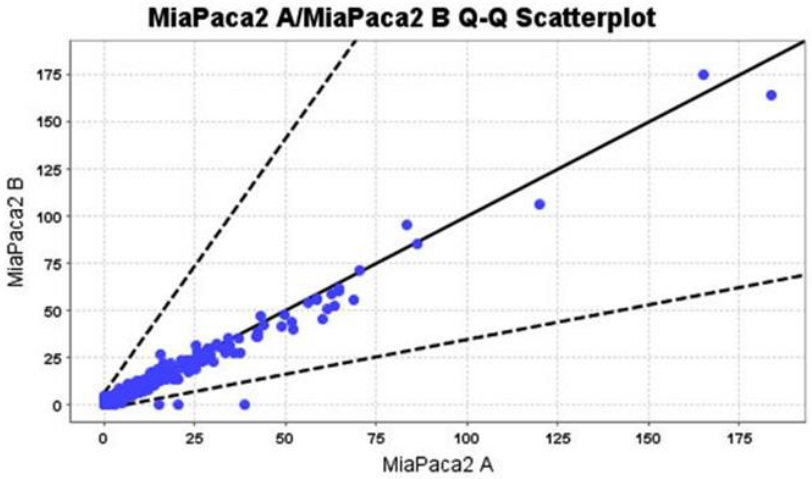

Figure 15. Qualitative analysis of the number of proteins identified by LC-MS using fractionated and unfractionated MiaPaca2 peptide digest. Proteins were identified with ≥two peptides with 90% and 95% confidence at peptide and protein level respectively and an FDR of 0% (**A**). Quantitative analysis of the two replicates of fractionation. Spectral counts of proteins identified in the two replicates are plotted on the x and y axes. The solid line represents optimal correlation while the dashed lines represent ±2 SD (**B**).

We then assessed the performance of our proteomics approach using normal pancreas FFPE and the same protein extraction protocol as will be used in the PNI proteomic profiling experiment (Liquid Tissue buffer). 10µg of normal pancreas FFPE peptide digest were fractionated and analysed in the same way as MiaPaca2 digest. The fractionation was similarly reproducible chromatographically (**Figure 16**) and the two fractionated samples yielded 1057 protein IDs compared to 187 from the two unfractionated samples, demonstrating again a five-fold increase. The reproducibility of protein IDs between the two fractionated samples was also similar to MiaPaca2 digest (74%), only 8% lower than the technical reproducibility of the LC-MS itself for the technical replicates of unfractionated samples (82%) (**Figure 17A**). Quantitatively, the two duplicates of normal pancreas FFPE fractionated digests also showed good correlation (**Figure 17B**).

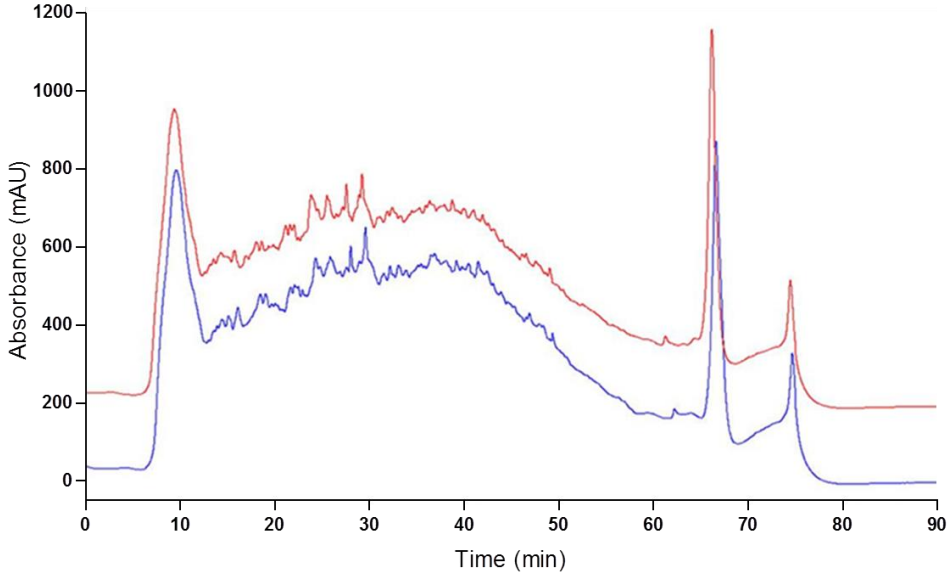

Figure 16. Chromatograms of duplicate runs of normal pancreas FFPE tissue digest fractionation showing good reproducibility.

(A)

	Protein (peptide) identifications				
	1st replicate	2nd replicate	Common	Total	Reproducibility (Protein IDs)
Unfractionated NL pancreas	169(871)	172(865)	154(736)	187(1000)	82%
Fractionated NL pancreas	913(5009)	930(5034)	786(3811)	1057(6232)	74%

(B)

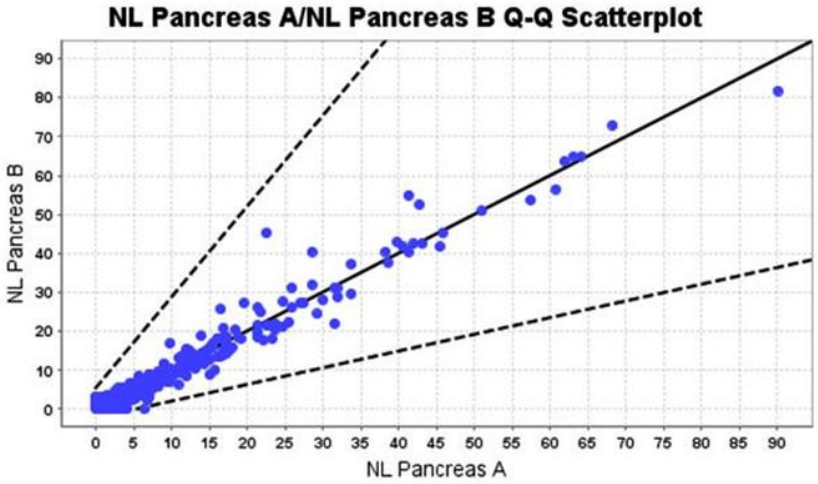

Figure 17. Qualitative analysis of the number of proteins identified by LC-MS/MS using fractionated and unfractionated normal pancreas FFPE tissue digest. Proteins were identified with ≥two peptides with 90% and 95% confidence at peptide and protein level, respectively and an FDR of 0.2% (**A**). Quantitative analysis of the two replicates of fractionation. Spectral counts of proteins are plotted on the x and y axes. The solid line represents optimal correlation while the dashed lines represent ±2 SD (**B**).

Of note, the number of peptides and proteins identified from FFPE tissues was less than those from cell lines. However, whilst the number of peptides identified in the MiaPaca2 samples was twice as those identified in the FFPE normal pancreas, the number of proteins was only a third higher. This discrepancy can be explained by the higher average sequence coverage (representing the part of the protein sequence that was identified in LC-MS relative to the full sequence of that protein) of proteins in the MiaPaca2 samples (~25%) compared to FFPE normal pancreas (~16%) which suggests that proteins in the cell line were identified with more peptides than was the case in the pancreas samples. Furthermore, only one third of the acquired MS spectra were identified in the FFPE samples compared to 50% in the cell line samples, probably reflecting formalin-induced modifications and/or the presence of non-tryptic peptides in the FFPE samples. These factors combined, in addition to the differences in the sample preparation method and biological differences between the samples would account for the observed difference in the number of protein identifications. Nonetheless, these results demonstrate excellent qualitative and quantitative reproducibility of the high pH RP fractionation using the converted HPLC platform as well as significantly wider proteome coverage in the two dimensional (2D) LC-MS approach compared to the 1D analysis.

3.3. Proteomic analysis of cancer cells and nerves in PNI

3.3.1. Analysis of PNI and non-PNI cancer

1D LC-MS analysis

1µg of peptide digest of each of five matched PNI and non-PNI cancer samples was subjected to LC-MS analysis in duplicate. We identified 1,432 proteins in the PNI samples (1,083-1,266 per sample) and 1,542 proteins in the non-PNI samples (1,092-1,258 per sample). A total of 1,610 proteins were identified from all samples with at least two unique peptides/protein (the complete list will be deposited in the Pancreatic Expression Database, www.pancreasexpression.org).1,346 proteins were common to both types of samples, whereas 86 and 196 proteins were unique to PNI and non-PNI, respectively. Only 31 proteins (1.9%) were differentially regulated (p≤0.05) (**Table 5** and **6**). Applying a fold change of ≥1.5 in addition to the p value resulted in only eight up-regulated and 11 down-regulated proteins.

Table 5. Up-regulated proteins in PNI compared to non-PNI cancer samples analysed using 1D LC-MS (p≤0.05). Mean values are the average intensity of five FFPE samples. FC: fold change.

Protein ID	Gene Name	Protein name	PNI	Non-PNI	p value	FC
Q15582	TGFBI	Transforming growth factor-beta-induced protein ig-h3	4E+07	2E+07	0.0000	2.29
P07942	LAMB1	Laminin subunit beta-1	3E+07	7E+06	0.0150	4.01
Q16363	LAMA4	Laminin subunit alpha-4	1E+07	2E+06	0.0179	7.32
P26368	U2AF2	Splicing factor U2AF	1E+07	1E+07	0.0195	1.26
P14543	NID1	Nidogen-1	1E+07	3E+06	0.0231	4.47
P62269	RPS18	40S ribosomal protein S18	8E+07	6E+07	0.0292	1.33
O94973	AP2A2	AP-2 complex subunit alpha-2	2E+06	6E+05	0.0334	3.21
P62899	RPL31	60S ribosomal protein L31	3E+07	2E+07	0.0353	1.35
P11047	LAMC1	Laminin subunit gamma-1	4E+07	1E+07	0.0360	3.20
Q6PCB0	VWA1	von Willebrand factor A domain-containing protein 1	4E+06	0	0.0448	-
P40222	TXLNA	Alpha-taxilin	2E+06	3E+05	0.0448	5.65
Q13509	TUBB3	Tubulin beta-3 chain	8E+07	5E+07	0.0466	1.53
P49721	PSMB2	Proteasome subunit beta type-2	3E+07	2E+07	0.0487	1.30

Table 6. Down regulated proteins in PNI compared to non-PNI cancer samples analysed using 1D LC-MS (p≤0.05). Mean values are the average intensity of five FFPE samples. FC: fold change.

Protein ID	Gene name	Protein name	PNI	Non-PNI	p value	FC
P35749	MYH11	Myosin-11	2E+07	1E+08	0.0054	0.16
P60660	MYL6	Myosin light polypeptide 6	2E+08	2E+08	0.0057	0.77
P56537	EIF6	Eukaryotic translation initiation factor 6	1E+06	6E+06	0.0067	0.22
P09525	ANXA4	Annexin A4	7E+08	1E+09	0.0069	0.64
O15144	ARPC2	Actin-related protein 2/3 complex subunit 2	5E+07	6E+07	0.0080	0.80
P45880	VDAC2	Voltage-dependent anion-selective channel protein 2	2E+07	3E+07	0.0083	0.68
O15143	ARPC1B	Actin-related protein 2/3 complex subunit 1B	7E+06	1E+07	0.0092	0.61
O43396	TXNL1	Thioredoxin-like protein 1	2E+06	4E+06	0.0116	0.45
P21291	CSRP1	Cysteine and glycine-rich protein 1	2E+07	2E+07	0.0129	0.69
Q13232	NME3	Nucleoside diphosphate kinase 3	3E+06	6E+06	0.0143	0.55
O75436	VPS26A	Vacuolar protein sorting-associated protein 26A	6E+06	1E+07	0.0226	0.54
Q9H0E2	TOLLIP	Toll-interacting protein	6E+06	8E+06	0.0253	0.74
P21333	FLNA	Filamin-A	3E+08	5E+08	0.0277	0.73
O14880	MGST3	Microsomal glutathione S-transferase 3	6E+06	1E+07	0.0283	0.54
P09493	TPM1	Tropomyosin alpha-1 chain	8E+06	2E+07	0.0361	0.37
Q9UJU6	DBNL	Drebrin-like protein	1E+07	2E+07	0.0410	0.78
Q01995	TAGLN	Transgelin	9E+07	2E+08	0.0418	0.58
P23142	FBLN1	Fibulin-1	5E+06	1E+07	0.0486	0.39

ArrayTrack™ software was used to perform unsupervised hierarchical cluster analysis of these samples based on all identified proteins. PNI and non-PNI samples from each case clustered together, further supporting the largely similar nature of those samples (**Figure 18**).

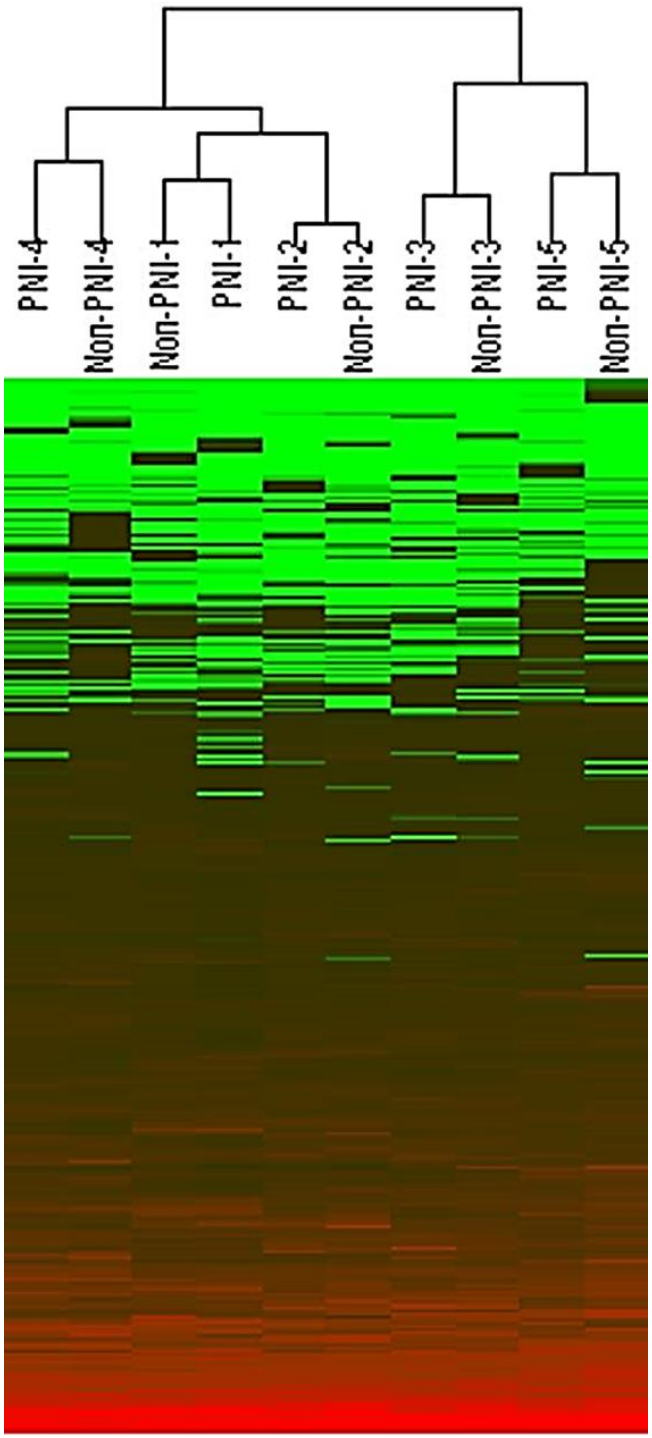

Figure 18. Hierarchal clustering of PNI and non-PNI cancer samples according to their protein expression profile. Each PNI sample clustered with its matching non-PNI sample. Clustering was performed using ArrayTrack^{TM} software.

2D LC-MS analysis

As the 1D LC-MS analysis of PNI and non-PNI cancer revealed limited number of differentially regulated proteins, and in order to achieve in depth proteomic analysis of these samples, we performed 2D LC-MS using pooled material from three of the five cases that had sufficient peptide digest. For this, we pooled equal amount of peptides from PNI cancer from those three cases into one sample and similarly pooled non-PNI cancer from the same cases. The two pooled samples were then fractionated in duplicate into 12 fractions using high pH RP HPLC (**Figure 19**). Each fraction was subsequently submitted to LC-MS analysis in the same way as the 1D analysis.

(A)

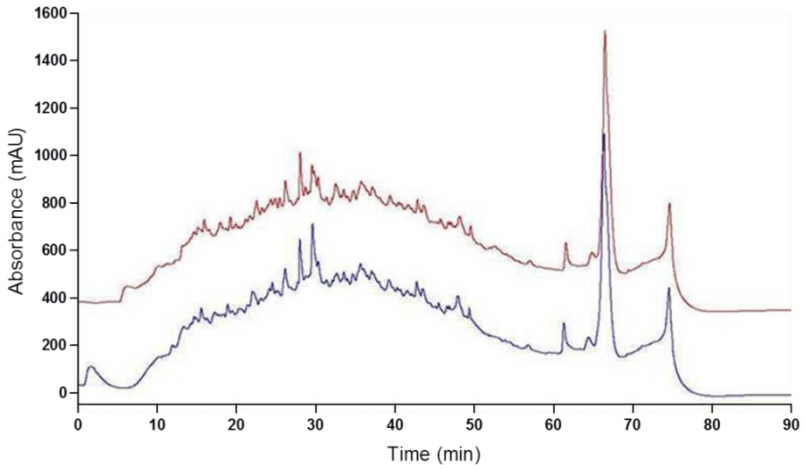

(B)

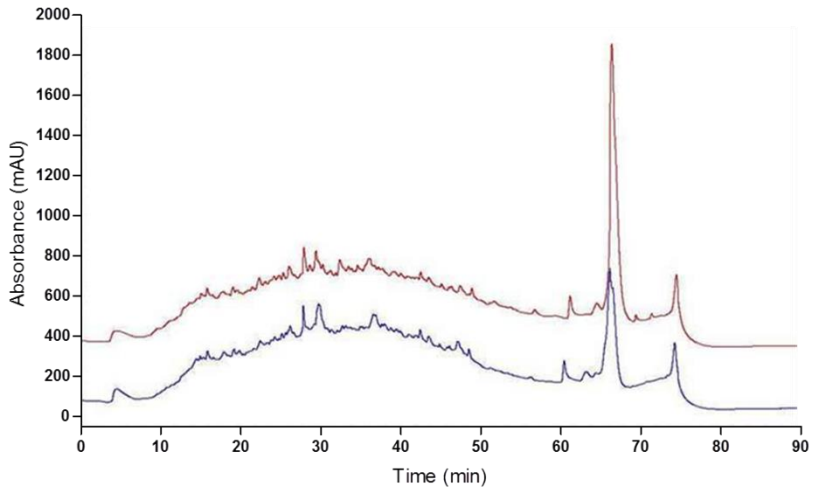

Figure 19. Chromatograms of high pH RP HPLC of pooled PNI cancer (**A**) and non-PNI cancer (**B**) samples. Fractions were collected every 5min (12 fractions per sample).

This in-depth profiling resulted in the identification of 3,229 proteins (3,160 in the PNI and 3,136 in the non-PNI samples) with an FDR of 1% (the complete list will be deposited in the Pancreatic Expression Database, www.pancreasexpressio.org). 97% of the proteins identified in 1D LC-MS were also identified in 2D LC-MS, only 39 proteins (1.2%) were found to be differentially expressed (p≤0.05) (**Table 7** and **8**). Using a fold change of ≥1.5 as an additional filter, we identified 18 up-regulated and 15 down-regulated proteins in PNI compared to non-PNI cancer samples.

Table 7. Up-regulated proteins in PNI compared to non-PNI cancer samples analysed using 2D LC-MS (p≤0.05). Mean values are the average spectral counts of the two technical replicates. FC: fold change.

Protein ID	Gene name	Protein name	PNI	Non-PNI	p value	F/C
P41219	PRPH	Peripherin	37	1.5	0.0000	24.67
P24043	LAMA2	Laminin subunit alpha-2	12.5	0	0.0003	-
Q6UX06	OLFM4	Olfactomedin-4	76	39.5	0.0006	1.92
P02511	CRYAB	Alpha-crystallin B chain	11	0	0.0009	-
P24821	TNC	Tenascin	12	0.5	0.0012	24.00
P48681	NES	Nestin	19.5	4.5	0.0024	4.33
P09622	DLD	Dihydrolipoyl dehydrogenase, mitochondrial	25.5	8	0.0026	3.19
P55011	SLC12A2	Solute carrier family 12 member 2	21	5.5	0.0028	3.82
Q2UY09	COL28A1	Collagen alpha-1(XXVIII) chain	9	0	0.0035	-
P07942	LAMB1	Laminin subunit beta-1	23.5	7.5	0.0043	3.13
Q14112	NID2	Nidogen-2	15.5	3.5	0.0068	4.43
P12111	COL6A3	Collagen alpha-3(VI) chain	134	94.5	0.0082	1.42
P14543	NID1	Nidogen-1	12	2	0.0093	6.00
P68133	ACTA1	Actin, alpha skeletal muscle	115	80.5	0.0127	1.43
P12036	NEFH	Neurofilament heavy polypeptide	7	0	0.0128	-
P46821	MAP1B	Microtubule-associated protein 1B	7.5	0.5	0.0200	15.00
P12110	COL6A2	Collagen alpha-2(VI) chain	41	22.5	0.0205	1.82
P07196	NEFL	Neurofilament light polypeptide	6	0	0.0245	-
Q05707	COL14A1	Collagen alpha-1(XIV) chain	16.5	6	0.0305	2.75
Q16363	LAMA4	Laminin subunit alpha-4	10.5	2.5	0.0336	4.20

Table 8. Down-regulated proteins in PNI compared to non-PNI cancer samples analysed using 2D LC-MS (p≤0.05). Mean values are the average spectral counts of the tow technical replicates. FC: fold change.

Protein ID	Gene name	Protein name	PNI	Non-PNI	p value	F/C
P01275	GCG	Glucagon	5	46	0.0000	0.11
P35749	MYH11	Myosin-11	16.5	69.5	0.0000	0.24
Q01995	TAGLN	Transgelin	50	91	0.0006	0.55
O60218	AKR1B10	Aldo-keto reductase family 1 member B10	6	23.5	0.0014	0.26
P67936	TPM4	Tropomyosin alpha-4 chain	44	78	0.0023	0.56
P15924	DSP	Desmoplakin	102.5	151	0.0027	0.68
P58107	EPPK1	Epiplakin	20.5	44	0.0038	0.47
O00338	SULT1C2	Sulfotransferase 1C2	0	8	0.0068	0.00
P21333	FLNA	Filamin-A	104.5	148	0.0071	0.71
Q12929	EPS8	Epidermal growth factor receptor kinase substrate 8	29	53.5	0.0078	0.54
Q9UHG2	PCSK1N	ProSAAS	0	7.5	0.0095	0.00
Q7Z406	MYH14	Myosin-14	248.5	309.5	0.0118	0.80
P00488	F13A1	Coagulation factor XIII A chain	2	10.5	0.0217	0.19
P23141	CES1	Liver carboxylesterase 1	1.5	9.5	0.0220	0.16
Q15149	PLEC	Plectin	619.5	706	0.0225	0.88
P21397	MAOA	Amine oxidase [flavin-containing] A	7.5	19.5	0.0246	0.38
O95833	CLIC3	Chloride intracellular channel protein 3	1.5	9	0.0289	0.17
P12814	ACTN1	Alpha-actinin-1	62.5	89.5	0.0317	0.70
P05408	SCG5	Neuroendocrine protein 7B2	0	5	0.0473	0.00

GO analysis (geneontology.org) of the PNI, non-PNI and the differentially expressed proteins (**Figure 20**) revealed that our LC-MS analysis detected less membranous and more cytoplasmic proteins compared to all GO annotated proteins. The distribution of subcellular localisation of the detected proteins is broadly consistent with published literature [214-216] and reflects the difficulty of extracting hydrophobic membranous proteins. The GO annotations for both PNI and non-PNI samples were similar, however the differentially expressed proteins included a significantly higher percentage of the extracellular proteins compared to the whole cohort of identified proteins.

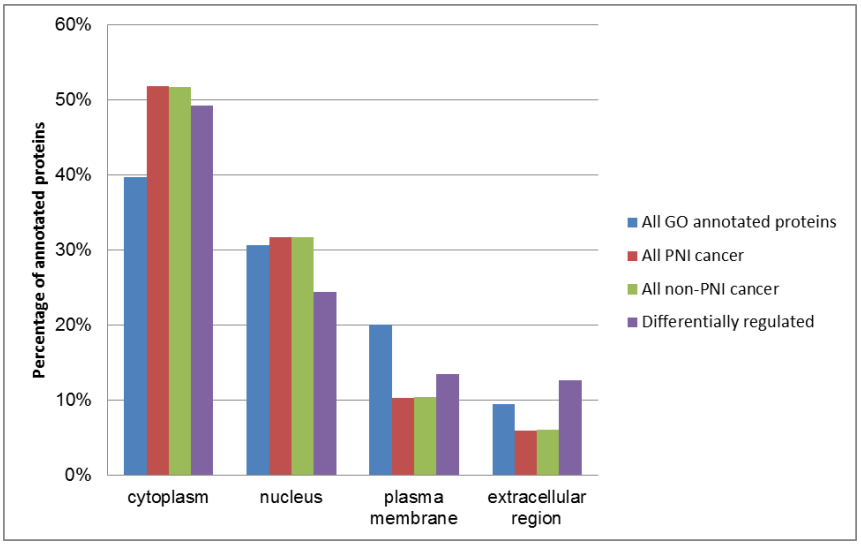

Figure 20. Cell component GO annotations comparing all GO annotated proteins detected in PNI cancer and non-PNI cancer as well as differentially regulated proteins.

To further explore this and look into the overall functional roles of the differentially expressed proteins, we performed GO enrichment analysis of the differentially expressed proteins against the background of all identified proteins using Gene Enrichment Analysis and Visualization (GOrilla) tool (http://cbl-gorilla.cs.technion.ac.il). This analysis confirmed the significant enrichment of extracellular proteins and to a lesser degree basement membrane and intermediate filaments proteins in addition to others (**Figure 21**).

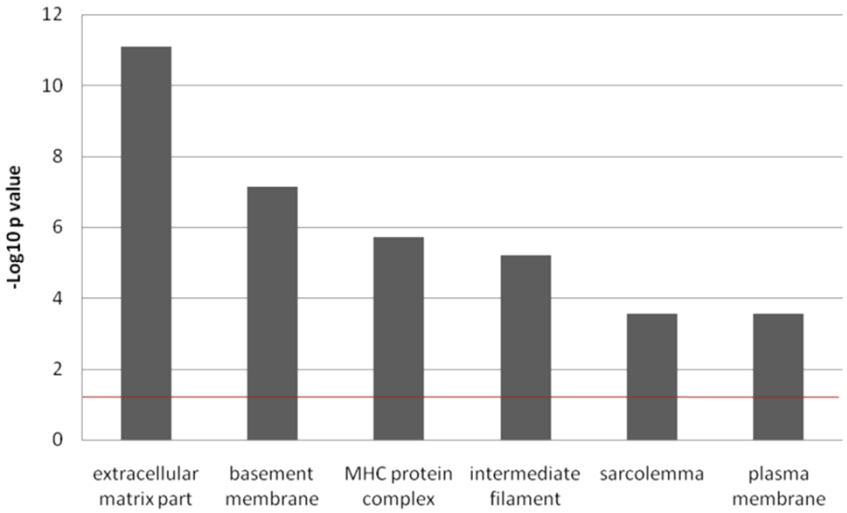

Figure 21. GO cellular component enrichment analysis of the differentially regulated proteins. Red line represents the –log10 of 0.05.

Ingenuity Pathway Analysis (IPA) was also used to explore the Molecular and Cellular functions and Disease processes attributed to the differentially regulated proteins. The top enriched functions included ‘Cellular Assembly and Organisation’ and ‘Cellular Function and Maintenance’ (such as cytoskeleton organisation, microtubule formation and axonogenesis). Enrichment in proteins related to ‘Cellular Movement’ included migration, chemotaxis and invasion, whereas ‘Cell Death and Survival’ enrichment included functions related to tumour and neuronal cell survival (**Figure 22**).

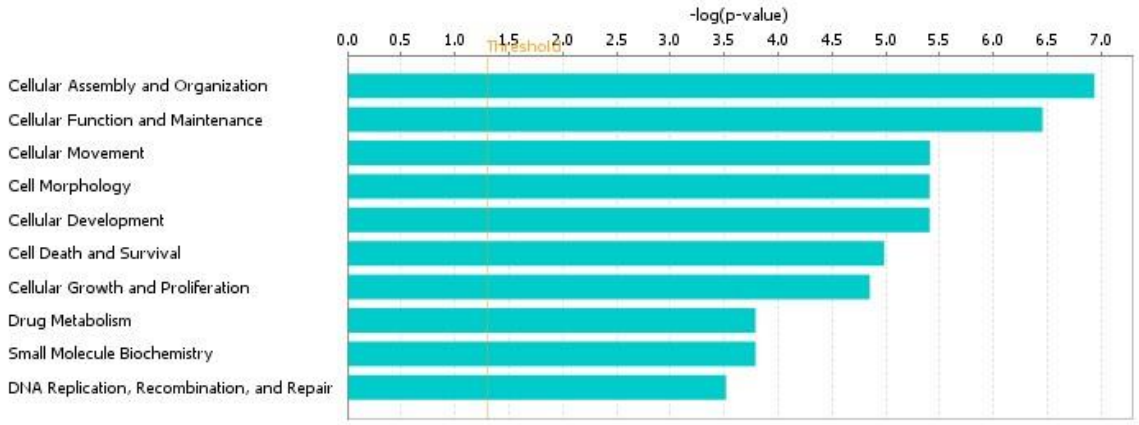

Figure 22. IPA analysis of GO Molecular and Cellular function enrichment of the differentially expressed proteins in PNI and non-PNI cancer samples. The threshold line represents -log (0.05).

3.3.2. 1D LC-MS analysis of invaded and non-invaded nerves

1µg of peptide digest of each of matched invaded and non-invaded nerve samples from five cases was subjected to LC-MS analysis in duplicate. A total of 925 unique proteins were identified from all samples with at least two unique peptides/protein. In the invaded nerves, we identified 847 proteins (681-729 proteins per sample) whereas in the non-invaded nerves 833 proteins (578-729 proteins per sample) were detected. 167 proteins (18%) were differentially expressed ($p \leq 0.05$) (**Appendix table 1** and **2**), 99 of which had a fold change of ≥1.5. Selected up-regulated and down-regulated proteins are shown in **Tables 7** and **8**, respectively.

Table 9. Selected up-regulated proteins in invaded compared to non-invaded nerves analysed using 1D LC-MS ($p \leq 0.05$ and fold change ≥1.5). Mean values are the average intensity from five FFPE samples. FC: fold change, IN: Invaded nerves, NIN: non-invaded nerves

Protein ID	Gene name	Protein name	Mean IN	Mean NIN	p value	FC
P07942	LAMB1	Laminin subunit beta-1	7E+08	4.1E+08	0.0031	1.60
P54577	YARS	Tyrosine--tRNA ligase, cytoplasmic	2E+06	258950	0.0040	7.57
P48681	NES	Nestin	4E+08	1.1E+08	0.0048	3.35
P24043	LAMA2	Laminin subunit alpha-2	5E+08	2.7E+08	0.0072	1.69
P21796	VDAC1	Voltage-dependent anion-selective channel protein 1	1E+07	5364680	0.0080	2.40
O15240	VGF	Neurosecretory protein VGF	1E+08	2.7E+07	0.0086	5.15
P24821	TNC	Tenascin	5E+07	2E+07	0.0088	2.57
P45880	VDAC2	Voltage-dependent anion-selective channel protein 2	1E+07	6897500	0.0118	2.04
Q9UHG2	PCSK1N	ProSAAS	3E+07	6256750	0.0123	4.69
P54920	NAPA	Alpha-soluble NSF attachment protein	5E+06	2404260	0.0123	2.16
O15075	DCLK1	Serine/threonine-protein kinase DCLK1	4E+06	886260	0.0142	4.26
O00429	DNM1L	Dynamin-1-like protein	1E+07	5517700	0.0174	1.76
P61803	DAD1	Dolichyl-diphosphooligosaccharide--protein glycosyltransferase subunit DAD1	4E+06	1026970	0.0190	3.76
Q15063	POSTN	Periostin	1E+08	4.1E+07	0.0201	3.54
P61981	YWHAG	14-3-3 protein gamma	9E+07	5.4E+07	0.0209	1.60
P78559	MAP1A	Microtubule-associated protein 1A	9E+06	4469180	0.0213	1.93
P17677	GAP43	Neuromodulin	2E+08	8.9E+07	0.0311	2.14
Q9NRW1	RAB6B	Ras-related protein Rab-6B	4E+07	2E+07	0.0365	1.84
Q05193	DNM1	Dynamin-1	3E+07	1.7E+07	0.0368	1.70
O60716	CTNND1	Catenin delta-1	3E+06	476250	0.0374	6.31
P18509	ADCYAP1	Pituitary adenylate cyclase-activating polypeptide	7E+06	0	0.0499	-

Table 10. Selected down-regulated proteins in invaded compared to non-invaded nerves analysed using 1D LC-MS ($p \leq 0.05$ and fold change ≥ 1.5). Mean values are the average intensity from five FFPE samples. FC: fold change. IN: Invaded nerves, NIN: Non-invaded nerves

Protein ID	Gene name	Protein name	Mean IN	Mean NIN	p value	FC
P32119	PRDX2	Peroxiredoxin-2	2.1E+08	6E+08	0.0010	0.37
P11532	DMD	Dystrophin	2.6E+07	6E+07	0.0012	0.42
P13591	NCAM1	Neural cell adhesion molecule 1	1.3E+08	3E+08	0.0079	0.44
P12429	ANXA3	Annexin A3	2.2E+07	4E+07	0.0118	0.62
P04271	S100B	Protein S100-B	7.9E+08	4E+09	0.0179	0.19
Q01118	SCN7A	Sodium channel protein type 7 subunit alpha	6975530	5E+07	0.0347	0.14
P69905	HBA1	Hemoglobin subunit alpha	7363660	2E+07	0.0357	0.36
P68871	HBB	Hemoglobin subunit beta	6752000	1E+07	0.0357	0.65
P08294	SOD3	Extracellular superoxide dismutase [Cu-Zn]	1084070	7E+06	0.0368	0.16
P00915	CA1	Carbonic anhydrase 1	1.9E+07	4E+07	0.0400	0.51
P11166	SLC2A1	Solute carrier family 2, facilitated glucose transporter member 1	4366370	2E+07	0.0408	0.23
Q9NZN4	EHD2	EH domain-containing protein 2	1.4E+07	2E+07	0.0480	0.62
P11277	SPTB	Spectrin beta chain, erythrocyte	3.7E+07	6E+07	0.0482	0.63
P00918	CA2	Carbonic anhydrase 2	5196460	1E+07	0.0492	0.54

Unsupervised hierarchal cluster analysis was performed as described for cancer samples. Interestingly, all invaded nerves clustered together, separate from the four out of five non-invaded nerves (**Figure 23**). The clustering of NIN-1 with IN samples could be due to microdissection of some nerves that were in fact invaded at a different depth in the tissue. Nonetheless, the clustering pattern strongly suggested common features of molecular changes upon neural invasion that surpasses the biological matching of samples.

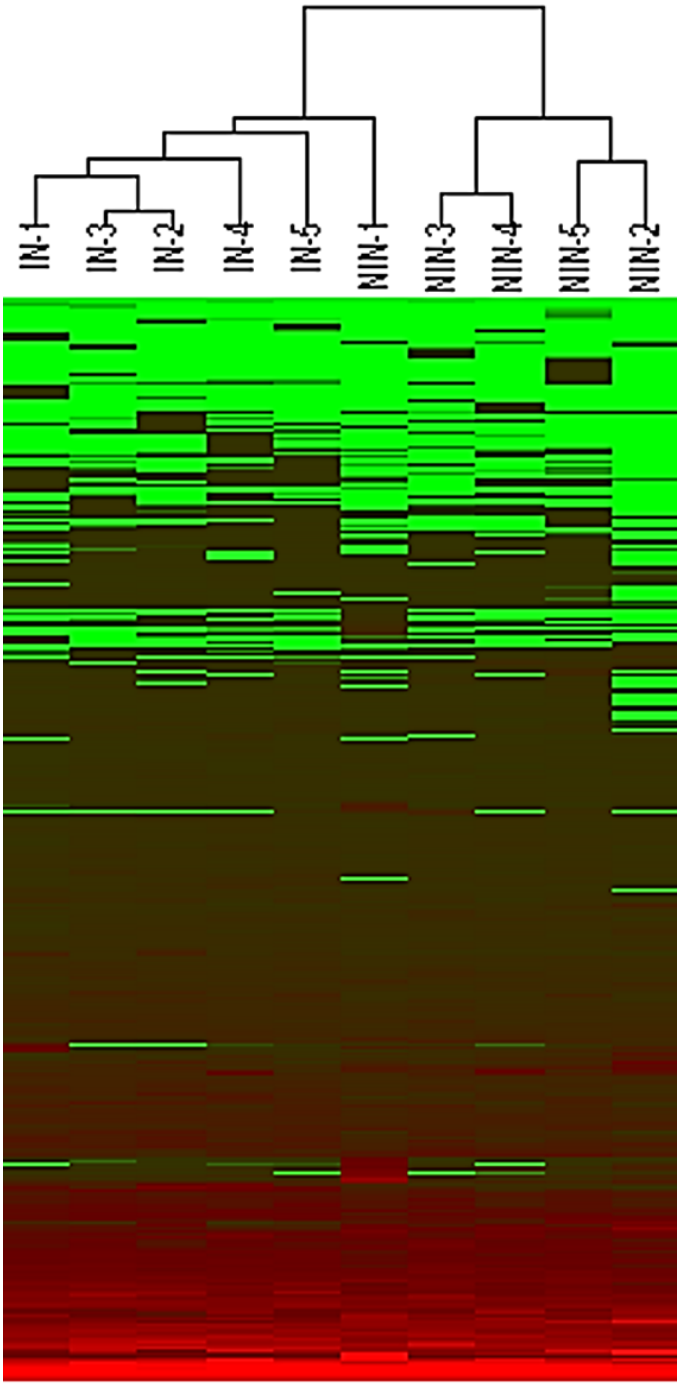

Figure 23. Hierarchal clustering of invaded and non-invaded nerve samples according to their protein expression profile. Clustering was performed using ArrayTrack™ software.

IPA analysis was also performed to identify enriched cellular functions and disease processes. Not surprisingly, 'Neurological Diseases' was the most enriched disease category. In addition, other interesting disease processes included 'Immunological Diseases' and 'Inflammatory Response' **(Figure 24**).

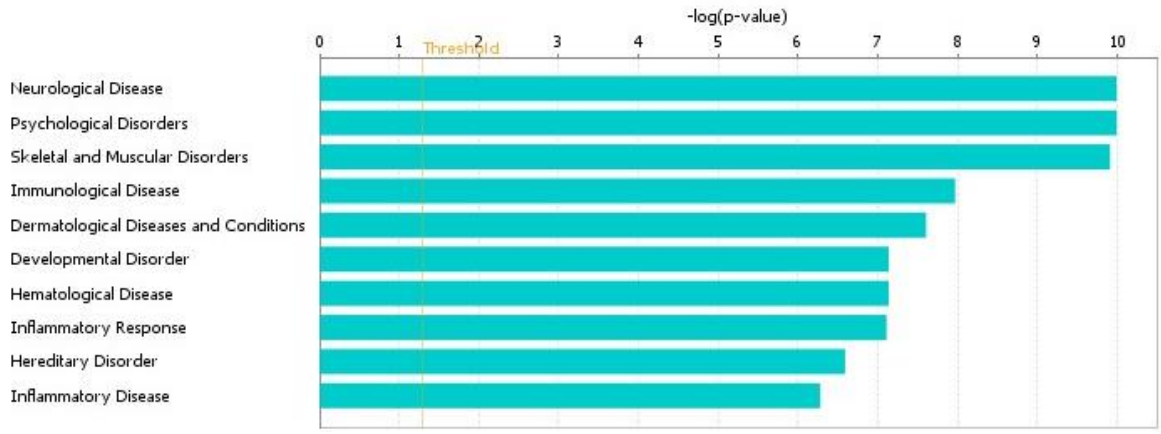

Figure 24. IPA analysis of diseases and disorders enrichment of the differentially expressed proteins in invaded and non-invaded nerves. Top 10 disease processes are shown.

Analysis of molecular and cellular function revealed enrichment in 'Cell Death and Survival' function including neuronal cell survival as well as 'Cell Morphology' (mostly relating to axonogenesis and neurite formation). Other enriched functions included 'Cellular Growth and Proliferation' and 'Cellular Movement' (such as migration and invasion) (**Figure 25**).

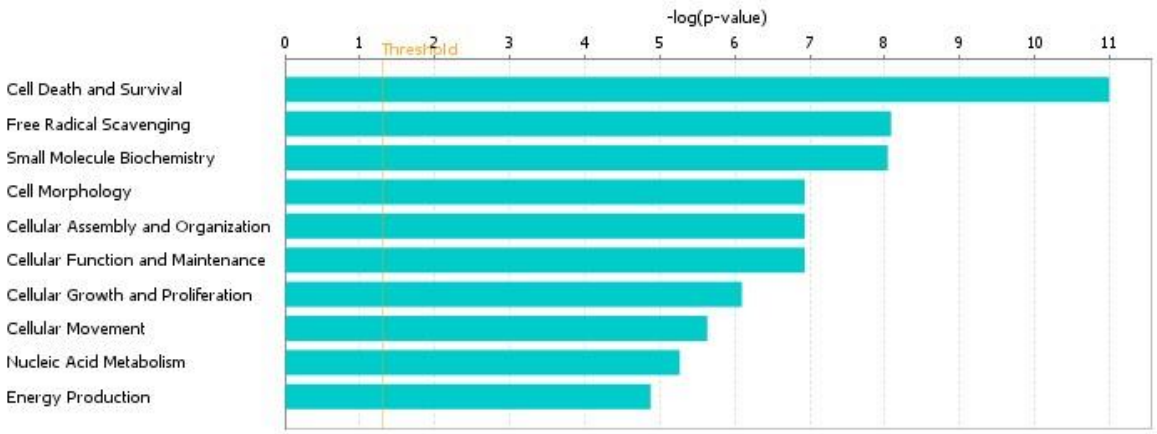

Figure 25. IPA analysis of molecular and cellular enrichment of the differentially expressed proteins in invaded and non-invaded nerves. Top 10 function categories are shown.

Overall, the proteomics data from the nerve samples reveal extensive molecular and thus biological alterations that are closely related to the neuroplasticity phenotype that has been described in PNI by several studies.

3.3.3. Assessment of the purity of LCM samples

One of the important factors to consider in LMD is the degree of cross contamination between closely related samples such as in our case PNI cancer and invaded nerves. We therefore attempted to estimate the degree of contamination based on the assumption that for a neuronal protein, for example, the level of expression in the PNI cancer relative to the invaded nerves is indicative of the degree of contamination of cancer sample by the adjacent nerve. We identified four known neuronal markers in the nerves dataset: Glial fibrillary acidic protein (GFAP), S100B, neurofilament heavy polypeptide (NEFH) and neurosecretory protein VGF. We first calculated the abundance of each protein relative to the sample in which it was identified. The obtained value for each protein in the PNI cancer sample was then expressed as a percentage of its abundance in the matching invaded nerve sample (**Figure 26**). Whilst most of these proteins were not detected in most PNI cancer samples, the relative abundance varied between proteins in the same sample pair (PNI cancer and invaded nerve) as well as for the same protein in different sample pairs particularly for GFAP.

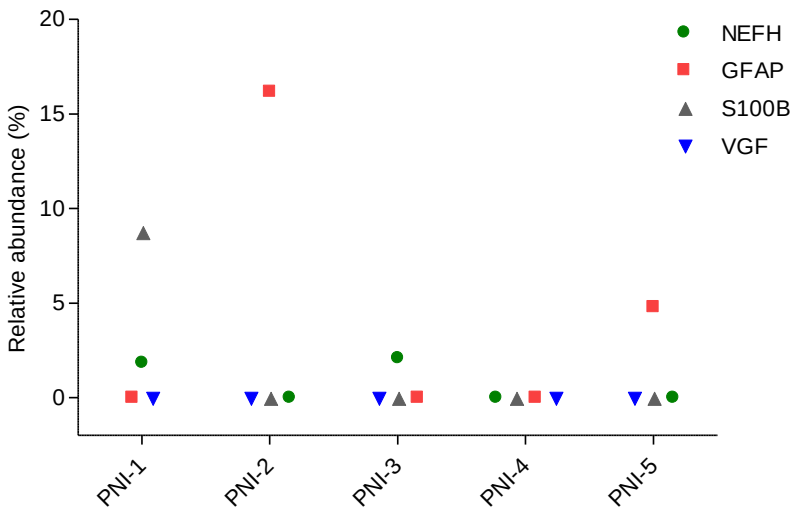

Figure 26. Abundance of selected neuronal proteins in PNI cancer samples relative to invaded nerves. The relative abundance for each protein was calculated by dividing the expression level in PNI cancer by the level in invaded nerves in the same PDAC case.

We then used the relative abundance of the other four proteins in each sample pair to estimate the degree of contamination of the PNI-cancer sample by the matching invaded nerves' sample. The estimated purity of the microdissected PNI cancer samples based on the average relative abundance of the four proteins was 98 and 96% for PNI-1 and PNI2, respectively, and ≥99% for the last three samples (**Figure 27**). Although the average clearly does not reflect the fact that most of these proteins were not detected, it still indicates high degree of purity of the PNI cancer samples at this depth of proteomic analysis. In fact, except for sample PNI cancer sample two (PNI-1) in which two of the four proteins were detected, not more than one protein was detected in three samples whilst none of the four proteins was identified in PNI-4 (**Figure 26**).

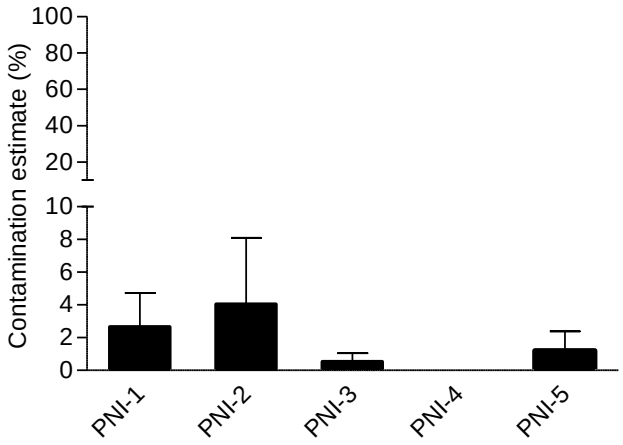

Figure 27. Estimation of contamination of PNI cancer samples by invaded nerves. The abundance of four proteins (NEFH, GFAP, S100B and VGF) in the PNI cancer samples relative to the matching invaded nerves samples was used to estimate the degree of contamination for each PNI cancer sample.

We were not able to identify any epithelial specific protein in the invaded nerves samples, which would suggest even higher degree of purity of those samples. A similar analysis of contamination in the 2D dataset was not possible, as we did not perform 2D LC-MS analysis of the nerves. However, the peptide digest that was used for this analysis was pooled from PNI-1, PNI-3 and PNI-4 cancer samples, which demonstrated high degree of purity in the above analysis.

3.4. IHC validation:

3.4.1. Expression of OLFM4 in PNI

Olfactomedin 4 (OLFM4) was one of the most significantly up-regulated proteins in the PNI compared to non-PNI cancer samples in the 2D analysis (**Table 7**). It was selected for validation using immunohistochemistry as it has been reported to have antiapoptotic properties [217] as well as conferring poor prognosis in PDAC [218]. IHC was performed on 30 PDAC cases. All PDAC cases displayed OLFM4 expression to varying degree and OLFM4 immunoreactivity varied also within the same section. However, cancer cells in PNI lesions usually displayed strong immunoreactivity (**Figure 28**). This was significantly higher than in non-PNI cancer (p=0.028) (**Figure 29**).

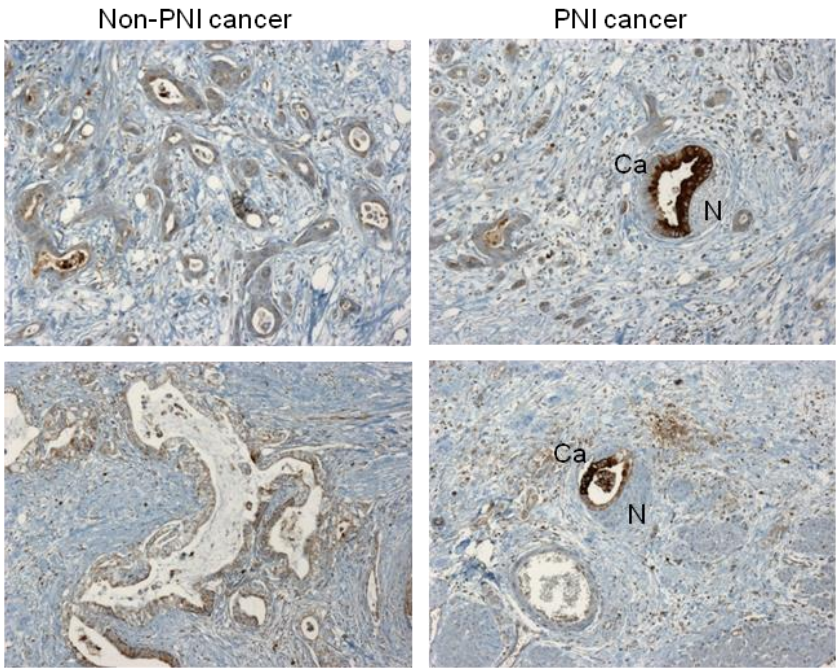

Figure 28. Immunohistochemsitry analysis of OLFM4 expression in PNI and non-PNI cancer. Representative images of two different PDAC cases (100x magnification) illustrate that OLFM4 showed variable expression in non-PNI cancer (left panel) while PNI cancer was usually strongly positive (right panels).

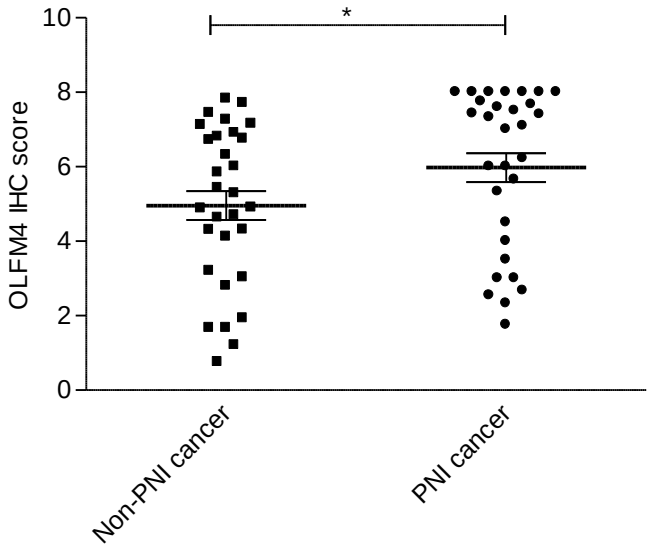

Figure 29. Semiquantitative analysis of OLFM4 in PNI and non-PNI cancer using immunohistochemistry. OLFM4 was significantly over-expressed in PNI compared to non-PNI cancer. Each data point represents the average score of all PNI cancer or at least 10 HPFs of non-PNI cancer for one patient. *p=0.028

3.4.2. Expression of VGF in the nerves

Neurosecretory protein VGF (non-acronymous) was one of the top up-regulated proteins in the invaded compared to non-invaded nerves (**Table 9**). VGF has been implicated in the generation of neuropathic pain [219] as well as in cell survival [220], both of which are closely linked to PNI, and was therefore selected for further validation and analysis.

VGF expression was evaluated in normal pancreas, CP and PDAC cases. In normal pancreas, VGF expression was limited to the islets which served as the internal positive control. VGF expression in normal pancreas nerves was occasionally weak but predominantly absent as shown on the left panel (**Figure 30A**).

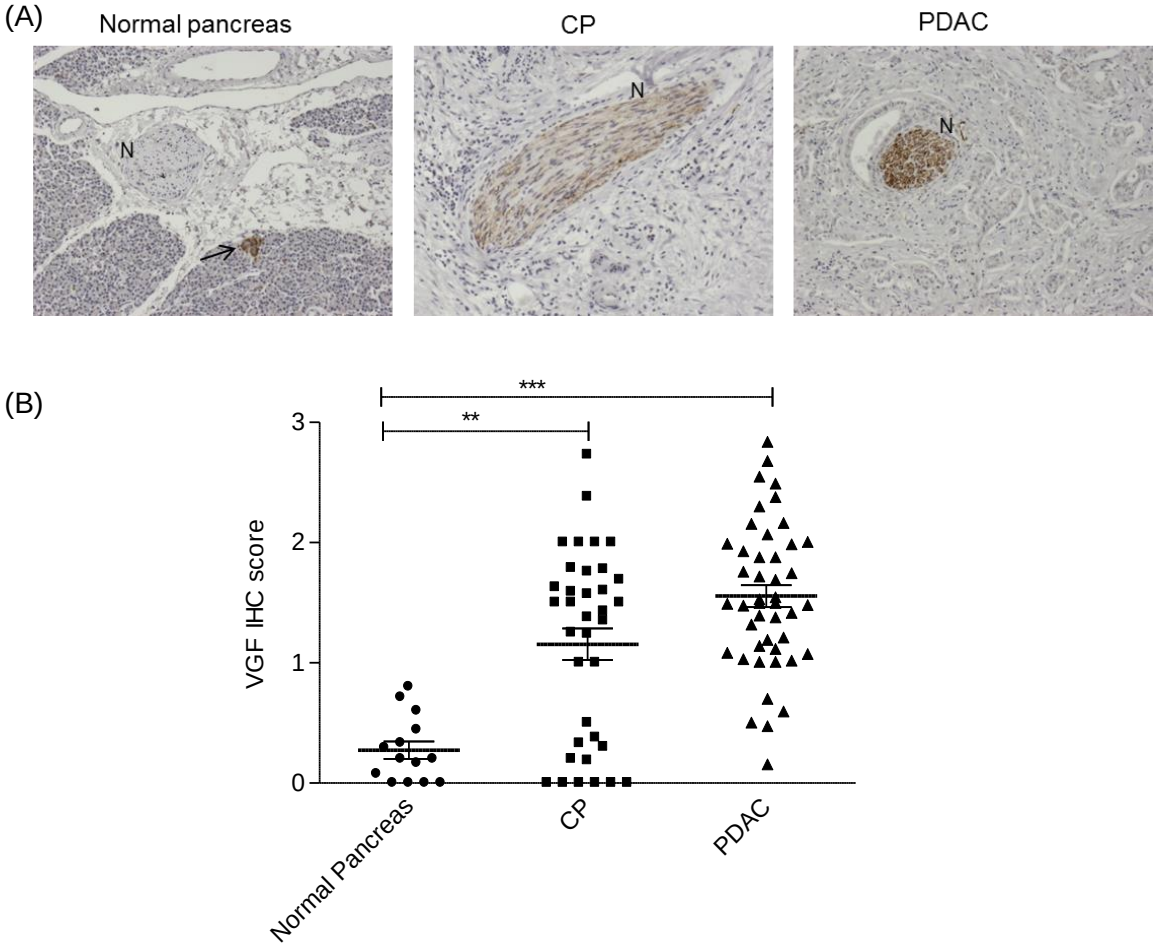

Figure 30. VGF expression in normal pancreata (n=14), CP (n=36) and PDAC (n=45). Representative images (200x magnification) showing that VGF is significantly over-expressed in both CP and PDAC nerves (N) compared to normal pancreas (**A**). No significant difference in the levels of VGF expression between CP and PDAC was detected (**B**). Arrow head pointing towards an islet which expresses VGF. Each data point represents one patient (the average score of all nerves in the indicated category). **p≤0.01, ***p≤0.001

In addition to the islets, nerves in the setting of CP and PDAC showed diverse immunoreactivity that ranged from weak to strong. Quantitation of VGF expression revealed a significant difference between both CP and PDAC and normal pancreas, however, the difference between CP and PDAC did not reach statistical significance (**Figure 30**).

In PDAC, nerves displayed a spectrum of immunoreactivity from absent to strong. Nerves invaded with cancer displayed, in the majority of cases, moderate to strong expression that was significantly higher than non-invaded nerves (**Figure 31A** and **B**). However, we noticed an interesting pattern of VGF expression in the non-

invaded nerves where nerves outside the tumour/stroma mass did not usually express VGF whereas nerves within the tumour showed weak to moderate expression (**Figure 31A**). Based on this observed pattern, we classified nerves into invaded nerves, intra-tumoural non-invaded nerves and extra-tumoural non-invaded nerves. VGF expression was significantly different between these three groups of nerves (**Figure 31C**).

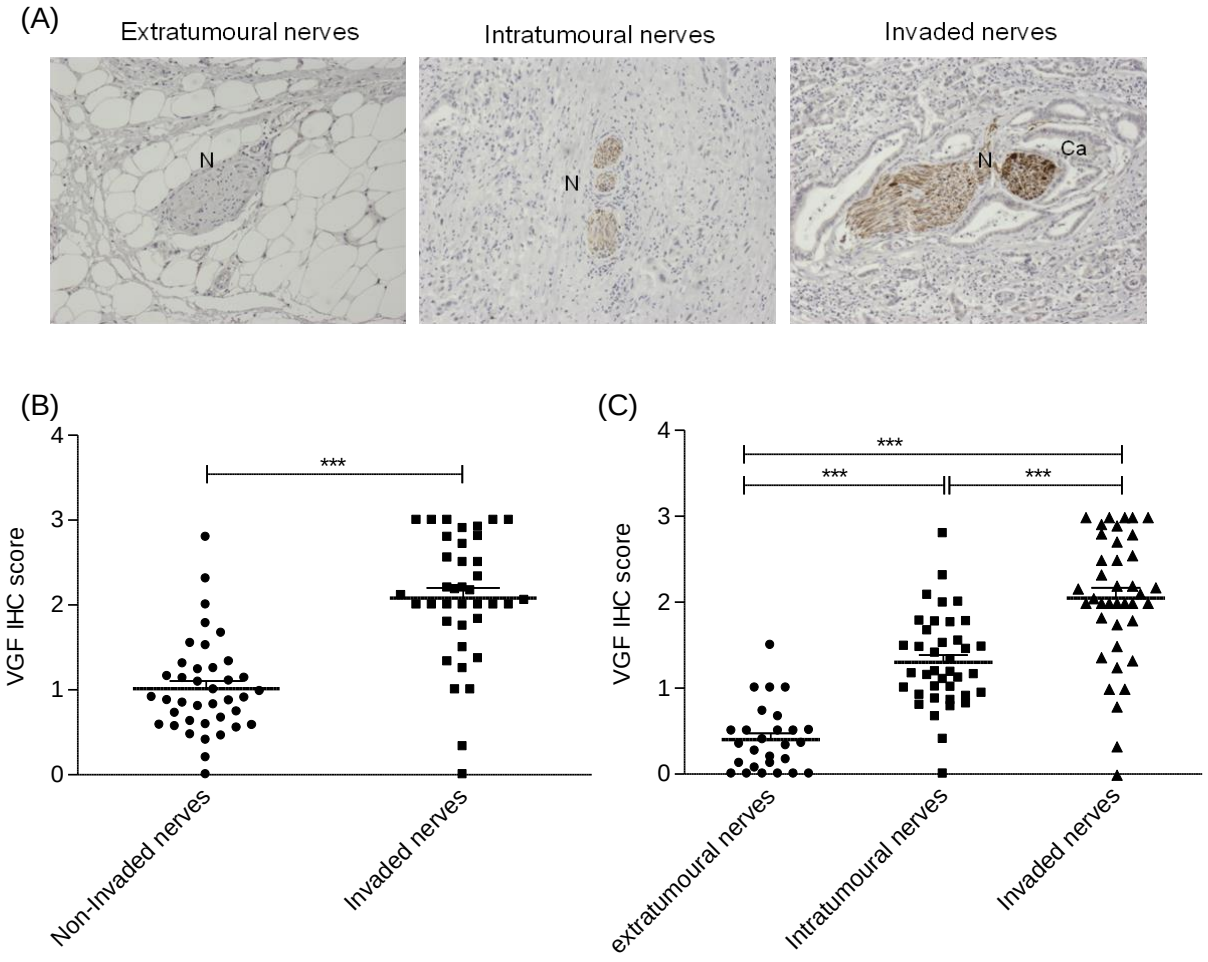

Figure 31. Analysis of VGF expression in PDAC cases using IHC. Representative images (200x magnification) of PDAC nerves (N) showed a range of immunoreactivity. Extratumoural nerves (left) were usually negative, whereas intratumoural non-invaded nerves were weakly to moderately positive (middle) and invaded nerves strongly positive (right, Ca is invading cancer) (**A**). VGF expression was significantly higher in invaded compared to non-invaded nerves (**B**). VGF expression was also significantly different between the three groups of nerves in PDAC (**C)**. Each data point represents one patient (the average score of all nerves in the indicated category). ***p<0.001

3.4.3. Correlation of pain and VGF expression

Because VGF has been linked to neuropathic pain, we further investigated whether VGF expression in CP and PDAC patients is related to pain. The severity and frequency of pain was used to classify CP and PDAC patients into three groups as described in the Methods section: no pain, mild pain (G1 pain) or moderate-severe pain (G2 pain). VGF was significantly over-expressed in CP patients with pain compared to those who did not have pain ($p<0.01$) (**Figure 32A & B**). There was also a trend of increased VGF expression with increasing degree of pain but this was not statistically significant (**Figure 32C**).

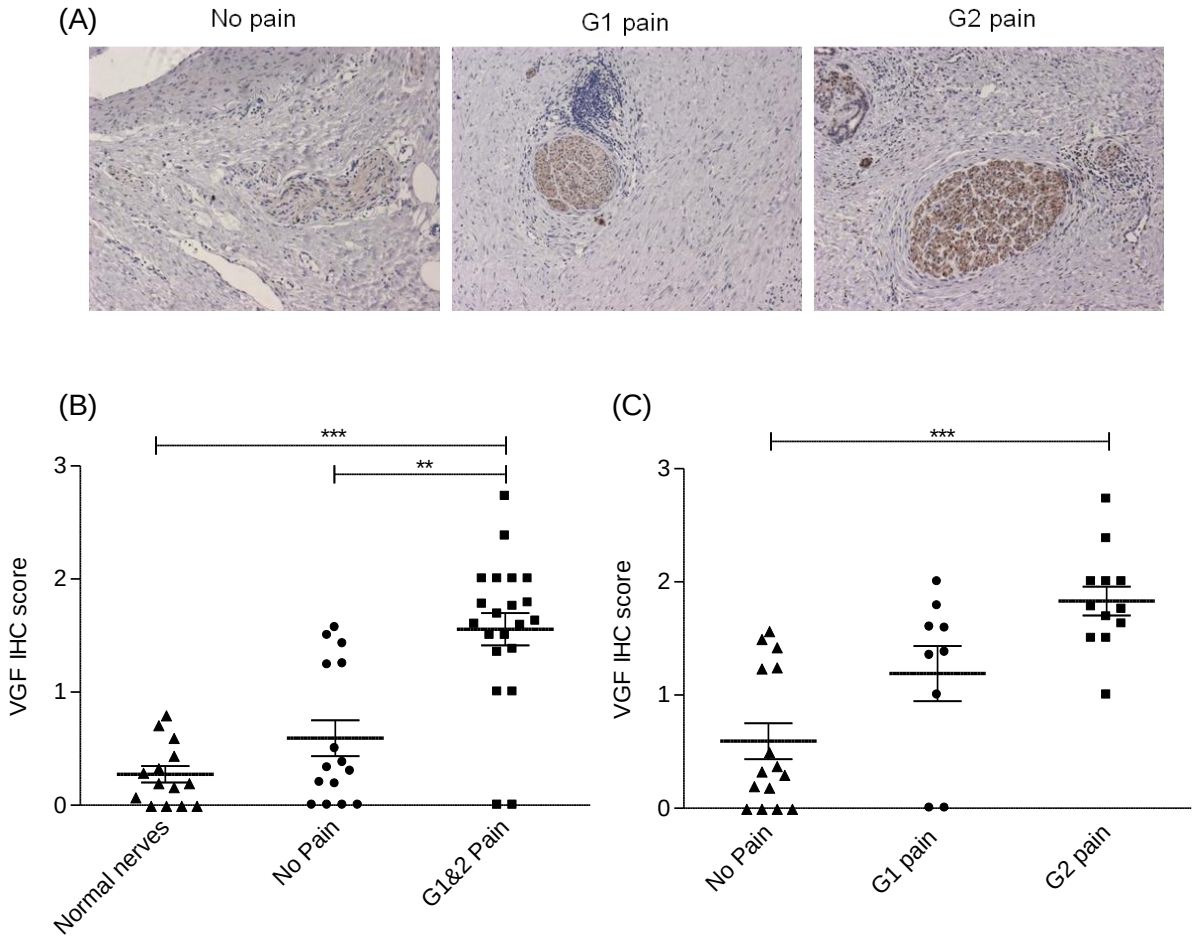

Figure 32. Correlation between VGF expression and pain in CP patients. Representative images (200x magnification) of three different CP cases with increasing pain and levels of VGF expression are shown (**A)**. VGF expression was significantly higher in patients with pain compared to those without pain (**B**). There was a trend of increasing VGF expression with the increasing degree of pain but this was statistically significant only for G2 pain (**C**).

This is likely due to the small number of cases in the subgroups as Spearman's correlation analysis revealed a strong correlation between VGF expression and the degree of pain (correlation coefficient 0.7, $p<0.0001$). Noticeably, pancreatic nerves from CP patients with no pain displayed weak or absent VGF expression similar to what was observed in normal pancreata.

Furthermore, nerves were classified according to their VGF expression into low expression (absent or weak) and high expression (moderate to strong) groups and expressed as percentage of the total number of nerves in each tissue section. This analysis reveals that as pain increases, the percentage of nerves with high VGF expression also increases (**Figure 33**), (Pearson's correlation coefficient 0.66, $p<0.0001$).

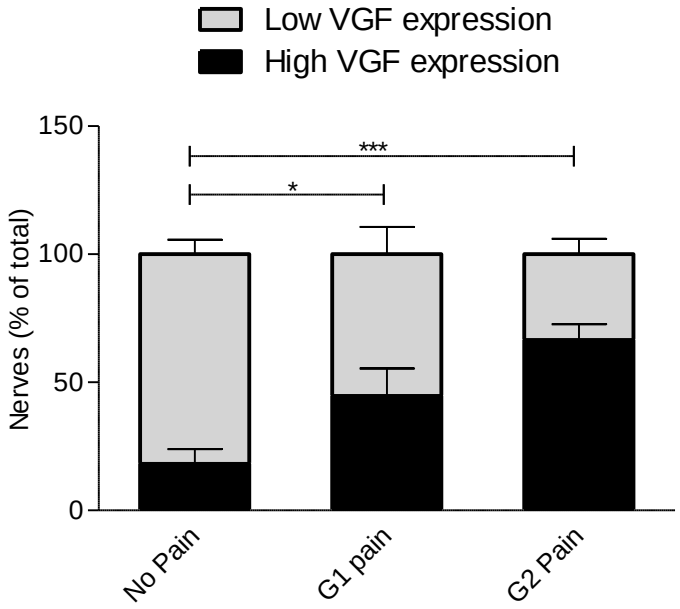

Figure 33. Correlation between VGF expression and degree of pain in CP patients. Nerves were divided into low expression or high expression groups. As the degree of pain increases, the percentage of nerves with high VGF expression increases. *p<0.05, **p<0.01

Unfortunately, up till now, we had only limited number of clinically annotated PDAC cases to complete the critical investigation of the relationship between VGF expression in nerves in PDAC. Disappointingly, this analysis is thus still pending and due to time constraints will have to be performed as soon as we receive the outstanding tissue sections.

3.5. *In vitro* modelling of neuro-epithelial interactions

We established an *in vitro* co-culture model in order to further validate molecular changes observed in our proteomic analysis and characterise the molecular mechanisms underlying them focusing, initially, on neuronal alterations.

For this model, we used PC12 cells as the neuronal element. PC12 cells are rat pheochromocytoma cell line that was established by Greene [221]. Upon exposure to NGF, PC12 cells differentiate into sympathetic like neurons, exit the cell cycle, extend neurites and become electrically excitable [221]. Due to their molecular and phenotypic response to neurotrophins, PC12 cells have been extensively used to study neuronal plasticity, neuronal differentiation, toxicity and response to injury [222-224]. We therefore hypothesized that PC12 cells could represent a useful model to study neuro-epithelial interactions.

3.5.1. Transwell co-culture system

Using Transwell inserts, PC12 cells were co-cultured with several PDAC cell lines in serum-free media for 24 hours. As a control, PC12 cells were cultured on their own and their number was adjusted to match the total number of cells in the co-culture system with cancer cells. In addition, PC12 cells were grown in serum free media with or without NGF as additional controls. Co-culture with MiaPaca2, Capan1 and BxPc3 induced neurite extension in PC12 cells similar to that induced by NGF. Panc1 cells, however, failed to induce neurite extension (**Figure 34 and 35**).

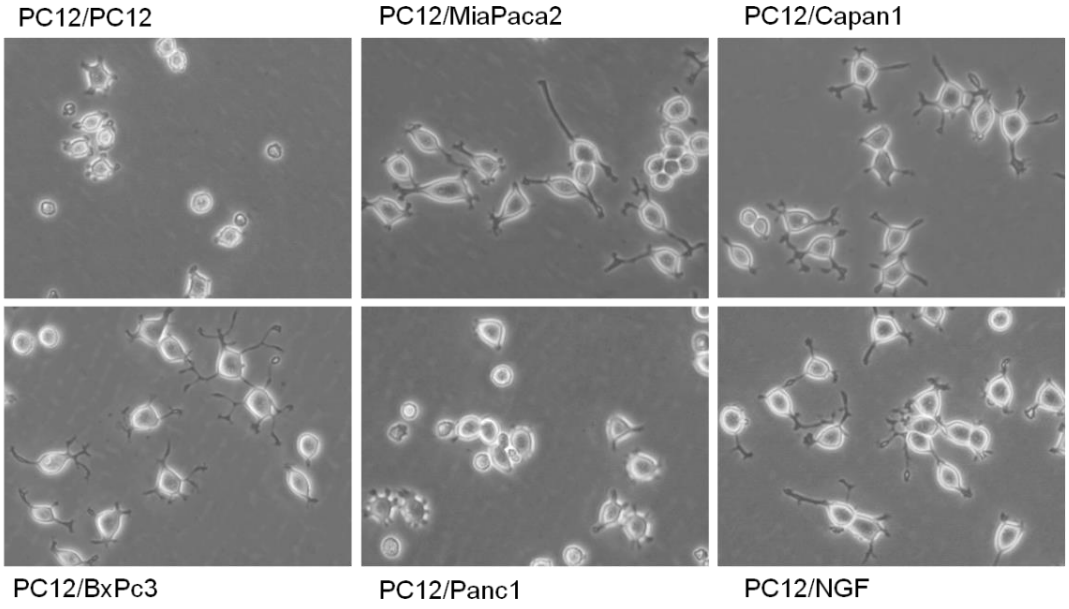

Figure 34. Representative images of PC12 neurite growth in co-culture with PDAC cell lines (200x magnification). NGF was used as positive control.

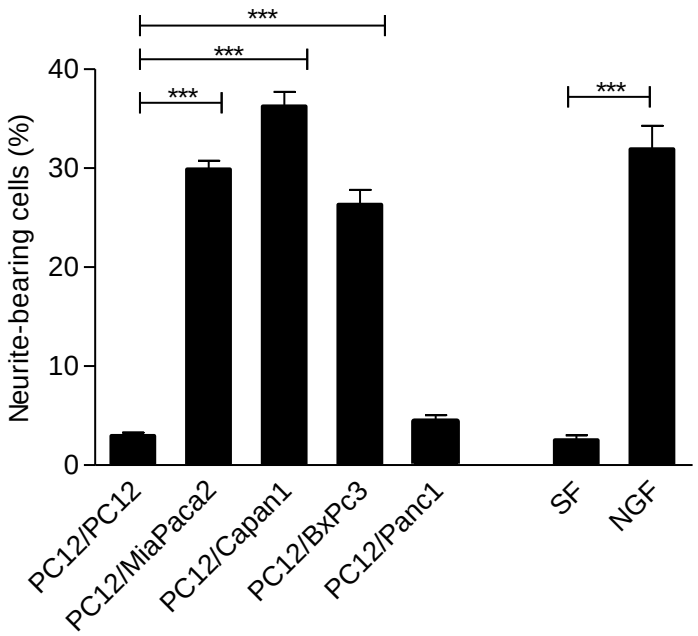

Figure 35. Neurite growth in Transwell co-culture of PC12 cells with several PDAC cell lines. PC12 co-cultured on their own were used as controls. NGF (50ng/ml) treatment was used as a positive control. Cells extending neurites longer than the maximum diameter of the cell body were counted and represented as a percentage of total number of cells. Data represents three independent experiments.***$p<0.001$. SF: serum free media.

PC12 cells are known to undergo apoptotic cell death in serum-free media whilst NGF promotes their survival under these conditions [225]. We wanted to explore whether PDAC cell lines could also provide protection against apoptosis in PC12 cells.

Following 24 hours co-culture, floating and attached PC12 cells were harvested for survival analysis using Annexin V and DAPI as described in the Methods section. Co-culture with MiaPaca2, Capan1 and BxPc3 protected PC12 cells from serum starvation induced apoptosis similar to complete media and NGF. Again, Panc1 cells did not provide significant protection (**Figures 36** and **37**).

In agreement with this, we observed an abrogation in the levels of cleaved Caspase-3 (CASP3) in PC12 cells when co-cultured with MiaPaca2, Capan1 and BxPc3, which was comparable to the effect of NGF (**Figure 36B**).

This data shows that three out of four PDAC cells lines were able to induce neuronal plasticity in PC12 cells similar to the effects of NGF and consistent with the features of neuronal plasticity in human PDAC tissues and in other *in vitro* models of PNI [81, 149].

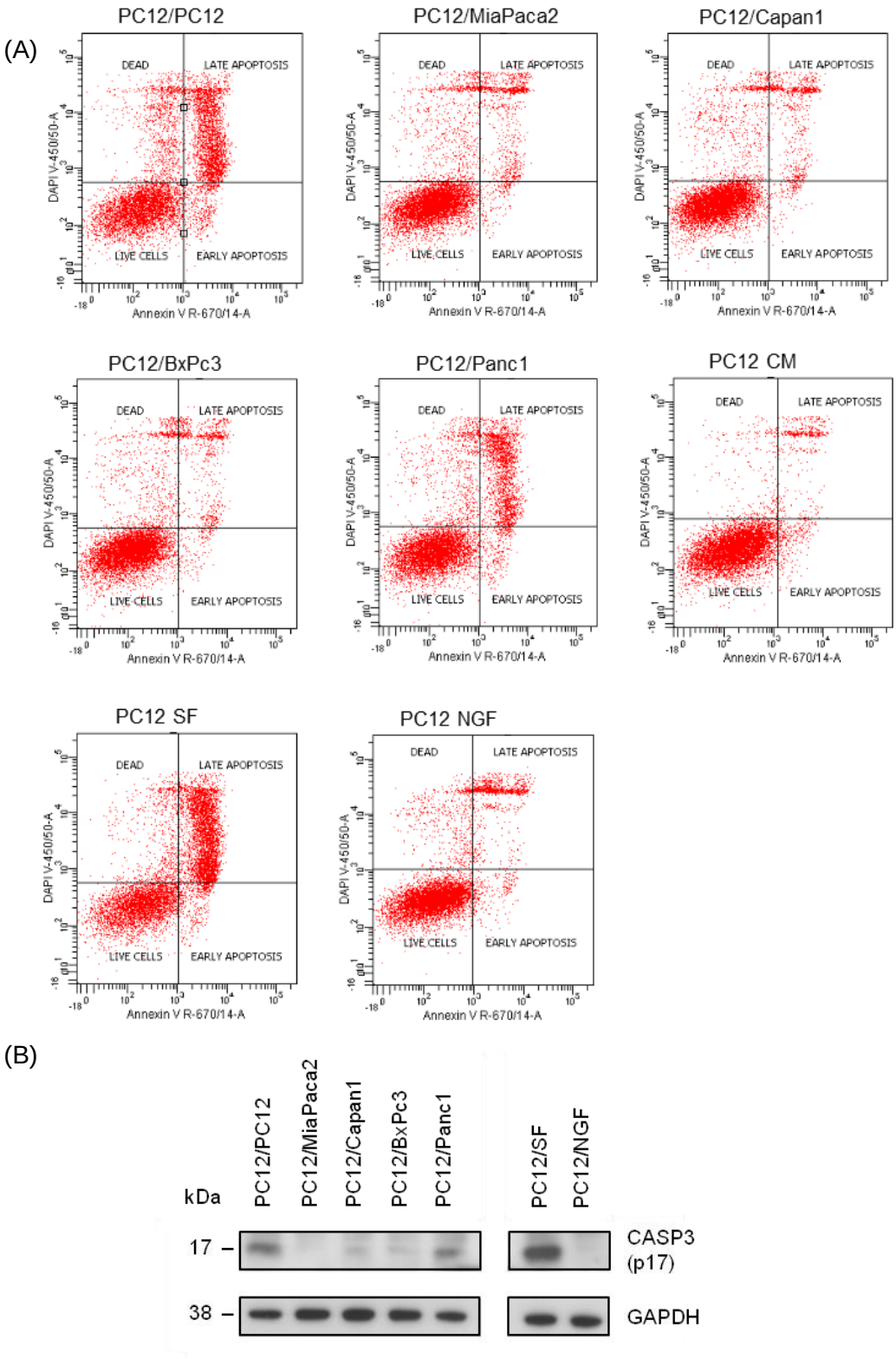

Figure 36. PC12 survival in transwell co-cultures using Annexin V/DAPI flow-cytometry assay. SF (serum-free) conditions were used as positive control for apoptosis whereas CM (complete media) and NGF (50ng/ml) were negative controls. Following 24 hours co-culture in serum-free-media, floating and attached PC12 cells were harvested, stained with Annexin and DAPI and analyzed as detailed in Methods section (**A**). Western blot showing decrease in CASP3 (p17) levels in PC12 cell co-cultured with three PDAC cell lines indicating reduced apoptosis comparable to the effect of NGF. GAPDH was used as a loading control (**B**).

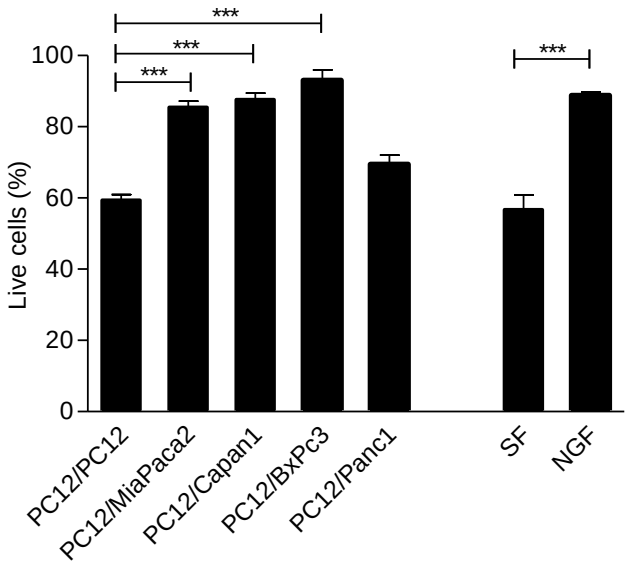

Figure 37. Annexin V/DAPI flow-cytometry apoptosis assay of PC12 cells co-cultured with PDAC cells lines or NGF (50ng/ml). The percentage of live cells (negative for both Annexin V and DAPI) in each condition was expressed relative to live cells in complete media.
***p<0.001

In addition to the phenotypic changes, PC12 cells exposure to NGF induces the expression of a variety of genes including VGF [226]. Therefore, we investigated whether PDAC cell lines can also induce molecular alterations in PC12 cells similar to what we have observed in the proteomic analysis of cancer-invaded nerves. QRT-PCR analysis revealed significant induction of VGF gene expression in PC12 cells co-cultured with MiaPaca2, Capan1 and BxPC3 cells but not with Panc1 cells (**Figure 38**).

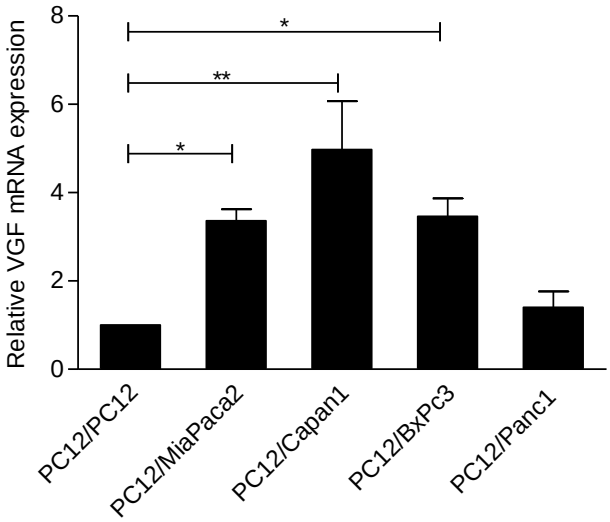

Figure 38. VGF gene expression in PC12 cells co-cultured with several PDAC cell lines. Values are relative to PC12 only co-culture. *p<0.05, **p<0.01

Next, we determined the level of VGF protein expression under these conditions using Western blot. Similar to gene expression, VGF protein was up-regulated by two fold in PC12 cells co-cultured with the same cell lines (**Figure 39**). Hence, MiaPaca2, Capan1 and BxPc3 cells are able to, induce VGF expression in PC12 cells in the Transwell co-culture system at both mRNA and protein levels.

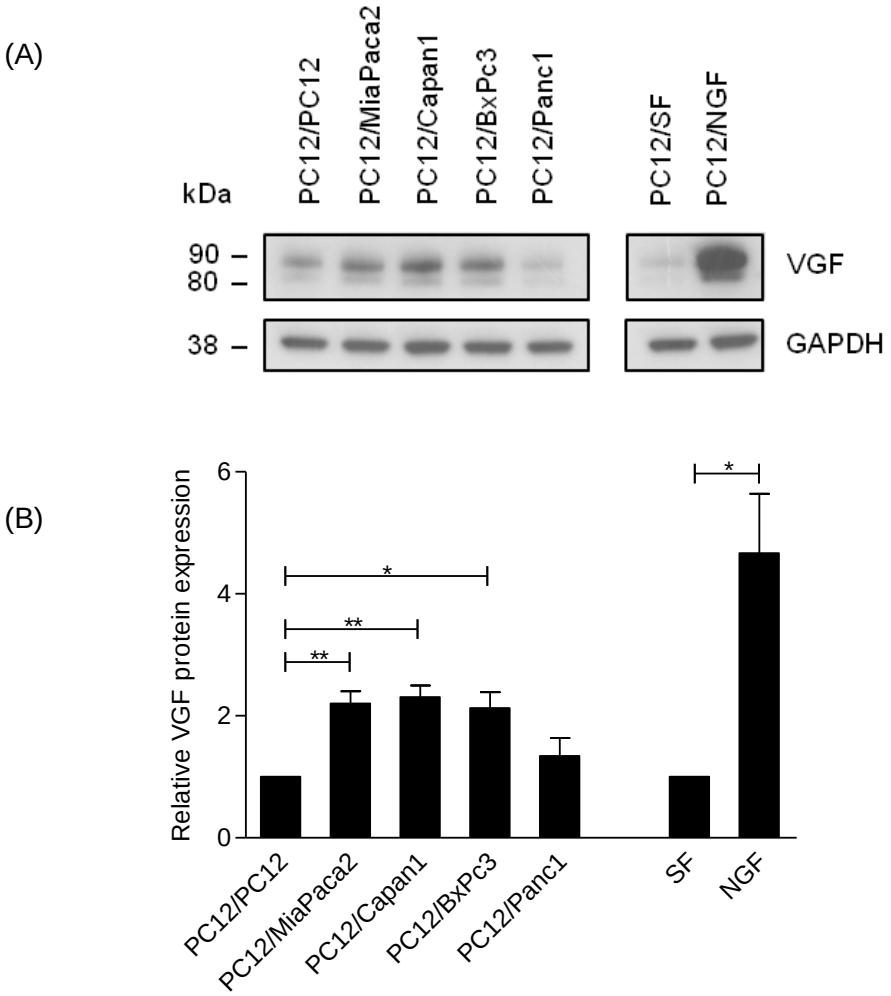

Figure 39. VGF protein expression in PC12 cells in Transwell co-culture with PDAC cell lines or with PC12 as control. A representative Western blot is shown. VGF appear as a doublet at ~80 and ~90kDa, the lower band is thought to be a limited proteolytic product of the upper one [227] (**A**). Densitometry analysis of three independent experiments. Bands are normalized to GAPDH as a loading control and the results are expressed as fold change relative to control (**B**). SF: serum free media. *p<0.05, **p<0.01

As PDAC cell lines were able to induce plasticity in PC12 cells along with up-regulation of VGF, we investigated whether PDAC cell lines are also able to induce the expression of other proteins that we have observed as up-regulated in invaded nerves in our proteomic analysis. We selected two of these proteins, Nestin (NES) and Neuromodulin (GAP43) as they have been linked with neuronal plasticity in PDAC and CP. NES has been reported to be associated with PNI and expressed at a higher level in invaded nerves [195, 228]. Similarly, Neuromodulin (GAP43) is a neuroplasticity marker that has been shown to be up-regulated in PDAC and CP related pancreatic neuropathy and neuroplasticity [81]. Indeed, the expression of both proteins was significantly increased in PC12 cells co-cultured with Capan1 or BxPc3 cells (**Figure 40**). Interestingly, VGF and GAP43 but not NES were induced in PC12 upon NGF treatment.

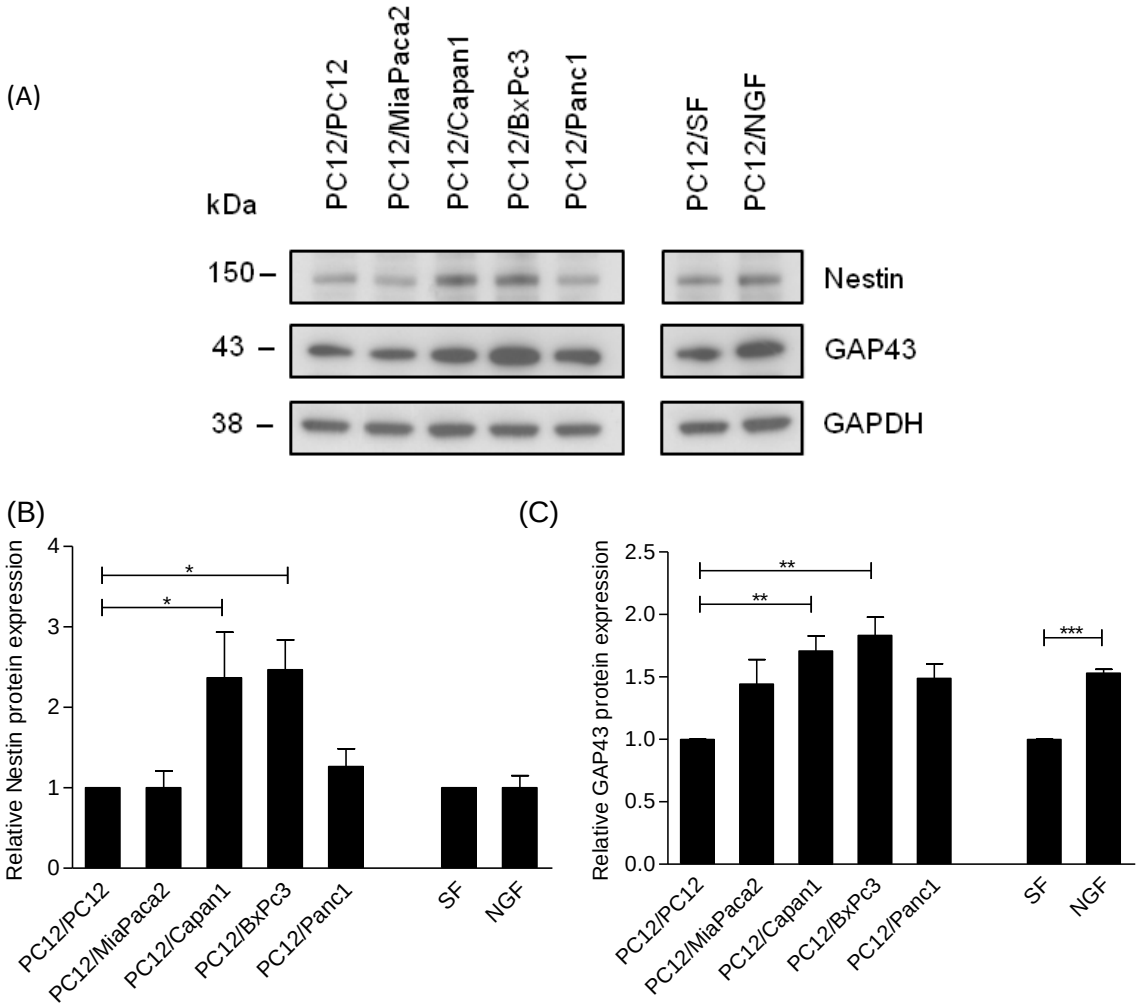

Figure 40. Western blot analysis of PC12 cells in Transwell co-culture. Representative Western blot of the expression of Nestin, Gap43 and cleaved caspase-3 (**A**). Densitometry quantitation of Nestin (**B**) and GAP43 (**C**). GAPDH was used as a loading control.*p<0.05, **P<0.01, ***p<0.001

3.5.2. Contact co-culture system

The Transwell co-culture model allows free exchange of media and soluble factors between the two cell types in a similar manner to PNI. Our data indicate that PDAC cell lines are able to induce phenotypic and molecular plasticity in PC12 cells similar to published observations and our proteomic data. However, because we observed even stronger VGF immunoreactivity in the nerves as they come in close contact with cancer cells, we used a contact co-culture to further test whether our co-culture system could recapitulate this pattern of VGF expression in human PDAC tissues. In this system, PC12 cells were seeded, stained with CellTracker fluorescent dye and PDAC cell lines were subsequently added to achieve a direct contact with PC12 cells as detailed in the Methods section.

24 hours later, the co-cultured cells were separated based on the CellTracker using FACS sorting, and PC12 cells were collected and used for downstream analysis. For Annexin V/DAPI assay, both floating and attached cells in the co-culture were collected and following Annexin V and DAPI staining, survival was measured in PC12 cells (positive population for the CellTracker).

PC12 isolated using FACS sorting were re-checked for purity using the same FACS setting. Purity of the samples was 97% ±1.6 (mean ± SD). In addition, aliquots of the post-sorting PC12 cells were seeded on coverslips and immunocytochemistry staining with anti-CK19 antibody was performed to assess epithelial contamination. The purity of PC12 cells was >99% based on CK19 staining (**Figure 41**).

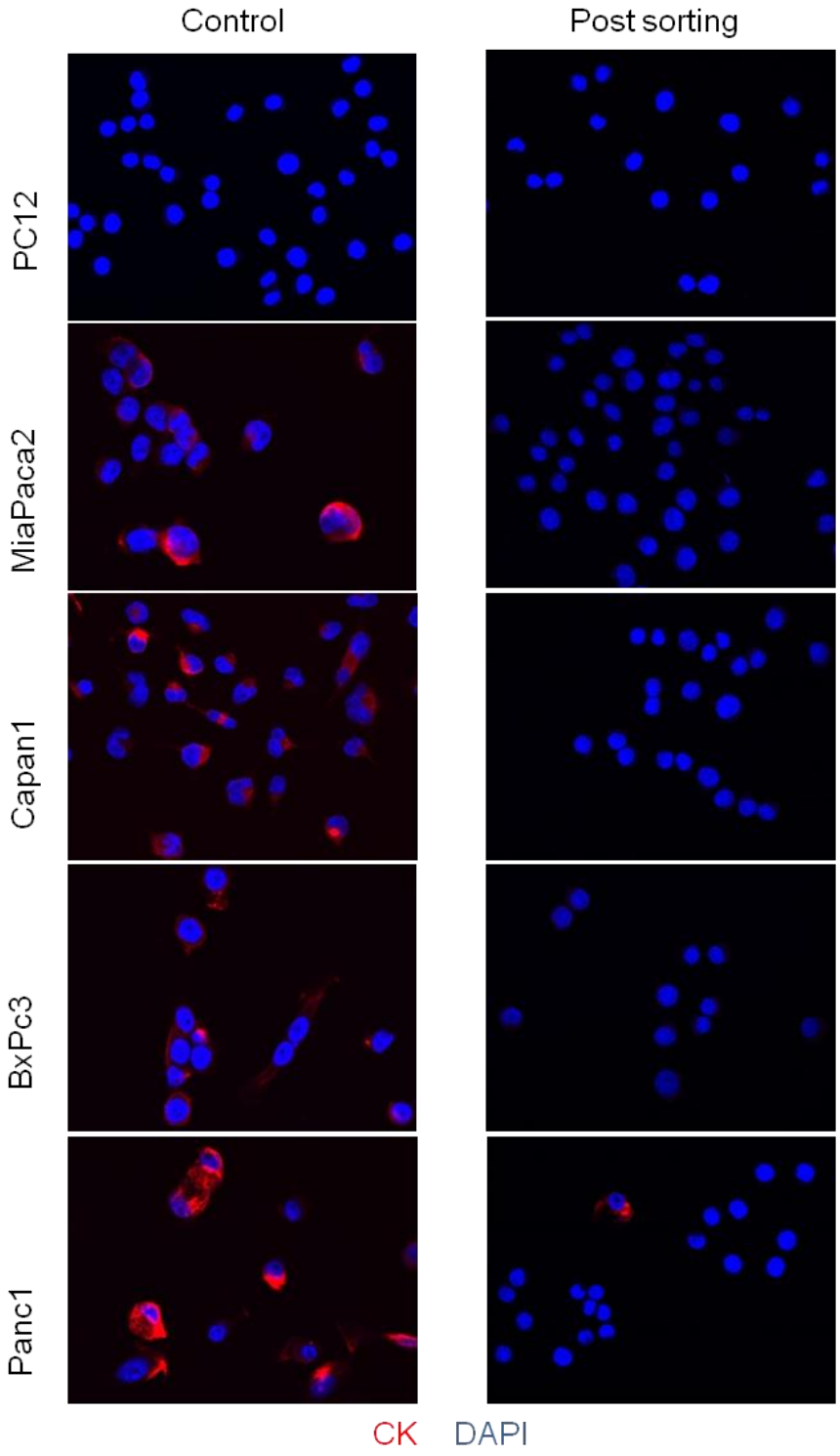

Figure 41. Immunocytochemistry staining of post-sorting PC12 using anti-CK19 antibody. Representative images (x400 magnification) of post-sorting PC12 cells (right panel), the lack of CK staining indicates high degree of purity. PC12 cells and PDAC cells on their own were used as negative and positive controls, respectively (left panel). DAPI was used to stain nuclei.

Similar to what was seen in the Transwell co-cultures, PDAC cell lines in the contact co-culture protected PC12 cells from serum-starvation induced apoptosis (**Figure 42A**). Furthermore, PC12 cells co-cultured with Capan1 cells appear to survive even better in the contact compared to the Transwell co-culture (**Figure 42B**).

(A)

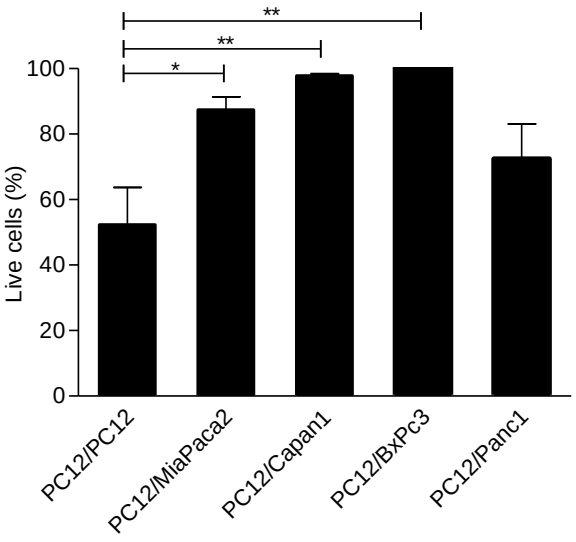

(B)

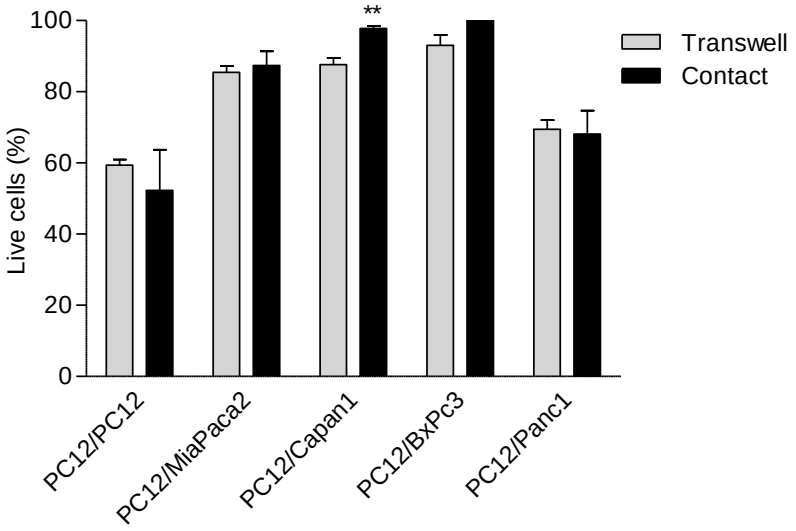

Figure 42. PC12 cell survival measured using Annexin V /DAPI flow-cytometry assay in contact co-culture (**A**) and both Transwell and contact co-cultures depicted on the same graph (**B**). Capan1 cells further increased the survival of PC12 cells when in direct contact compared to Transwell co-culture. *p<0.05, **p<0.01

Furthermore, VGF induction in PC12 cells was stronger in contact compared to Transwell co-culture. This, approximately two-fold, increase in VGF protein expression was observed for all PDAC cell lines including Panc1, which did not induce strong expression of VGF in the Transwell co-cultures (**Figure 43**). This is therefore reminiscent of what we have observed in pancreatic nerves in the context of PDAC.

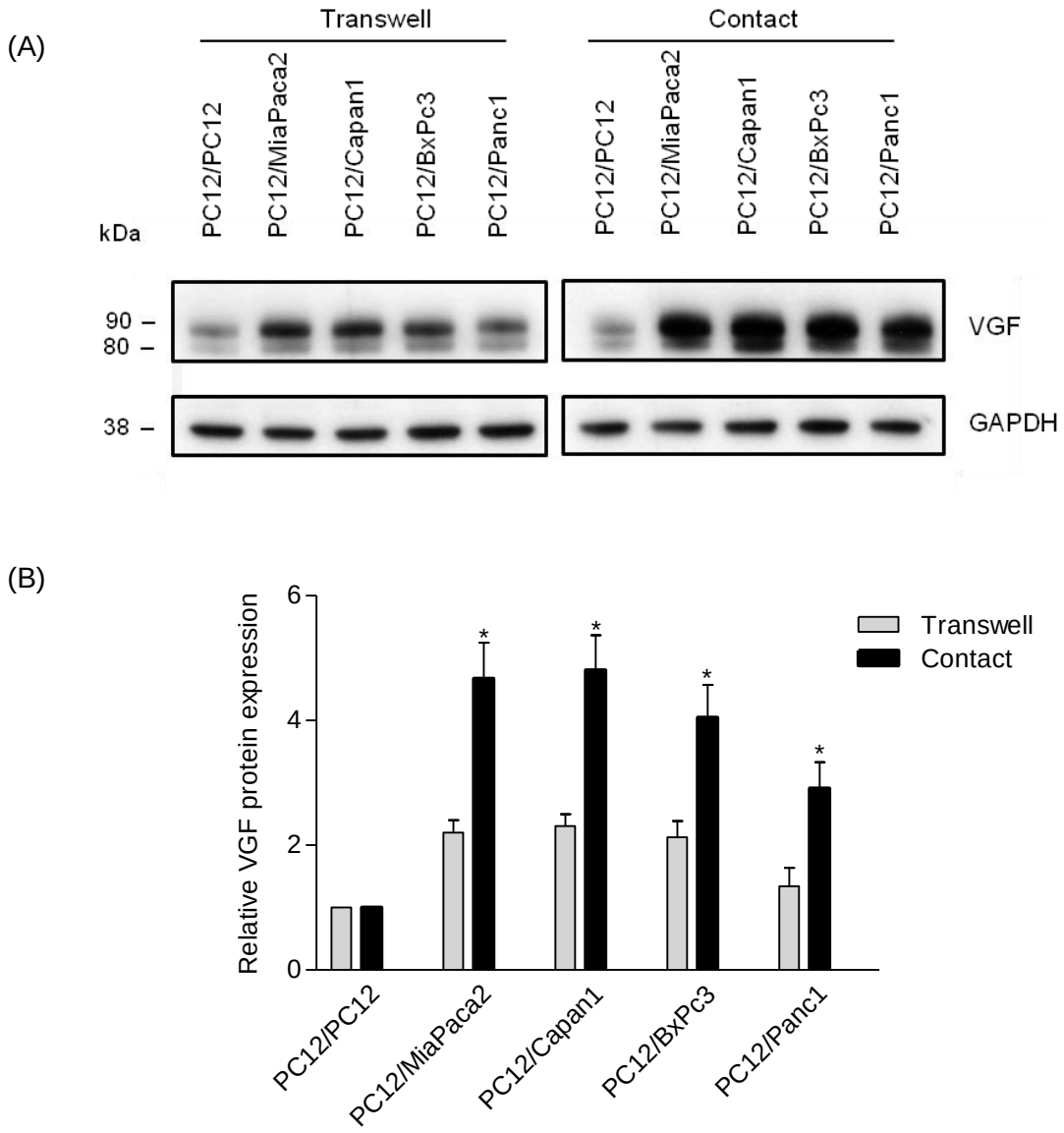

Figure 43. Induction of VGF protein expression in PC12 cells in Transwell and contact co-culture systems. Representative Western blot showing the higher increase in VGF protein expression in the contact co-culture for all four PDAC cell lines tested (**A**). Densitometry of three independent experiments illustrates the statistically significant increase in VGF expression (**B**). GAPDH was used as a loading control and data expressed as fold change relative to control. *p<0.05

3.5.3. Role of NGF in PC12 plasticity induced by PDAC cells

NGF has been suggested to be an important factor in PNI as well as in generation of pain in pancreatic cancer, CP and other non-pancreatic diseases [71, 106, 107]. Clinical trials are ongoing to evaluate targeting of NGF-Trk signalling pathway as a potential pain modulation strategy [107]. NGF is also a well-known inducer of neuroplasticity and differentiation in PC12 cells as mentioned previously and as our data show.

Because several of the effects of PDAC cell lines on PC12 cells mimic those of NGF, we sought to investigate whether the observed effects are mediated via NGF. In the first instance, we tried to determine whether the three PDAC cell lines that induced PC12 plasticity (MiaPaca2, Capan1 and BxPc3) express and secret NGF. It has been previously reported, using ELISA, that whilst MiaPaca2 and Panc1 and to a lesser extent Capan1 cells express NGF, only MiaPaca2 and Panc1 secreted NGF in their conditioned media [160]. Of note, Panc1 cells were not able to induce PC12 plasticity in our co-culture system. We used the same ELISA to measure NGF in the lysates and conditioned media from MiaPaca2, Capan1 and BxPc3. However, the ELISA did not work in our hands, including with the positive control (rat brain lysate). Using Western blot, we observed, inconsistently, bands corresponding to NGF in the lysates and sometimes in BxPc3 conditioned media (data not shown). The authenticity of our cell lines have been confirmed using STR profiling. Nonetheless, we determined that functional testing for potential effects of NGF would answer whether NGF is contributing to the PC12 plasticity phenotype we observed in the co-culture system. To achieve this, we treated PC12 cells with conditioned media from MiaPaca2, Capan1 and BxPc3 cells with or without K252a, a known inhibitor of TrK receptor (NGF receptor) that blocks the phosphorylation of the Trk receptors (A, B and C) and thus blocks the effects of NGF as well as other neurotrophins that act through the same receptor such as BDNF and NT3 [207].

We initially optimised the dose of K252a required to neutralise NGF effect on PC12 cells. Based on literature reports, we tested three different concentrations of K252a and found that at 30nM, K252a blocked the survival (**Figure 44**), neurite extension (**Figur45A**) as well as VGF expression induced by NGF (**Figure 45B** and **C**).

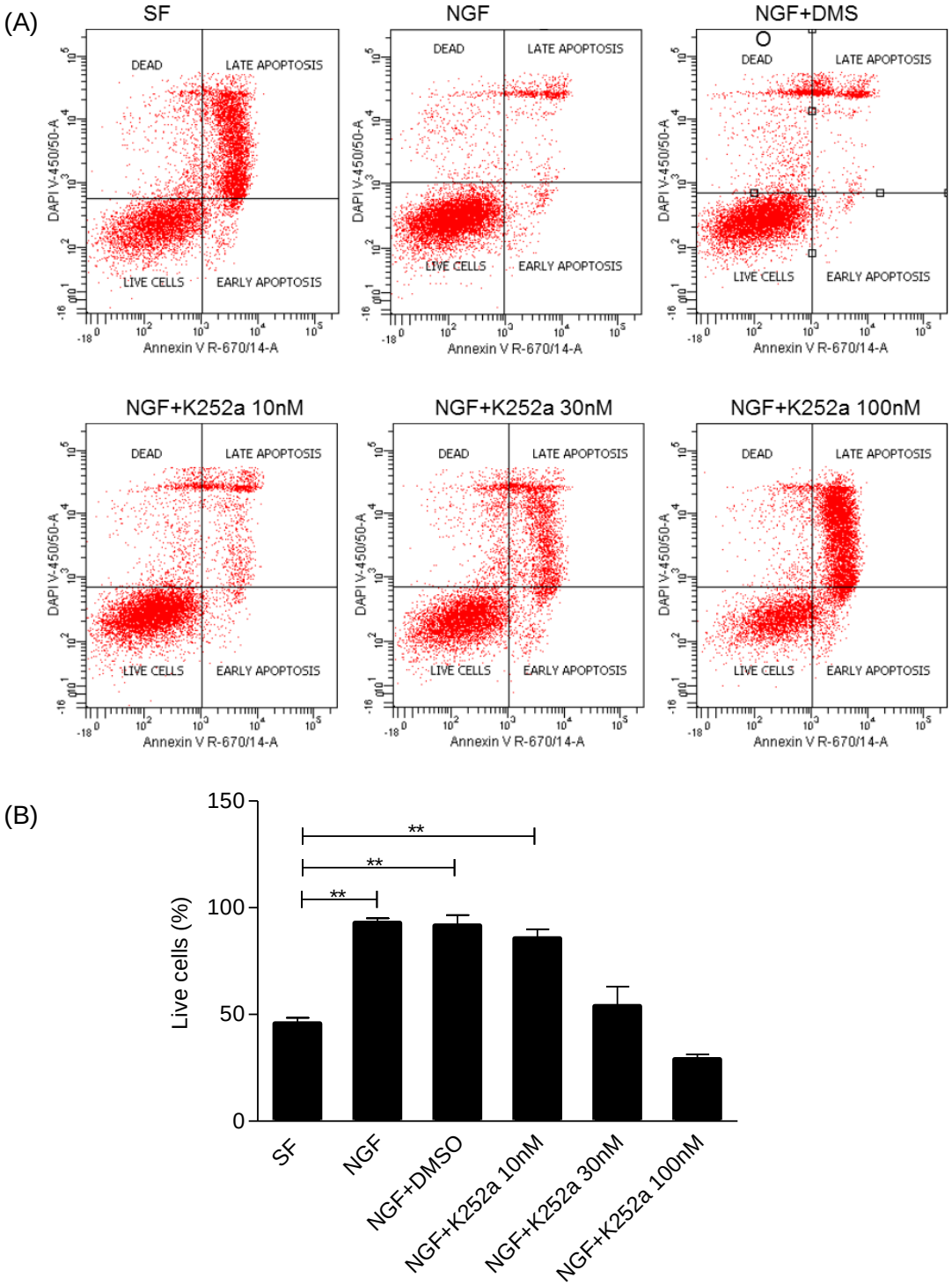

Figure 44. Optimisation of the K252a concentration required to block NGF effects on PC12 cells. PC12 cells were treated with 50ng/ml NGF with either K252a in various concentrations or vehicle only (DMSO) in serum-free (SF) conditions. Serum-free alone and NGF alone were used as positive and negative control, respectively. Flow cytometry analysis using Annexin V/DAPOI (**A**). Quantitation of flow-cytometry data from two independent experiments. Live cells are expressed as a percentage relative to live PC12 cells growing in complete media (**B**). ** $p<0.01$

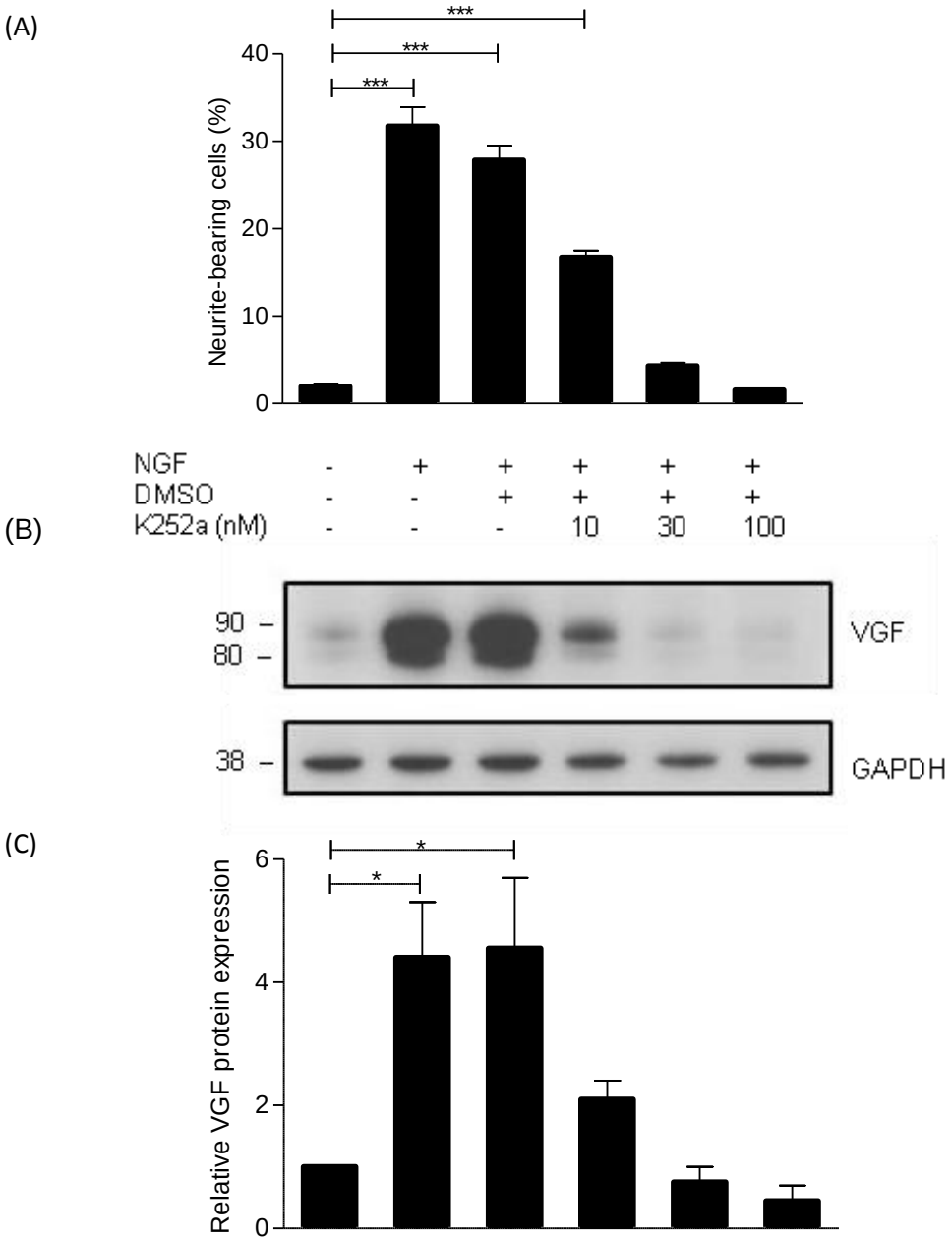

Figure 45. Optimisation of K252a concentration required to block NGF-induced neurite extension and VGF induction. PC12 cells were treated with 50ng/ml NGF with either K252a in the stated concentrations or vehicle only (DMSO) in serum-free conditions. Serum-free alone and NGF were used as positive and negative controls respectively. Number of PC12 cells extending neurites was expressed as a percentage of total cells (A). A representative Western blots showing VGF protein expression (B), and Densitometry quantitation of VGF protein expression (n=2). *p<0.05 *** p<0.001

Next, PC12 cells were treated with PDAC cell lines conditioned media in addition to either 30nM K252a or DMSO and PC12 cells survival, neurite extension as well as induction of VGF expression were determined. K252a failed to abrogate PC12 cells

neurite extension and VGF expression induced by PDAC cells conditioned media suggesting that these effects are not mediated via NGF (**Figure 46**). It was somewhat surprising that the neuritogenic effect of MiaPaca2 conditioned media was in fact augmented by K252a. Similar trend was noted for BxPc3 conditioned media although this did not reach statistical significance.

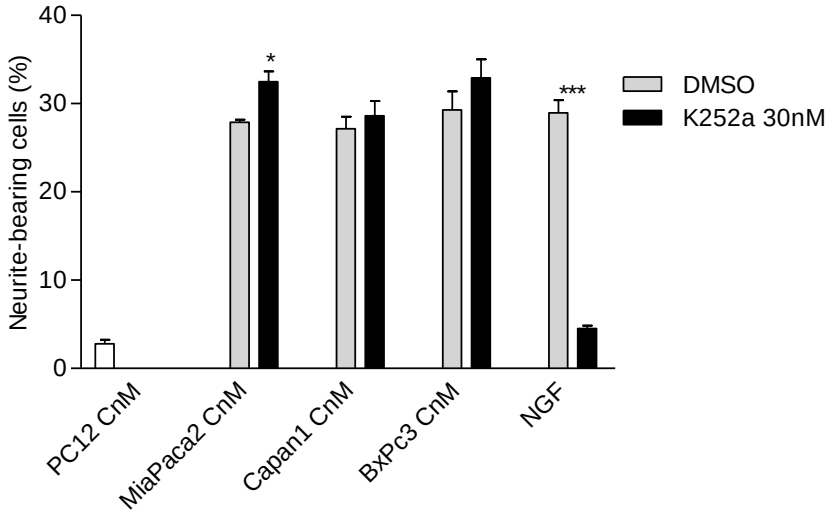

Figure 46. PC12 neurite extension following treatment with PDAC cell lines conditioned media (CnM) with 30nM K252a or DMSO. NGF was used as a positive control. *p<0.05

Treatment with K252a also could not reverse PC12 survival induced by PDAC cells conditioned media (**Figure 47**).

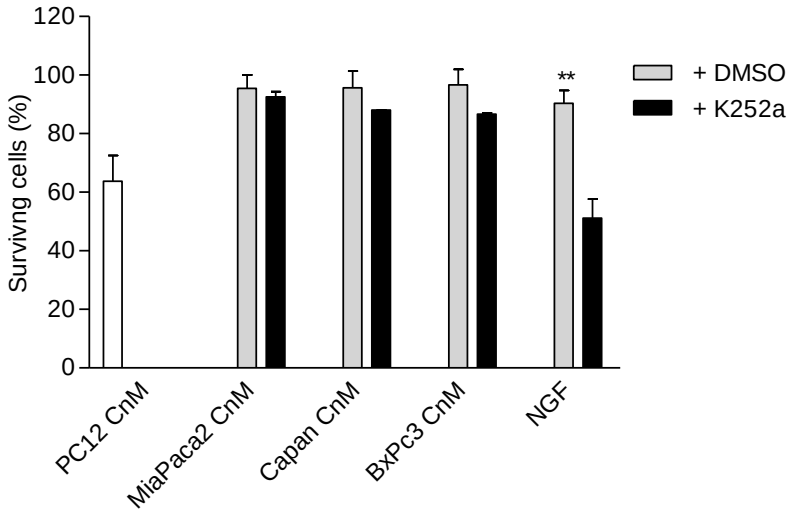

Figure 47. PC12 cells survival as determined by Annexin V/DAPI flow-cytometry assay following treatment with PDAC cell lines conditioned media (CnM) with 30nM K252a or DMSO. NGF was used as a positive control. **p<0.01

Finally, K252a was also not able to block the PDAC cells mediated up-regulation of VGF protein in PC12 cells (**Figure 48**).

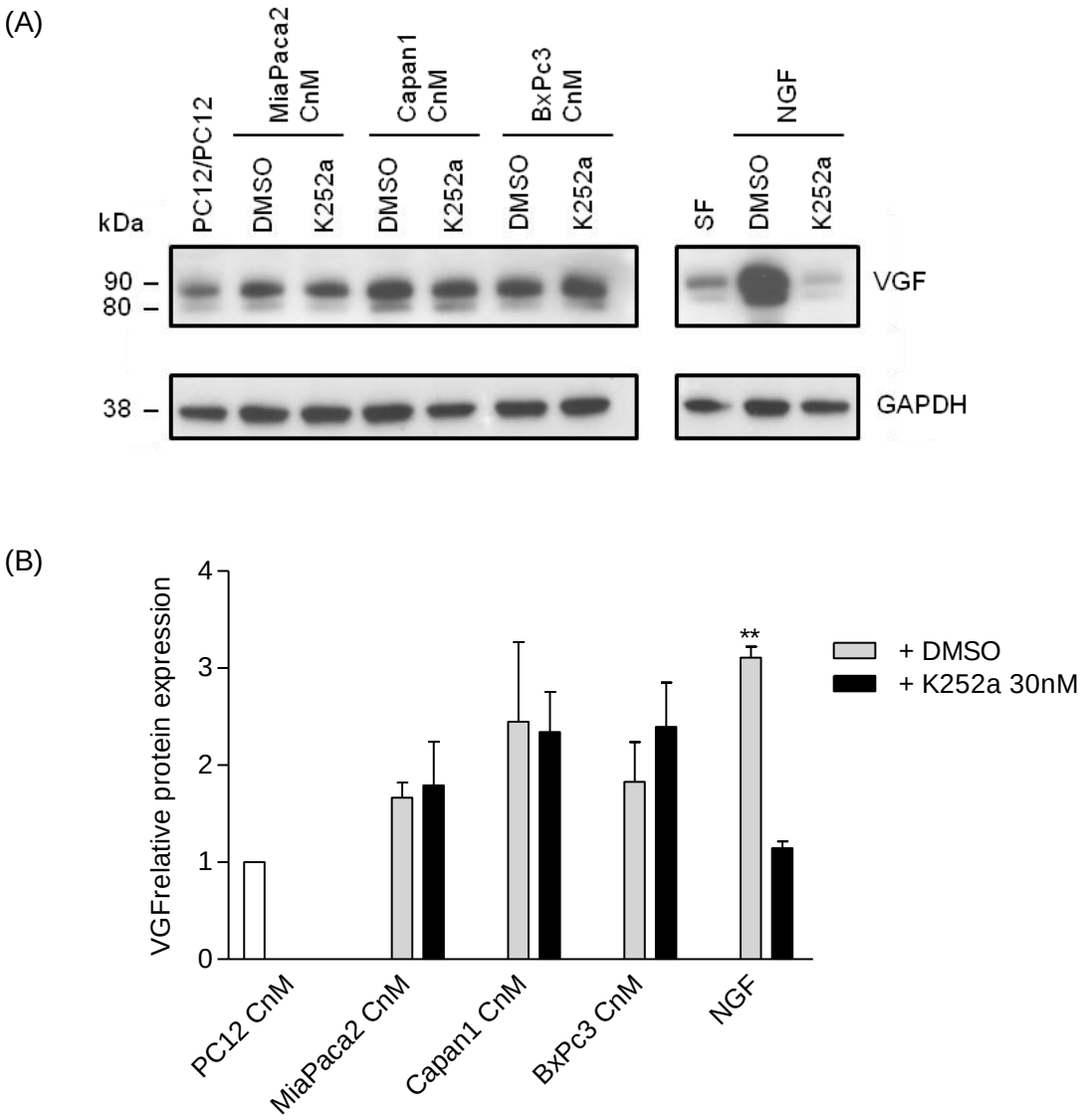

Figure 48. VGF protein expression in PC12 cells following treatment with PDAC cell lines conditioned media (CnM) with 30nM K252a or DMSO. NGF was used as a positive control. A representative Western blot (**A**) and densitometry quantification of VGF protein expression relative to control (PC12 CnM treatment) (**B**). GAPDH was used as a loading control.

These experiments indicated that while NGF is capable of inducing PC12 cell plasticity, its presence in the PDAC cells conditioned media is not necessary for the plasticity induced by PDAC cells.

3.5.4. Role of VGF in PC12 cells plasticity induced by PDAC cells

VGF has been recently suggested to play a role in cell survival [220] and neuronal plasticity [229]. Due to the observed pattern of induction of VGF that mirrors the PC12 survival and neurite extension, we tested whether VGF could mediate some of these changes. In order to investigate that, we used VGF-specific siRNA to block the induction of VGF expression by PDAC cell lines conditioned media. The siRNA successfully prevented the up-regulation of VGF as shown in **Figure 49**. Of note, we optimised the siRNA experiment to block the induced VGF expression but to maintain the basal levels of VGF at our time point of interest (24 hours).

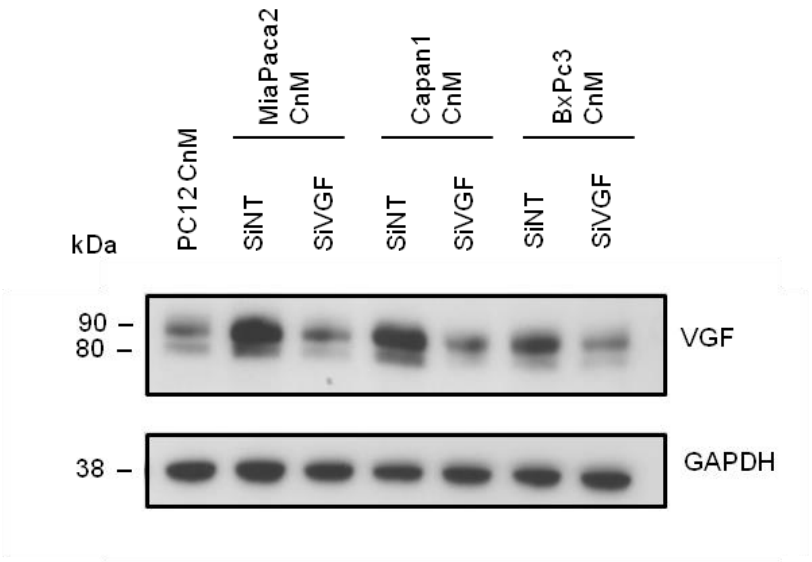

Figure 49. SiRNA mediated block of VGF induction by PDAC cells conditioned media (CnM). Following gene silencing using VGF-specific siRNA or a non-targeting siRNA, PC12 cells were then treated with PDAC cells as detailed in the Methods section. Cells were harvested following 24 hours treatment with CnM. Representative Western blot showing that the VGF siRNA maintained the baseline level of VGF preventing its up-regulation.

24 hours after treatment with conditioned media, we measured neurite extension as well as cell survival. Using Annexin/DAPI flow-cytometry assay we could not detect any significant difference in survival after blocking VGF induction (**Figure 50**).

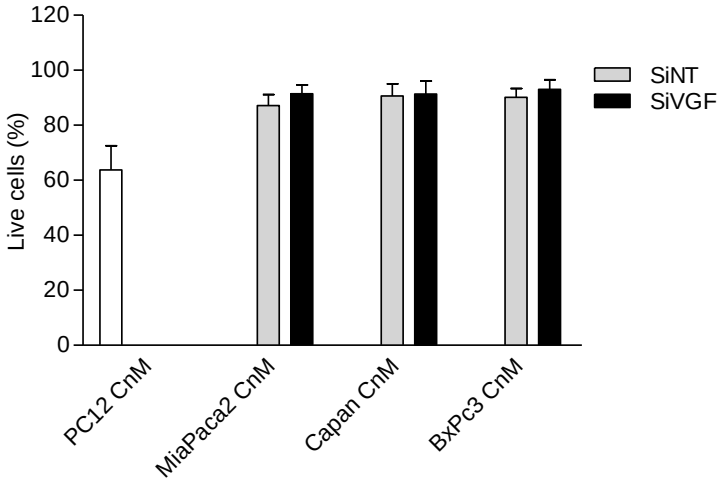

Figure 50. PC12 cell survival analysis following VGF siRNA or non-targeting siRNA using Annexin v/DAPI flow-cytometry assay. Survival was expressed relative to live cells in complete growth media.

PC12 neurite extension, on the other hand, was reduced with all PDAC cell lines' conditioned media treatment when blocking VGF induction. This was statistically significant for both MiaPaca2 and BxPc3 conditioned media but did not reach statistical significance for Capan1 conditioned media (p=0.09) (**Figure 40**). Hence, VGF appears to contribute significantly to the neuroplasticity response of PC12 cells to PDAC cells. It is clear however, that VGF is only part of the molecular machinery driving this response.

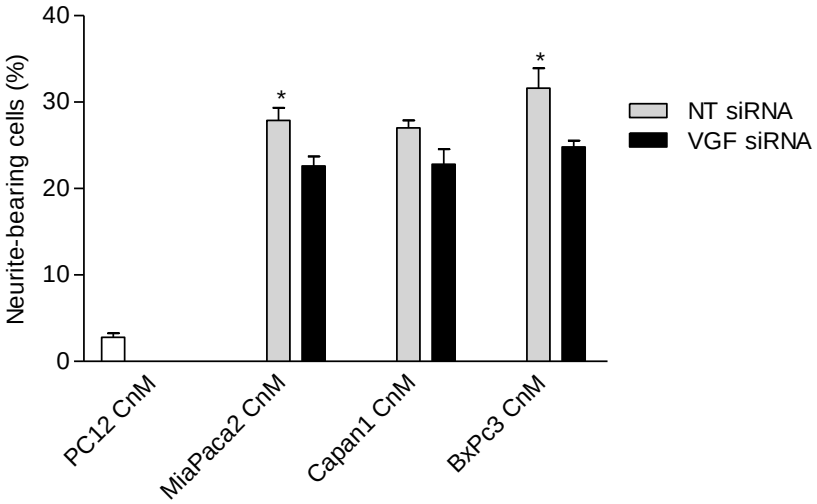

Figure 51. PC12 cells neurite extension induced by PDAC cells CnM with or without blocking VGF induction by siRNA pre-treatment. Blocking VGF induction significantly reduced the neurite extension in PC12 cells mediated by both MiaPaca2 and BxPc3 conditioned media.*p<0.05

Chapter Four: Discussion

4. Discussion

4.1. 1D and 2D Proteomics of FFPE tissues

In this project, we set out to investigate the molecular alterations in nerves and cancer cells involved in PNI in PDAC and develop an *in vitro* model that would recapitulate these changes. Firstly, we performed proteomic analysis of PNI lesions to identify differentially regulated proteins and pathways between PNI and non-PNI cancer as well as between invaded and non-invaded nerves. The limited availability of fresh frozen tissues and the infrequent occurrence of PNI lesions within histological sections of small fresh frozen material necessitated the use of FFPE PDAC tissues. Until recently, protein expression profiling of FFPE tissue samples has been met with very limited success due to formalin-induced modifications resulting in difficulties in extracting good quality soluble proteins from such samples [230, 231]. Proteomic analysis using FFPE tissues has, therefore, been largely limited to immunohistochemistry, a technique that can only target previously known single proteins in order to assess their expression in a particular tissue types. However, recent advances in protein extraction and MS techniques allowed an unprecedented ability to compare global protein expression in the large archives of FFPE samples enabling the discovery of potential novel disease biomarkers in several tissue types [232, 233]. Plethora of studies have demonstrated the equivalence of proteomic profiles of FFPE tissues to those obtained from fresh frozen samples using a variety of tissue types and proteomic analysis platforms including gel-based methods [234, 235], MS [214, 215, 236, 237] and protein arrays [230, 238]. Furthermore, proteins extracted from FFPE tissues also retain protein expression data related to subproteomes such as phosphoproteins and glycoproteins [239]. In pancreatic cancer, a recent study has demonstrated, using gel-based techniques, comparable protein pattern between FFPE and frozen PDAC tissues but a lower concentration of proteins was obtained from the FFPE samples [235]. In addition, comparison of the proteomic profiles of fresh frozen and FFPE normal pancreas using LC-MS revealed similar protein identifications and subcellular localisation [231]. This success is mainly attributed to the newly developed protein extraction methods that rely principally on heat-induced antigen retrieval methods as well as detergents [215, 216, 236]. In this project, we used Liquid Tissue (LT) buffer, a proprietary reagent that was specifically designed to extract proteins from FFPE tissues and particularly tailored to minute amounts of samples such as those procured by laser microdissection [240]. Using LC-MS, this

buffer enabled the acquisition of equivalent proteomic data from fresh frozen and FFPE liver and kidney tissues [214, 233]. Several other studies have also successfully reported the usage of this buffer for large scale MS based proteomic profiling of FFPE tissues resulting in identification of hundreds of proteins from several tissue types including prostate, lung and brain tissues [214, 241-243]. This method allowed us to extract ~15µg of peptide digest/10mm^2 tissue area, which is in line with published literature using LT [237] as well as other protein extraction protocols [238]. Using 1µg of normal pancreas digest we were able to confidently identify 1,000 peptides and 187 proteins with ≥ 2 peptides/proteins and an FDR of 0% from two replicate LC-MS analyses. It is difficult to compare this head to head with other studies due to differences in sample processing, LC-MS protocols and platforms and data analysis methods. In a review of FFPE proteomics studies, Reimel *et al* reported the identification of 1,168 peptides and 370 proteins from normal pancreas FFPE tissue and 990 peptides and 340 proteins from frozen samples [231]. Our results are comparable in terms of peptide identifications; however, the minimum number of peptides used for protein identification in the mentioned study was not specified. Also consistent with our findings, a recent study using LC-MS/MS and mice pancreas tissue reported the identification of 237 and 271 proteins from 8 biological replicates of FFPE and fresh frozen samples respectively with 80% overlap and similar molecular function and subcellular localization [244]. Cheung *et al* also reported proteomic profiling of pancreatic intraductal papillary mucinous neoplasm (IPMN) from FFPE tissues using LT and LC-MS. They identified 1,534 peptides corresponding to 523 proteins, 95 of which were identified with ≥2 peptides [241]. Our results are also consistent with studies using other tissues such as colon and kidney [214, 233, 243].

Proteomic analysis using 1D LC-MS provides proteomic coverage limited to the highly abundant proteins and multidimensional fractionation is necessary to achieve adequate depth of complex proteome analysis [245]. To perform 2D LC-MS using our samples, several challenges had to be resolved. Firstly, the amounts of proteins obtained from laser microdissected samples, particularly for PNI, are typically minute necessitating some degree of pooling to allow downstream fractionation. Secondly, our protein extraction protocol allows only for fractionation at the peptide level, as the final product is a mixture of peptides rather than full-length proteins. Lastly, HPLC fractionation of such minute amounts of peptides requires a capillary/nano HPLC platform whereas the system available to us was a standard analytical HPLC.

The most commonly used technique of peptide fractionation is strong cation exchange (SCX) in different formats including off-line, on-line and MudPIT [246]. In this method, peptides are first fractionated primarily based on their charge using SCX stationary phase; each fraction is then submitted to RP LC-MS analysis in the second dimension. Because SCX and RP utilize two different properties of peptides for separation, charge and hydrophobicity, respectively, a good orthogonality is achieved [247, 248]. Recently, high pH RP fractionation in the first dimension has been introduced and is being increasingly used. In this workflow, peptides are separated based on hydrophobicity using RP stationary phase in both dimensions with a high pH mobile phase in the first dimension and low pH in the second [249]. This change in pH results in modification of the charges of some amino acids and therefore peptide hydrophobicity resulting in different selectivities in the two dimensions [250]. Several studies have evaluated this method in comparison to other techniques particularly SCX [250, 251]. High pH separation in the first dimension has an orthogonality that is comparable to SCX, however, because of the high resolving power of RP, the practical peak capacity of RP-RP workflow is much higher than SCX-RP resulting in superior separation efficiency and therefore higher number of peptide and protein identifications [247, 249, 252] In addition, RP separation results in lesser sample loss often associated with SCX, especially the off-line variety and avoids the need for sample preparation, particularly desalting prior to fractionation [252, 253].

With these considerations in mind, our proteomic analysis workflow involved 1D LC-MS analysis of all samples, individually, and 2D LC-MS analysis of pooled and matched samples of PNI cancer and non-PNI cancer. To perform the latter, we, firstly, converted our standard analytical HPLC into a capillary system using T-piece and restriction capillary to split the flow and validated the reproducibility and enhancement of protein coverage achieved by high pH fractionation using the converted system. At 380µl pump flow rate and using a 50cm restriction capillary with 50µm internal diameter, we were able to achieve a stable and reproducible column flow of 5µl/min throughout the separation gradient. The chromatographic reproducibility of BSA digests fractionation and inter- and intra-day reproducibility further demonstrated the robustness of the system. To further assess the degree of reproducibility and the improvement in the depth of proteomic analysis following high pH RP fractionation, we first fractionated 10µg of MiaPaca2 cell line digest into 14 fractions, in duplicate, and submitted each fraction as well as unfractionated samples to LC-MS analysis. This demonstrated high qualitative and quantitative

reproducibility of proteomic data obtained from 2D LC-MS analysis approaching the analytical reproducibility of the LC-MS itself. Equally important, the fractionation process resulted in a 5-fold increase in the number of proteins identified (340 vs 1602 proteins). In an on-line version of 2D LC-MS using high pH fractionation in the first dimension, Siu *et al* identified ~12,000 peptides and ~2,500 proteins (≥1peptides/protein) from 13 fractions of mouse fibroblast peptide digest over 52 hours of MS time [254]. Another study also obtained protein identifications comparable to ours (1,338 proteins from 12 fractions of frozen mouse cardiac tissue digest, 100µg fractionated) [251]. The number of proteins identified from normal pancreas FFPE tissue digest (~1,000) was smaller but the improvement in the depth of analysis as well as reproducibility was similar to that of the cell lines. In agreement with our results, a recent study using FFPE renal tissues identified ~ 250 and ~500 proteins (≥1peptide/protein) from 1D and five fractions 2D LC-MS, respectively, using high pH RP fractionation [216]. Of note, collecting only 14 fractions largely reduces the resolving power of the first dimension and therefore the power of the 2D LC-MS method; however, larger number of fractions would have large impact on LC-MS time and therefore the throughput and the overall cost of the whole method.

The largest FFPE proteome coverage using MS was achieved in the laboratory of M. Mann [255, 256]. In their latest report, extensive proteomic analysis of microdissected FFPE tissue from colon adenoma was performed using a combination of heat and detergent based protein extraction, multi-enzyme digestion, strong anion exchange fractionation and the latest MS platform resulting in the identification of ~8500 proteins per sample [257]. This not only illustrates the importance of incorporating multiple strategies in order to increase the proteome coverage but also the rapid progress in the field of proteomics and particularly FFPE proteomics.

4.2. Laser microdissection

In the last decade, Laser Microdissection (LMD) has emerged as an effective and elegant way of collecting homogeneous cell populations whilst avoiding many of the pitfalls of manual microdissection. Several recent reports have emphasized the role of LMD in revealing tumour cell specific molecular alterations that could not be detected using bulk tissue analysis [258, 259]. Furthermore, the authenticity of the dissected material can be directly verified and documented by microscopic visualisation. LMD can be used to dissect groups of cells, individual cells or even subcellular organelles for a variety of downstream molecular analyses including genomic, RNA and protein analysis using various platforms [260]. The process of LMD itself appears to have minimal impact on downstream molecular analysis [261-263]. Most of the biological material in the path of the narrow cutting laser is completely destroyed and does not take part in subsequent analysis and heat conduction to the dissected material is limited to <1µm for few microseconds [264] .

On the other hand, optimal microscopic visualisation requires preparation and staining of tissue sections that could interfere with downstream analysis and add to the experimental variables. For example, whilst both toluidine blue and hematoxylin have been shown to be compatible with proteomics analysis using both gel-based and MS-based methods, toluidine blue should be removed prior to analysis [262, 265]. Eosin, on the other hand, may affect protein focusing in 2 dimensional electrophoresis (2DE) [266]. We used a short (15min) preparation protocol for tissue sections that involved rapid deparafinization, rehydration and hematoxylin-only staining as this is compatible with our protein extraction protocol and downstream LC-MS analysis. The sections were then dehydrated, stored at 4°C and used within two weeks. Of note, the samples that were microdissected were completely matched, not only biologically but also technically, as they were microdissected from the same tissue sections. Therefore, PNI and non-PNI cancer samples as well as nerve samples have undergone the same tissue fixation and processing as well as tissue section preparation, staining and storage. From the point of microdissection, downstream experiments were performed in parallel.

Samples collected using LMD are typically limited and require optimised protocols for extraction and subsequent analysis of biological molecules. The number of cells required depends on the desired molecular analysis. While mutation analysis can be performed on single cells, gene expression profiling often requires 100s-1000s of

cells while proteomics often require thousands of cells depending on the analytical platform [260]. Recently, several approaches have been developed for proteomic analysis of laser microdissected specimens [262, 267]. As previously mentioned, in this project we used a commercially available kit, Liquid Tissue (LT) (Expression Pathology) that has been specifically designed for protein extraction from small FFPE samples for subsequent MS-based proteomic analysis [237].

Despite the advantages of LMD, it remains true, that procurement of samples using this technique is time consuming. The obtainment of our specimens involved more than 600 hours of laser microdissection time. However, the high homogeneity of the specimens was necessary in order to generate high quality data in downstream profiling experiments. In addition, the nature of PNI lesions requires high degree of precision to isolate cells from such specific tissue compartments. The collection of both the nerves and cancer specimens would not have been possible without the LMD technique.

Purity of samples collected by LMD

Because the aim of LMD is to procure highly homogenous and pure samples, one of the key issues is the degree of purity of the collected material and its potential contribution to aberrant differential expression. This was particularly important in this study as cancer and nerves are in a close proximity within the PNI lesions. Several studies assessed the relative purity of collected material within the context of gene expression profiling [268, 269]. This is relatively straightforward task, as global gene expression studies involve hybridization of all samples to a known set of probes and therefore the signal attributed to a particular gene relies primarily on its absolute expression level, the levels of cell-specific genes can subsequently be used to assess the cross contamination. In global proteomic analysis using MS, on the other hand, peptides (and hence proteins) compete for identification and the detection of a particular protein in two different samples relies primarily on its abundance in the sample relative to the other proteins as well as the depth of proteomic coverage (assuming similar protein modifications, equal digestion and MS/MS fragmentation efficiency). This is particularly true for low abundance proteins such as cross-contaminants. Although qualitative assessment of the purity of LCM samples have been attempted in the context of proteomic analysis [270], we are not aware of any proteomic studies that tried to evaluate that quantitatively. Here we

used an approach that, similar to ones used in gene expression studies, relies on the expression of known tissue-specific markers to gain insight into the relative enrichment or depletion of that particular tissue type. Because this requires the analysis of both tissue types in a similar way, our 1D analysis of cancer and nerve samples allows us to perform this type of analysis. Using this approach, we looked at the expression levels of several neuronal makers in the PNI cancer samples and compared their relative abundance to that in invaded nerves. This revealed variation in the estimated contamination depending on the protein evaluated. Using the relative abundance values for four neuronal proteins (NEFH, GFAP, S100B and VGF), the estimated purity of three of the five PNI cancer samples was ≥99%, whilst the other two samples showed 96% and 98% enrichment. Whilst this represents high degree of purity, several factors could have contributed to the low level of contamination observed. In addition to the close proximity of PNI cancer and invaded nerves, inadvertent catapulting of loose non-target tissue could have contributed. Furthermore, as the tissue section thickness is 10µm, the demarcation between neuronal and epithelial components is not necessarily similar on the top of the section compared to the bottom [270]. This, however, is unavoidable except by using thinner sections, which would, in turn, reduce protein yield and significantly increase the total dissection time.

Using the same approach, we were not able to identify any epithelial specific proteins in the invaded nerves' samples, which would suggest high purity of those samples. We also could not perform a similar contamination assessment for the 2D data because only cancer samples were analyzed using this approach. Finally, whilst the main concern in this work would be cross contamination between cancer and nerves within PNI lesions, other potential sources of contamination, including adjacent stroma could not be assessed, as we did not perform the same proteomic analysis for those compartments.

4.3. Proteomic analysis of PNI and non-PNI cancer

1D LC-MS analysis of PNI and non-PNI cancer identified ~1600 proteins, surprisingly, only a few were differentially regulated as further illustrated by hierarchal clustering. Using 2D LC-MS to achieve wider coverage of the proteome, we identified ~3,200 proteins, which represent the largest proteomic profile in pancreatic cancer to date. In comparison, a previous study from our laboratory comparing the proteomes of PDAC cells from matched primary and lymph node metastasis identified ~1500 proteins using 10-fractions MudPIT approach [271], highlighting the advantages of high pH RP fractionation. Nonetheless, even using 2D analysis, only 39 proteins were differentially expressed, indicating relatively high degree of similarity between the two samples.

In the only study that investigated laser microdissected PNI and non-PNI cancer using human tissues, Chen *et al* performed gene expression profiling of these cells from fresh frozen salivary adenoid cystic carcinoma [74]. The authors described 54 deregulated genes (out of 18,716 genes) and validated the up-regulation of MCAM in PNI cancer compared to non-PNI cancer. We did not see any commonalities between their deregulated gene list and the differentially regulated proteins in our data set. This is not surprising considering the different tissue types and the different technologies used, as proteomics has a limited depth of coverage compared to gene expression in addition to the recognized lack of agreement between gene and protein expression [272].

In another study, using bulk prostate cancer tissue from cases with or without PNI, Prueitt *et al* investigated the expression profiles of genes and microRNAs [196]. Whilst the clustering pattern of microRNAs could differentiate the two groups of samples, the RNA expression failed to do so and only 34 transcripts out of 13,000 were differentially regulated, none of which again corresponded to our dataset [196]. To our knowledge, the two studies mentioned above are the only studies that used human tissues for large scale expression profiling in the context of PNI, and despite the different approaches, the largely similar profiles in PNI and non-PNI cancer is highly consistent with our findings.

Although the overall proteomic profiles of PNI and non-PNI cancer were similar, there were some interesting differences. IPA analysis of differentially regulated proteins in both the 1D and the 2D datasets revealed largely similar enrichment in biological functions such as Cell Movement (migration and invasion), Cellular

Organization as well as Cell Survival and Proliferation. Furthermore, subcellular localization analysis revealed enrichment of extracellular proteins (such as laminins, collagens and nidogens) consistent with published literature suggesting a role for ECM proteins in pancreatic cancer migration and invasion [273, 274]. For example, TGFβ induced protein (TGFBI) is an extracellular protein that was shown to be over-expressed in several cancers including pancreatic cancer [275] and has been suggested to play roles in cellular adhesion and migration [276] as well as metastasis of colon cancer cells [277]. TGFBI was one of the top up-regulated proteins in PNI cancer samples using 1D LC-MS. Unfortunately, attempts at validating its expression using immunohistochemistry were not successful due to the low signal to noise ratio.

Ryschich *et al* showed that PDAC cell lines migration was significantly increased by laminin, fibronectin and collagen IV [192] whilst ECM proteins including laminin increased pancreatic cancer cells survival [278]. A study of PNI using an *in vivo* sciatic nerve model found that the level of expression of several laminins, most significantly LAMC2 correlated with the distance of PNI [194]. Furthermore, laminins as well as several of their receptors, including integrins, are widely expressed in the nervous system and play important roles in neurite growth and regeneration [279]. Indeed, amongst other ECM proteins, laminins have been shown to induce the highest neurite outgrowth in mouse DRG neurons and LAM1-mediated neuritogenesis was independent of neurotrophic factors [280]. Similarly, LAMC1 was shown to be vital for peripheral nerve regeneration and myelination following injury [281]. It has also been suggested that axonal guidance molecules secreted by cancer cells could contribute to neurogenesis and axonogenesis [142, 282] which is also supported by the unidirectional growth of neurites from DRGs towards cancer cell colonies *in vitro* [140, 149]. The dual effects of ECM proteins on both cancer cells and nerves could represent one of the key mechanisms underlying neuro-epithelial interactions and driving neurotropism. This extends beyond just ECM proteins, for example, NES, one of the proteins that were up-regulated in the PNI cancer, have been described previously in the context of PNI. Using IHC, Kawamoto *et al* showed that NES was over-expressed in PDAC and its expression correlated with PNI [195]. However, NES was also up-regulated in invaded nerves and plays an important role in neuronal response to injury as will be discussed later on.

Several studies have previously shown that interaction of nerves and cancer cells induces up-regulation of antiapoptotic pathways resulting in enhanced survival of

cancer cells [140, 144, 145]. We identified several apoptosis related proteins as differentially regulated in the PNI cancer including Alpha-crystallin B chain (CRYAB), monoamine oxidase A (MAOA) and OLFM4. CRYAB is a small heat shock protein that has oncogenic properties; it increased the migration and invasion of breast cancer cells and predicted poor outcome as well as resistance to chemotherapy in this malignancy [283, 284]. Although there is no data describing CRYAB in pancreatic cancer, *in vitro* studies using other cell lines have shown its ability to promote cell survival through several mechanisms such as prevention of protein aggregation, regulation of caspase-3 activation as well as sequestration of Bax and Bcl-X(S) proteins [285, 286].

MAOA is a mitochondrial enzyme that is highly expressed in neuroendocrine tissue and has been shown to induce oxidative stress and apoptosis of neuronal cells [287, 288]. The expression of MAOA in pancreas cancer has not been studied in details although there was a report suggesting it is expressed in human PDAC tissues [289]. In a meta-analysis of gene expression studies in PDAC, MAOA was reported to be consistently down-regulated in PDAC [290]. Our proteome data indicates that in PNI-cancer, MAOA expression is further down-regulated consistent with reduced apoptosis in these cells [140].

OLFM4 was one of the most significantly up-regulated proteins in PNI compared to non-PNI cancer. OLFM4 is a stem cell marker that displays anti-apoptotic properties and plays a role in cell-cell adhesion [291]. Induction of OLFM4 in myeloid cells was shown to be regulated by NF-κB and mediated through ERK1/2 MAPK pathway [292]. OLFM4 also attenuated apoptosis in the presence of cellular stress and promoted prostate cancer cell growth *in vivo* [293]. Similar anti-apoptotic effects of OLFM4 regulated via NF-κB were also demonstrated in gastric cancer [217]. In Panc1 PDAC cell line, OLFM4 promoted cellular proliferation but its silencing did not increase apoptosis [294]. Clinically, OLFM4 was reported to correlate with better differentiation in gastric cancer [295], although another study did not find such correlation, but revealed the association between OLFM4 expression and lymph node metastasis as well as poor prognosis in these patients [296]. In colon cancer, OLFM4 expression also correlated with differentiation and its levels were reduced in advanced compared to early stage tumours precancerous adenomas [297, 298]. It is notable, however, that OLFM4 expression was significantly higher in tumours with activated KRAS-NF-κB pathway [297]. In pancreatic cancer, OLFM4 expression did not correlate with differentiation but its expression predicted poor outcome [218].

We found that OLFM4 was widely expressed in PDAC but with striking heterogeneity within the same tissue section; poorly differentiated areas of the tumour tended to secrete OLFM4 into the ECM, whereas the immunoreactivity was largely cytoplasmic and membranous in the well-differentiated cancer glands; however this was not anlaysed quantitatively.

Despite this variability, PNI cancer demonstrated higher OLFM4 expression compared to non-PNI cancer. Interestingly, we have throughout this project, observed that PNI cancer foci were almost always moderately to well-differentiated. This has also been previously observed [33], although we are aware of the risk of a potential bias due to the ease of detecting well differentiated PNI glands compared to poorly differentiated cells. In view of the literature reports of a correlation between OLFM4 expression and differentiation, it is conceivable that OLFM4 up-regulation in PNI cancer is a marker of differentiation. It will be interesting to quantify the differentiation of cancer in PNI foci and investigate further whether this has any correlation with OLFM4 expression. On the other hand, over-expression of OLFM4 in PNI cancer is consistent with the reported reduced apoptosis of cancer cells within the perineural environment and with the poor outcome associated with both PNI and OLFM4 expression in PDAC.

4.4. Proteomic analysis of invaded and non-invaded nerves

The molecular analysis of invaded and non-invaded nerves from human tissues including pancreatic cancer has not been performed before. In our analysis, we identified 925 proteins in the nerves, which is considerably less than the number of proteins detected through the similar analysis of PDAC cancer cells. This is not surprising as the nerve is less cellular and largely composed of axons and ECM proteins. Almost 20% of the identified proteins were differentially regulated. The significant alteration in the molecular profile of the nerves when invaded by cancer was further illustrated by the clustering of samples according to invasion status. IPA analysis revealed enrichment of several functional groups related, mainly, to 'Cell Survival', 'Cellular Organization', 'Morphogenesis' and 'Cellular Movement'. Sub-categories related to neuritogenesis and axonal development were also enriched. A core set of differentially regulated proteins including microtubule-associated protein 1B (MAP1B), doublecortin-like kinase 1 (DLCK1), LAMA1, LAMB1, Tenascin C (TNC), defender against cell death 1 (DAD1), VGF, NES as well as GAP43 contributed to several of these biological functions (**Figure 52** and **53**).

For example, MAP1B was shown to play an important role in the nervous system development and axonogenesis through cytoskeletal re-organisation that involves interactions with actin and microtubules [299, 300]. Equally important, this does not only depend on the level of MAP1B but also on alteration in its phosphorylation status [301]. Similarly, DLCK1 is a microtubule associated protein that contributes to axonogenesis through regulation of F-actin and stabilization of the microtubules in the growth cone thus facilitating response to axonal guidance cues [302, 303]. On the other hand, DAD1 has a protective role against apoptosis [304].

Some of the proteins that were identified as differentially regulated in our study have been previously reported in literature using immunohistochemistry, including NES and GAP43. GAP43 is a neuronal plasticity marker that has been shown to be up-regulated in nerves in PDAC as well as CP [81]. NES on the other hand, is an intermediate filament and a stem cell marker expressed in neuronal progenitor cells, its expression is usually absent in adult post mitotic neuronal cells [305]. NES is up-regulated in nerves in PDAC with invaded nerves showing higher expression levels compared to non-invaded nerves [195]. It is also up-regulated in CP nerves and its up-regulation is correlated with pain [104].

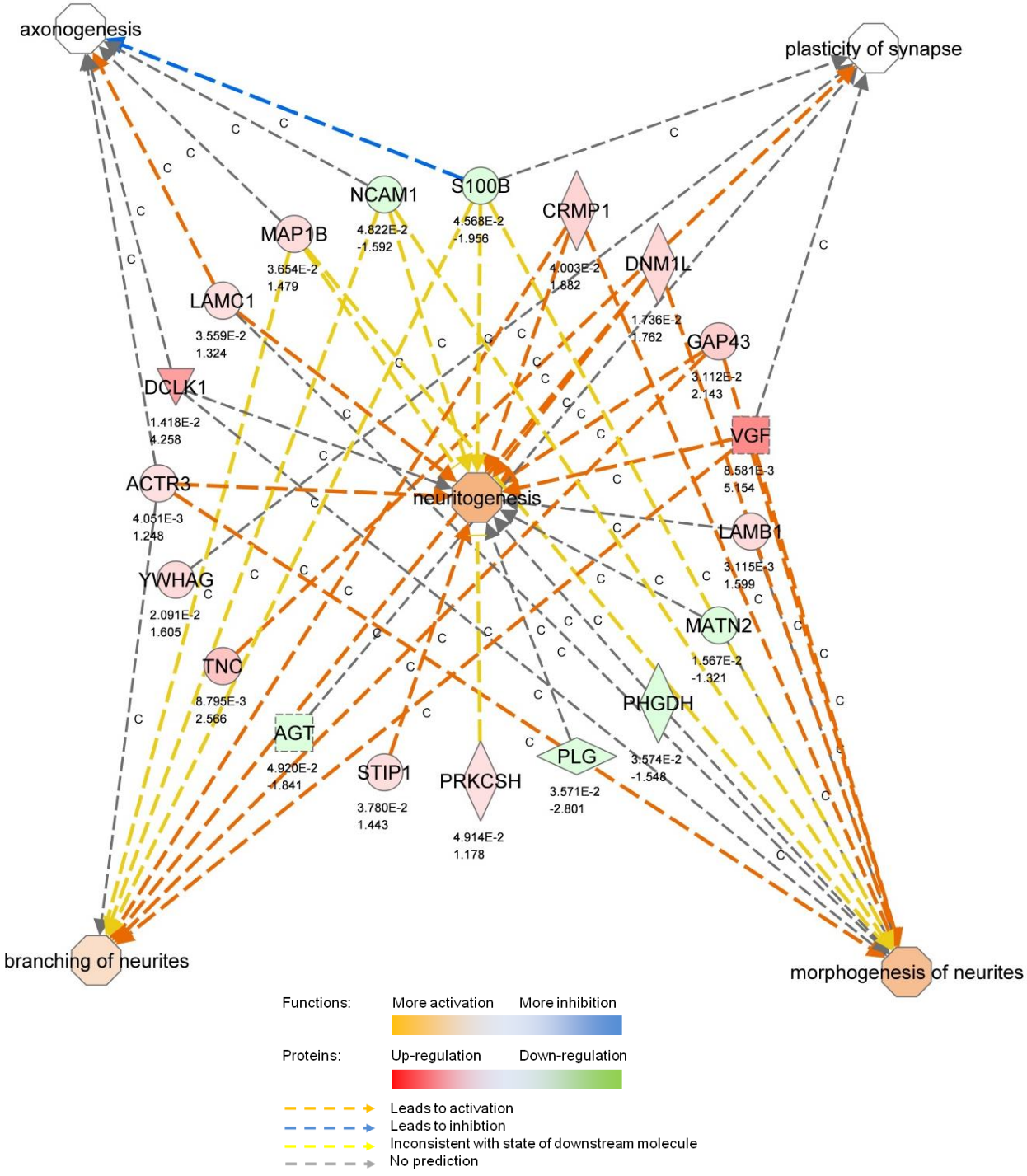

Figure 52. IPA functional enrichment showing neuritogenesis-related functions and the proteins contributing to those functions. Colours of the nodes reflect the level of activation/inhibition according to the colour key.

Strikingly, several of the proteins that were up-regulated in our dataset have been also shown to be up-regulated in peripheral nerve injury. For example, using gene expression profiling, VGF and GAP43 have been shown to increase in rat DRGs following spinal nerve ligation [306]. Similarly, Pituitary adenylate cyclase-activating polypeptide (ADCYAP1), Laminin A, NES as well as TNC were up-regulated under similar conditions [307]. NES has also been shown to be up-regulated in the spinal cord of mice following nerve injury [308], in rats major pelvic ganglion following cavernous nerve crush injury [309] as well as in the rat nucleus ambiguous following vagal nerve transection [310]. These similarities suggest common features of neuroplasticity that are independent of the underlying cause. In a recent review of neural plasticity in gastrointestinal disease, Demir *et al* concluded that common phenotypic, neurochemical and functional features of neuronal plasticity exist and are independent of the underlying aetiology [311]. We would suggest that some of these features also extend, beyond the gastrointestinal tract, to other neuropathies and neuronal plasticity responses in the peripheral nervous system in general. In the only reported expression analysis of nerves in the context of PNI and using a sciatic nerve *in vivo* model of PNI, Mitsunaga *et al* performed gene expression profiling of sciatic nerves proximal to either PNI or crush/suture injury to the nerve. Interestingly, not only was there no overlap with our findings, but also they could not detect any of the proteins commonly identified as up-regulated following peripheral nerve injury [194]. As they compared invaded nerves to nerves traumatized otherwise, this supports our assertion that many of the molecular changes that we observed are in common with changes following nerve injury in general. However, the presence or absence of certain molecular features that would represent a neuronal response to specific type of neuropathy cannot be ruled out and could depend, in part, on the nature of nerves involved.

As alluded to before, we identified several ECM proteins as up-regulated in invaded compared to non-invaded nerves that were similarly deregulated in PNI compared to non-PNI cancer including LAMA2, LAMB1, LAMC1, collagen VI A3 (COL6A3), nidogen 1 (NID1) and TNC. These would constitute, at least, part of the extracellular milieu within which cancer cells and nerves are interacting and many of them have dual roles in promoting cancer growth as well as neurogenesis. This provides further support to the notion that the PNI environment offers beneficial growth conditions for both cancer and nerves [312]. The extracellular nature of the aforementioned proteins, however, precludes firm conclusions as to their exact source based on proteomic methods and would require *in situ* hybridization experiments. For

example, COL6A3 is highly expressed in the stroma of PDAC, particularly in the vicinity of cancer cells [313], and its serum levels were significantly higher in PDAC patients compared to normal and benign controls [314]. Furthermore, COL6A3 provides neuronal protective effect against cellular stress such as UV irradiation through activation of PI3K pathway [315].

TNC, an extracellular glycoprotein, is also another intriguing example. It was shown to be up-regulated in both CP and PDAC stroma whilst PDAC cells were devoid of TNC expression using IHC [316]. The source of TNC is most likely the stellate cells [316]. However, PDAC cell lines do express TNC mRNA which increases their proliferation, migration and adhesion [317]. TNC is also expressed in the nervous system where it promotes neurite growth and regeneration following injury [318, 319]. We have previously used IHC to investigate the expression of TNC in PDAC (unpublished data) and found a similar stromal expression pattern. Within PNI lesions, and consistent with our proteomic data, TNC was seen expressed at the interface between cancer and endoneurium explaining its up-regulation in both PNI cancer and nerve samples.

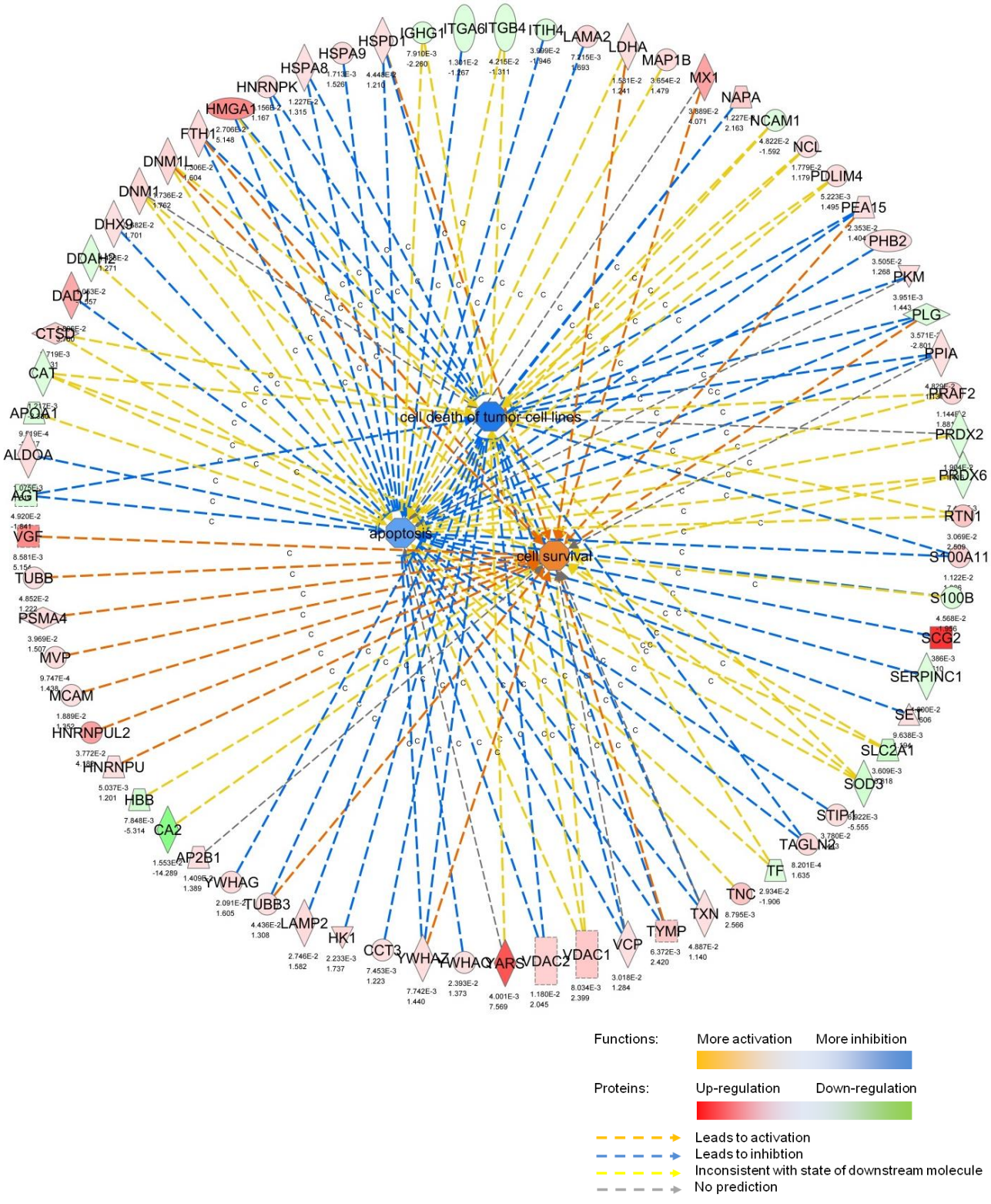

Figure 53. IPA analysis of differentially regulated proteins in the nerve samples demonstrating several proteins contributing to the activation of cell survival and inhibition of apoptosis. Colours of the nodes reflect the level of activation/inhibition according to the colour key.

4.5. Immunohistochemical evaluation of VGF expression

In our proteomic analysis, VGF was one of the most up-regulated proteins in invaded compared to non-invaded nerves. VGF was first described by Levi *et al* as a transcript that was rapidly up-regulated in PC12 cells following NGF treatment [320]. VGF is exclusively expressed in the central and peripheral nervous system as well as in neuroendocrine cells in the gut [321]. The protein is stored in secretory vesicles and released upon various stimuli in a similar manner to neuropeptides and neurotransmitters [227]. VGF is cleaved into at least a dozen of proteolytic peptides by the actions of peptidases including prohormone convertases 2 and 1/3, several of these peptides are biologically active [322, 323]. Several biological activities have been attributed to VGF and/or specific peptides including energy and water balance, and regulation of body weight, neuropathic pain as well as neuronal plasticity [227, 322].

Using IHC, we were able to confirm the up-regulation of VGF in invaded nerves and, interestingly, found that VGF expression is gradually increased as the nerves lie closer to cancer. This is consistent with previous observation of increasing neuroplasticity the closer the nerves are to cancer [199] . Several inducers of VGF that have been reported in the literature, including NGF [324] , BDNF [325] and basic fibroblast growth factor (bFGF) [326] are also expressed in pancreatic cancer [159, 327] and it is conceivable that one or more of them may contribute to VGF induction in PDAC nerves. Furthermore, the induction of VGF in CP suggests that the inflammatory stroma can also induce VGF expression in pancreatic nerves. In addition, pancreatic stellate cells have been suggested to play an important role in PNI as well as neuronal plasticity [200] and their potential ability to induce VGF could be related to their expression of neurotrophic factors such as NGF [328]. Furthermore, the up-regulation of VGF following nerve injury, as pointed out earlier, suggests that intrinsic mechanisms within the nerve components, activated by PDAC induced neuropathy may contribute to VGF induction.

The observed VGF distribution pattern and previous reports that neuroplasticity changes become more prominent the closer the nerves are to cancer, suggest that the differences we have observed in the proteome are attenuated due to the combining of intratumoural and extatumoural non-invaded nerves during microdissection. Comparison of normal nerves and invaded nerves would likely reveal even more extensive neuroplasticity changes.

VGF has been recently linked to neuropathic pain. In a mouse model of inflammatory pain using formalin, Rizzi *et al* showed that TLQP-21, a VGF derived peptide mediates inflammatory pain when injected peripherally but has an analgesic effect when injected centrally [329]. In a more detailed study of peripheral nerves injury, VGF was rapidly up-regulated in rat DRGs within 24 hours following nerve ligation or *in vitro* culture of DRGs. Injection of VGF derived peptides (AQEE-30 and LQEQ-19) intrathecally (around the spinal cord) resulted in a dose-dependent increase in thermal hyperalgesia [219].

We unfortunately obtained only a limited number of clinically annotated PDAC cases and were, therefore, not able to make any conclusions regarding association of pain and VGF expression in cancer specimens. Additionally, the fact that PNI is associated with pain in PDAC and that VGF expression is higher in invaded nerves necessitates relatively large number of cases to perform detailed statistics and multivariate analysis. We were able, however, to investigate the relationship of VGF expression and pain in CP cases. In CP, VGF expression strongly correlated with the degree of pain. In fact, pancreatic nerves from patients without pain showed either weak or no immunoreactivity, almost similar to VGF expression in nerves from normal pancreata. The mechanisms underlying VGF mediation of pain are not clear. Riedl *et al* reported that phosphorylation of p38 MAPK in spinal glial cells was necessary for thermal hyperalgesia induction by intrathecal injection of AQEE-30 and LQEQ-19 peptides [219]. In support of that, MAPK pathway has been extensively linked to neuronal plasticity and neuropathic pain development and maintenance and several noxious stimuli as well as pain-related neuropeptides such as SP can activate this pathway [330].

4.6. *In vitro* modelling of neuronal plasticity in neuro-epithelial interactions

Previous studies to model PNI *in vitro* relied largely on rodents' DRGs or their dissociated primary sensory neurons [140], whilst others used dissociated myenteric plexus cells from rats [149]. These primary cells and tissue explants are not easy to handle and require using large number of animals. In addition, while DRGs enable the study of the interaction between cancer cells and the whole nerve structure including all its components, it does not allow the study of interactions between specific nerve component and cancer cells. Finally, as mentioned earlier, harvesting DRGs and their dissociated cells itself represents a nerve injury in which several neuroplasticity alterations are already activated and continue to evolve over time in culture [307]. Immortalized cell lines, on the other hand, represent an infinite source of cells that can be manipulated in various ways, which are not always possible using DRGs or primary cells. They can also be used to investigate the role(s) of specific neuronal components.

In our experiments, we have used PC12 cells along with several PDAC cell lines to establish a co-culture model of neuro-epithelial interactions. As mentioned previously, PC12 is a rat pheochromocytoma cell line, which upon exposure to NGF, and several other neurotrophic factors, exits cell cycle, extends neurites and becomes electrically excitable, leading to a sympathetic-like neuronal phenotype [221]. In the field of PNI, PC12 cells have been used in only one study in which they were treated with media from DRG or DRG/prostate cancer cells co-culture; PC12 cells extended neurites under these conditions [142].

In our co-culture model, three out of four PDAC cell lines were able to recapitulate the major phenotypic features of neural plasticity associated with neuro-epithelial interactions that have been observed in tissues as well as *in vitro* model of PNI, namely survival and neuritogenesis. These effects were comparable to those induced by NGF. In addition, the model recapitulated several of the molecular changes that were observed in our proteomic analysis. PDAC cell lines were able to induce VGF expression reprising the VGF induction in human tissues and demonstrated the ability of PDAC cancer cell lines to up-regulate VGF independently of the stroma. It is important to note that we did not examine the expression of specific VGF proteolytic peptides due to lack of commercially available antibodies. This would be important because the proteolytic cleavage of VGF into

peptides with different biological activities represents an extra layer of its regulation, as it has been shown by the differential proteolytic profile that varies between tissues [331], which would not be captured by measuring its total levels. In support of this, one of the proteins which was up-regulated in invaded nerves in our proteomic dataset was PCSK1N, a known modulator of prohormone convertase 1, an enzyme responsible for VGF proteolytic cleavage [323].

Furthermore, PDAC cell lines were able to induce GAP43 as well as NES expression in PC12 cells, which was again consistent with our proteomics data. The induction of NES is particularly interesting, as NGF treatment could not induce NES expression in PC12 cells in the control experiments. The expression levels of NES in PC12 cells following NGF treatment have been reported twice in literature with one report showing a reduction in NES expression consistent with differentiation [332], and another reporting an increase in NES levels [333]. Both of these reports involved longer NGF treatment than the 24 hours point we used. As NES is a neuronal progenitors marker and its expression level is reduced in post-mitotic neurons, NES up-regulation following nerve injury suggests a possible de-differentiation in support of repair and regeneration [309, 310]. In view of this, our proteomics data and our observation of an increase in both neurite growth (differentiation) as well as NES (de-differentiation/regeneration), it is very tempting to suggest that cancer cells provide neuronal cues that keeps a delicate balance between the two processes resulting in not only growth of axons (axonogenesis) but also new neurons (neuronogenesis), the two phenomena which have already been described in human tissues in the context of neuro-epithelial interactions [142].

In view of the VGF expression pattern in PDAC nerves, we used both a Transwell and a contact co-culture to further model the physical proximity of nerves and cancer cells. Interestingly, the up-regulation of VGF in PC12 cells was even higher when cancer cells were in direct contact with PC12 cells. This could be due to exposure of PC12 cells to locally higher concentration of soluble cancer factors, direct cell-to-cell communication and/or interaction with ECM deposited by cancer cells. We believe, however, that both models represent direct neuro-epithelial interactions similar to PNI as there is a free exchange of soluble factors between both cell types with the added advantage of possible enhanced cellular communication in the contact model.

In addition to its effects on PC12 cells, NGF is thought to be involved in PNI and pancreatic cancer and CP associated neuropathy. We tested whether at least some

of the PC12 neuroplasticity changes induced by PDAC cells are mediated through NGF. Trk receptor inhibition with K252a failed to block survival, differentiation as well as VGF induction of PC12 cells treated with conditioned media from the three PDAC cell lines. Interestingly, and rather unexpectedly, K252a significantly increased PC12 neurite extension induced by MiaPaca2 conditioned media. Although the reason for this is unclear as yet, it has been reported that epidermal growth factor (EGF) can induce the extension of short neurites in PC12 cells and this effect is augmented by K252a [334]. It is possible that K252a enhanced an otherwise small effect of EGF in MiaPaca2 conditioned media. This indicated that in our model and using these cell lines, factor(s) other than NGF were responsible for the PC12 phenotype although this doesn't rule out contribution of NGF to PNI in human tissues.

Whilst the induction of VGF expression in nerves in human PDAC and CP tissues, and in PC12 cells in the co-culture systems as well as the association of VGF expression with pain in CP were clearly demonstrated, further functional relevance of VGF up-regulation in the setting of neuronal plasticity were still not obvious. VGF has been implicated in neuronal cell survival and plasticity. Previous studies indicated that TLQP-21, a VGF derived peptide protects cerebellar granular cells from serum and potassium deprivation induced apoptosis [220]. Furthermore, VGF mediated the protection of neuroblastoma cells from endoplasmic reticulum stress induced cell death [335]. Induction of VGF by BDNF has also been shown to mediate neuronal synaptic plasticity and memory in hippocampal cells [229]. On the other hand, PC12 cells undergo apoptosis in serum-free media and several factors including NGF, bFGF and cAMP are known to protect them from serum starvation mediated apoptosis via multiple initial signaling pathways that converge downstream [326]. There is, however, no data on whether VGF is involved in the survival of PC12 cells under these conditions. Using siRNA-mediated gene silencing, we blocked VGF up-regulation that is induced by PDAC cells conditioned media. This did not affect PC12 survival indicating that VGF is not necessary for this process. Blocking VGF however, resulted in significant reduction in neurite extension using both MiaPaca2 and BxPc3 conditioned media although it did not abrogate it completely. This indicated that whilst VGF is induced as part of the neuroplasticity response, it is also augmenting this process in an autocrine/paracrine fashion. This is likely as VGF is a secreted protein and some of its biological activities such as cell survival was reported to occur in this manner [220]. In support of this, VGF up-regulation in DRGs following peripheral nerve injury is limited to the neurons but not

glial cells [336], whilst its effects on pain behavior in the same setting is mediating through activation of glial cells [219].

Finally, we should point out that we have not yet investigated the functional and molecular alterations in PDAC cells in the co-culture system. The strong up-regulation of VGF in both invaded nerves as well as PC12 co-cultures poses an important question regarding potential roles of VGF in cancer cell biology. Barring the description of its expression in neuro-endocrine tumours [337], there is no data in the literature regarding its presence or putative functions in other tumours. Additionally, in our immunohistochemistry analysis, cancer cells did not show any VGF staining. The presence of reciprocal signaling pathways between cancer cells and nerves is widely perceived to underpin the mutual neuro-epithelial interactions; however, such a loop of reciprocal signaling has rarely been demonstrated experimentally. Due to the ability of VGF to activate, in a paracrine manner, MAPK signaling pathway in glial cells [219], and the central role this pathway plays in tumorigenesis and cancer progression [338], it is conceivable that VGF secreted by the nerves could also activate MAPK cascade in the cancer cells within the perineural environment. The ability of the neurotransmitter NE to activate p38 MAPK in pancreatic cancer cells enhancing their migration and proliferation is a prototype for such interaction [339]. This would potentially be an interesting loop whereby PDAC cells induce VGF expression which then activates survival, invasion and migration in cancer cells via MAPK and this could possibly further augment VGF induction. The presence of such signaling loop is yet to be elucidated and further characterization of the molecular alteration using our co-culture model may reveal further pathways. The flexibility of the model with regard to gene manipulation and obtaining relatively large quantities of condition media from both cancer cells as well as PC12 cells will undoubtedly facilitate such investigations and underscores the model's advantages compared to primary neuronal cells and neural tissue explants.

4.7. Conclusions

In this work we investigated the alterations in the proteomic profiles of PDAC cells and nerves within the PNI environment. Using laser microdissection and MS based proteomic analysis we were able to identify more than 3000 proteins from small amount of peptide digest derived from FFPE PDAC specimens. Our data revealed that despite some differences, of which we validated the up-regulation of OLFM4 in PNI compared to non-PNI cancer, these cells are largely similar. Nerves, on the other hand, displayed a wide range of molecular alterations driving the major phenotypic features of neuroplasticity observed in published literature. Several of these changes are similar to those observed in neuropathies associated with other clinical conditions such as chronic pancreatitis as well as peripheral nerve injury, underscoring the importance of common neuronal response to injury. We validated the up-regulation of VGF in invaded nerves as well as in nerves of chronic pancreatitis and unveiled a strong association between VGF expression and pain in CP. However, the correlation of VGF expression and pain in PDAC cases still remains to be established.

We also developed a model of neuro-epithelial interactions using co-culture of PC12 cells and PDAC cell lines. Several PDAC cell lines were able to induce neuronal plasticity changes in PC12 cells similar to what has been reported in PDAC tissues. In addition to neuritogenesis and cell survival, PDAC cell lines induced VGF, NES and GAP43 expression in PC12 cells. Interestingly, the induction of VGF was stronger when these cells were in direct contact which is consistent with our immunohistochemistry findings. Furthermore, we show that the effects of PDAC cell lines on PC12 cells are not mediated via NGF, a well-known effector of PC12 differentiation, and that VGF induction is not necessary for PC12 cell survival. However, VGF contributes to the neurite extension, likely in an autocrine/paracrine manner.

While PC12 model clearly recapitulated several phenotypic and molecular features of neuroplasticity seen in PDAC, and indeed, in other neuropathic conditions, the extent of functional and molecular alteration of cancer cells in this model and their resemblance to findings in human tissues remain to be established.

Chapter Five: Future Directions

5. Future directions

The work that was performed herein represents an important addition to our knowledge of the biology of neuro-epithelial interactions. While the proteomic analysis contains wealth of information, and the co-culture model adds a unique tool to the available armamentarium of PNI models, both present several questions and lines of inquiry that could be pursued using immunohistochemical and functional validation.

5.1. Correlation between VGF expression and pain in PDAC

We have illustrated a strong relationship between pain and VGF expression in CP patients. The clarification of the relationship between VGF expression and pain in PDAC patients remains outstanding as we are yet to receive the additional sections from our collaborators in order to have an adequate number of cases for robust statistical analysis. The experiment will be performed as soon as the sections are received. While this would, hopefully, answer the question of clinical correlation, it would not explain the underlying mechanisms. A VGF knock-out model has been described in the literature and used to investigate the role of VGF in the regulation of body weight and energy balance [340]. It would be interesting to investigate alterations in pain sensation in response to injury in such a model in comparison to VGF competent mice.

5.2. The regulation of VGF induction in PC12 cells by PDAC cells

We have demonstrated that PDAC cell lines as well as their conditioned media are able to induce phenotypic and molecular neuronal plasticity in PC12 cells and ruled out NGF as a contributing factor under our experimental conditions. However, the identification of the factor(s) responsible for this biological activity is crucial to the understanding of the mechanisms of these alterations and their relevance to neuro-epithelial interactions in human tissues. To achieve this, a combination of multi-dimensional HPLC fractionation (size exclusion, SCX) and mass spectrometry will be used to separate and identify proteins in PDAC cells conditioned media. HPLC

fractions will be tested for biological activity using PC12 survival, neurite extension and VGF induction as output assays. Biologically active fractions can then be further fractionated to narrow down the list of potential candidates. Depending on the putative factors and available reagents, we will subsequently use a combination of antibody-based neutralization, small molecular inhibitors and/or gene silencing to confirm the identity and validate the functions of putative candidates.

The expression of these proteins in human tissues will then be determined using immunohistochemistry prior to detailed investigation of their mechanisms of action, particularly in relation to the induction of VGF expression using the PC12 cells model.

5.3. The effects of VGF induction on PC12 cells

VGF gene silencing resulted in a significant attenuation of PC12 neurite extension in response to conditioned media from PDAC cells. We would like to further investigate how VGF is contributing to neuritogenesis and whether this is mediated through specific VGF derived peptides. We will use mass spectrometry to identify VGF proteolytic peptides in PC12 secretome to investigate the presence of differential proteolytic profile in response to PDAC conditioned media compared to NGF treatment. We will also use exogenous VGF derived peptides to establish whether VGF alone (or its peptides) are able to induce neurite extension.

5.4. The functional significance of NES up-regulation

We have observed up-regulation of NES in invaded nerves as well as in PC12 in co-culture with PDAC cells but not in PC12 treated with NGF. Of note, NES was shown to have prosurvival effects on neuronal cells via sequestration of Cdk5 [341], and whilst this doesn't seem to be required in the case of NGF treated PC12 cells, it may play a role in the co-culture system. It would be interesting to investigate, using gene silencing, whether NES serves similar functions in PC12 co-culture or if it contributes to other features of neuronal plasticity such as neurite extension.

On a similar note, we would like to investigate the expression of NES as well as the degree of differentiation of PC12 cells treated with PDAC cells conditioned media at further time points to determine whether, contrary to NGF treatment, a significant

proportion of these cells remain undifferentiated and expressing NES. Immunocytochemistry will also assist in clarifying whether all PC12 cells treated with conditioned media up-regulate NES or specific group of cells (differentiated or undifferentiated).

5.5. Investigation of the functional and molecular alterations in PDAC cells in the co-culture PNI model

As pointed out earlier, we have not yet investigated the changes in PDAC cells in the co-culture model. It will be interesting to investigate whether cancer cells display similar changes to what have been described in literature, including increasing migration and invasion as well as up-regulation of antiapoptotic pathways. We will use the same co-culture system but with larger pore size inserts allowing the quantitation of Transwell migration and invasion of PDAC cells in the inserts towards PC12 cells co-cultured in the bottom wells. Additionally we will investigate, in PDAC cells in co-culture, the expression of some of the proteins that were deregulated in our proteomic profiling starting with OLFM4 and further characterize its functional relevance.

5.6. Validation of differentially regulated proteins

Finally, we would also like to validate the differential expression of several other interesting proteins from our proteomic datasets. Clear candidates would be ECM proteins due to their role in both cancer progression and neuronal plasticity as discussed earlier. In the cancer samples, several antiapoptotic proteins that have not been studied in pancreatic cancer, such as CRYAB and MAOA, are potential candidates. This will rely in part on the availability and performance of reagents that are required for validation particularly antibodies.

References

1. Jemal, A., et al., *Cancer statistics, 2010.* CA Cancer J Clin, 2010. **60**(5): p. 277-300.

2. Fesinmeyer, M.D., et al., *Differences in survival by histologic type of pancreatic cancer.* Cancer Epidemiol Biomarkers Prev, 2005. **14**(7): p. 1766-73.

3. Wisnoski, N.C., et al., *672 patients with acinar cell carcinoma of the pancreas: a population-based comparison to pancreatic adenocarcinoma.* Surgery, 2008. **144**(2): p. 141-8.

4. Jung, K.W., et al., *Clinicopathological aspects of 542 cases of pancreatic cancer: a special emphasis on small pancreatic cancer.* J Korean Med Sci, 2007. **22 Suppl**: p. S79-85.

5. Sharma, C., et al., *Advances in diagnosis, treatment and palliation of pancreatic carcinoma: 1990-2010.* World J Gastroenterol, 2011. **17**(7): p. 867-97.

6. Zhou, J., et al., *Incidence rates of exocrine and endocrine pancreatic cancers in the United States.* Cancer Causes Control, 2010. **21**(6): p. 853-61.

7. Matsuno, S., et al., *Pancreatic Cancer Registry in Japan: 20 years of experience.* Pancreas, 2004. **28**(3): p. 219-30.

8. Doi, R., et al., *Surgery versus radiochemotherapy for resectable locally invasive pancreatic cancer: final results of a randomized multi-institutional trial.* Surg Today, 2008. **38**(11): p. 1021-8.

9. Conlon, K.C., D.S. Klimstra, and M.F. Brennan, *Long-term survival after curative resection for pancreatic ductal adenocarcinoma. Clinicopathologic analysis of 5-year survivors.* Ann Surg, 1996. **223**(3): p. 273-9.

10. Sener, S.F., et al., *Pancreatic cancer: a report of treatment and survival trends for 100,313 patients diagnosed from 1985-1995, using the National Cancer Database.* J Am Coll Surg, 1999. **189**(1): p. 1-7.

11. Alexakis, N., et al., *Current standards of surgery for pancreatic cancer.* Br J Surg, 2004. **91**(11): p. 1410-27.

12. Tsiotos, G.G., M.B. Farnell, and M.G. Sarr, *Are the results of pancreatectomy for pancreatic cancer improving?* World J Surg, 1999. **23**(9): p. 913-9.

13. Kuhlmann, K.F., et al., *Surgical treatment of pancreatic adenocarcinoma; actual survival and prognostic factors in 343 patients.* Eur J Cancer, 2004. **40**(4): p. 549-58.

14. Ferrone, C.R., et al., *Pancreatic adenocarcinoma: the actual 5-year survivors.* J Gastrointest Surg, 2008. **12**(4): p. 701-6.

15. Schnelldorfer, T., et al., *Long-term survival after pancreatoduodenectomy for pancreatic adenocarcinoma: is cure possible?* Ann Surg, 2008. **247**(3): p. 456-62.

16. David, M., et al., *Management and prognosis of pancreatic cancer over a 30-year period.* Br J Cancer, 2009. **101**(2): p. 215-8.

17. Furukawa, H., et al., *Clinicopathologic features of small pancreatic adenocarcinoma. A collective study.* Cancer, 1996. **78**(5): p. 986-90.

18. Hermanek, P., *Pathology and biology of pancreatic ductal adenocarcinoma.* Langenbecks Arch Surg, 1998. **383**(2): p. 116-20.

19. Beger, H.G., et al., *Treatment of pancreatic cancer: challenge of the facts.* World J Surg, 2003. **27**(10): p. 1075-84.

20. Sommerville, C.A., et al., *Survival analysis after pancreatic resection for ampullary and pancreatic head carcinoma: an analysis of clinicopathological factors.* J Surg Oncol, 2009. **100**(8): p. 651-6.

21. Morris-Stiff, G., et al., *Assessment of survival advantage in ampullary carcinoma in relation to tumour biology and morphology.* Eur J Surg Oncol, 2009. **35**(7): p. 746-50.

22. Wagner, M., et al., *Curative resection is the single most important factor determining outcome in patients with pancreatic adenocarcinoma.* Br J Surg, 2004. **91**(5): p. 586-94.

23. Shimada, K., et al., *Reappraisal of the clinical significance of tumor size in patients with pancreatic ductal carcinoma.* Pancreas, 2006. **33**(3): p. 233-9.

24. Riediger, H., et al., *The lymph node ratio is the strongest prognostic factor after resection of pancreatic cancer.* J Gastrointest Surg, 2009. **13**(7): p. 1337-44.

25. Iqbal, N., et al., *A comparison of pancreaticoduodenectomy with extended pancreaticoduodenectomy: a meta-analysis of 1909 patients.* Eur J Surg Oncol, 2009. **35**(1): p. 79-86.

26. Nagakawa, T., et al., *Perineural invasion of carcinoma of the pancreas and biliary tract.* Br J Surg, 1993. **80**(5): p. 619-21.

27. Kayahara, M., et al., *Lymphatic flow and neural plexus invasion associated with carcinoma of the body and tail of the pancreas.* Cancer, 1996. **78**(12): p. 2485-91.

28. Shimada, K., et al., *Prognostic factors after distal pancreatectomy with extended lymphadenectomy for invasive pancreatic adenocarcinoma of the body and tail.* Surgery, 2006. **139**(3): p. 288-95.

29. Garcea, G., et al., *Survival following curative resection for pancreatic ductal adenocarcinoma. A systematic review of the literature.* JOP, 2008. **9**(2): p. 99-132.

30. Meyer, W., et al., *Pathomorphological and histological prognostic factors in curatively resected ductal adenocarcinoma of the pancreas.* Surg Today, 2000. **30**(7): p. 582-7.

31. Cleary, S.P., et al., *Prognostic factors in resected pancreatic adenocarcinoma: analysis of actual 5-year survivors.* J Am Coll Surg, 2004. **198**(5): p. 722-31.

32. Pongprasobchai, S., et al., *Long-term survival and prognostic indicators in small (<or=2 cm) pancreatic cancer.* Pancreatology, 2008. **8**(6): p. 587-92.

33. Mitsunaga, S., et al., *Detail histologic analysis of nerve plexus invasion in invasive ductal carcinoma of the pancreas and its prognostic impact.* Am J Surg Pathol, 2007. **31**(11): p. 1636-44.

34. Deshmukh, S.D., J.K. Willmann, and R.B. Jeffrey, *Pathways of extrapancreatic perineural invasion by pancreatic adenocarcinoma: evaluation with 3D volume-rendered MDCT imaging.* AJR Am J Roentgenol, 2010. **194**(3): p. 668-74.

35. Yi, S.Q., et al., *Innervation of the pancreas from the perspective of perineural invasion of pancreatic cancer.* Pancreas, 2003. **27**(3): p. 225-9.

36. Kirchgessner, A.L. and M.D. Gershon, *Innervation of the pancreas by neurons in the gut.* J Neurosci, 1990. **10**(5): p. 1626-42.

37. Kiba, T., *Relationships between the autonomic nervous system and the pancreas including regulation of regeneration and apoptosis: recent developments.* Pancreas, 2004. **29**(2): p. e51-8.

38. Ushiki, T. and S. Watanabe, *Distribution and ultrastructure of the autonomic nerves in the mouse pancreas.* Microsc Res Tech, 1997. **37**(5-6): p. 399-406.

39. Love, J.A., E. Yi, and T.G. Smith, *Autonomic pathways regulating pancreatic exocrine secretion.* Auton Neurosci, 2007. **133**(1): p. 19-34.

40. Salvioli, B., et al., *Neurology and neuropathology of the pancreatic innervation.* JOP, 2002. **3**(2): p. 26-33.

41. Bockman, D.E., *Nerves in the pancreas: what are they for?* American Journal of Surgery, 2007. **194**(4A): p. S61-S64.

42. Sunderland, S., *The connective tissues of peripheral nerves.* Brain, 1965. **88**(4): p. 841-54.

43. Stolinski, C., *Structure and composition of the outer connective tissue sheaths of peripheral nerve.* J Anat, 1995. **186 (Pt 1)**: p. 123-30.

44. Gamble, H.J. and R.A. Eames, *An Electron Microscope Study of the Connective Tissues of Human Peripheral Nerve.* J Anat, 1964. **98**: p. 655-63.

45. Lorimier, P., et al., *Ultrastructural localization of the major components of the extracellular matrix in normal rat nerve.* J Histochem Cytochem, 1992. **40**(6): p. 859-68.

46. Bove, G.M., *Epi-perineurial anatomy, innervation, and axonal nociceptive mechanisms.* J Bodyw Mov Ther, 2008. **12**(3): p. 185-90.

47. Pina-Oviedo, S. and C. Ortiz-Hidalgo, *The normal and neoplastic perineurium: a review.* Adv Anat Pathol, 2008. **15**(3): p. 147-64.

48. Thomas, P.K., *The connective tissue of peripheral nerve: an electron microscope study.* J Anat, 1963. **97**: p. 35-44.

49. Rodin, A.E., D.L. Larson, and D.K. Roberts, *Nature of the perineural space invaded by prostatic carcinoma.* Cancer, 1967. **20**(10): p. 1772-9.

50. Dunn, M., M.B. Morgan, and T.W. Beer, *Perineural invasion: identification, significance, and a standardized definition.* Dermatol Surg, 2009. **35**(2): p. 214-21.

51. Liebig, C., et al., *Perineural invasion in cancer: a review of the literature.* Cancer, 2009. **115**(15): p. 3379-91.

52. Takubo, K., et al., *Light and electron microscopic studies of perineural invasion by esophageal carcinoma.* J Natl Cancer Inst, 1985. **74**(5): p. 987-93.

53. Carter, R.L., et al., *Perineural spread by squamous carcinomas of the head and neck: a morphological study using antiaxonal and antimyelin monoclonal antibodies.* J Clin Pathol, 1983. **36**(3): p. 269-75.

54. Nakao, A., et al., *Clinical significance of carcinoma invasion of the extrapancreatic nerve plexus in pancreatic cancer.* Pancreas, 1996. **12**(4): p. 357-61.

55. Ozaki, H., et al., *The prognostic significance of lymph node metastasis and intrapancreatic perineural invasion in pancreatic cancer after curative resection.* Surg Today, 1999. **29**(1): p. 16-22.

56. Sperti, C., et al., *Survival after resection for ductal adenocarcinoma of the pancreas.* Br J Surg, 1996. **83**(5): p. 625-31.

57. Takahashi, T., et al., *Perineural invasion by ductal adenocarcinoma of the pancreas.* J Surg Oncol, 1997. **65**(3): p. 164-70.

58. Mitsunaga, S., et al., *Important prognostic histological parameters for patients with invasive ductal carcinoma of the pancreas.* Cancer Sci, 2005. **96**(12): p. 858-65.

59. Hirai, I., et al., *Perineural invasion in pancreatic cancer.* Pancreas, 2002. **24**(1): p. 15-25.

60. Nagai, H., A. Kuroda, and Y. Morioka, *Lymphatic and local spread of T1 and T2 pancreatic cancer. A study of autopsy material.* Ann Surg, 1986. **204**(1): p. 65-71.

61. Li, Z., et al., *Overexpression of synuclein-gamma in pancreatic adenocarcinoma.* Cancer, 2004. **101**(1): p. 58-65.

62. Okusaka, T., et al., *Abdominal pain in patients with resectable pancreatic cancer with reference to clinicopathologic findings.* Pancreas, 2001. **22**(3): p. 279-84.

63. Li, J., et al., *Relationship between neural alteration and perineural invasion in pancreatic cancer patients with hyperglycemia.* PLoS One, 2011. **6**(2): p. e17385.

64. Shimada, K., et al., *Intrapancreatic nerve invasion as a predictor for recurrence after pancreaticoduodenectomy in patients with invasive ductal carcinoma of the pancreas.* Pancreas, 2011. **40**(3): p. 464-8.

65. Kayahara, M., et al., *The nature of neural invasion by pancreatic cancer.* Pancreas, 2007. **35**(3): p. 218-23.

66. Nagakawa, T., et al., *A clinicopathologic study on neural invasion in cancer of the pancreatic head.* Cancer, 1992. **69**(4): p. 930-5.

67. Chen, J.W., et al., *Predicting patient survival after pancreaticoduodenectomy for malignancy: histopathological criteria based on perineural infiltration and lymphovascular invasion.* HPB (Oxford), 2010. **12**(2): p. 101-8.

68. Nagakawa, T., et al., *Clinicopathological study on neural invasion to the extrapancreatic nerve plexus in pancreatic cancer.* Hepatogastroenterology, 1992. **39**(1): p. 51-5.

69. Wang, W., et al., *Patterns of expression and function of the p75(NGFR) protein in pancreatic cancer cells and tumours.* Eur J Surg Oncol, 2009. **35**(8): p. 826-32.

70. Dang, C., et al., *Expression of nerve growth factor receptors is correlated with progression and prognosis of human pancreatic cancer.* J Gastroenterol Hepatol, 2006. **21**(5): p. 850-8.

71. Zhu, Z., et al., *Nerve growth factor expression correlates with perineural invasion and pain in human pancreatic cancer.* J Clin Oncol, 1999. **17**(8): p. 2419-28.

72. Ma, J., et al., *Expression of nerve growth factor and tyrosine kinase receptor A and correlation with perineural invasion in pancreatic cancer.* J Gastroenterol Hepatol, 2008. **23**(12): p. 1852-9.

73. Ben, Q.W., et al., *Positive expression of L1-CAM is associated with perineural invasion and poor outcome in pancreatic ductal adenocarcinoma.* Ann Surg Oncol, 2010. **17**(8): p. 2213-21.

74. Chen, W., et al., *Gene expression profile of salivary adenoid cystic carcinoma associated with perineural invasion.* Tohoku J Exp Med, 2007. **212**(3): p. 319-34.

75. Koide, N., et al., *Establishment of perineural invasion models and analysis of gene expression revealed an invariant chain (CD74) as a possible molecule involved in perineural invasion in pancreatic cancer.* Clin Cancer Res, 2006. **12**(8): p. 2419-26.

76. Hibi, T., et al., *Synuclein-gamma is closely involved in perineural invasion and distant metastasis in mouse models and is a novel prognostic factor in pancreatic cancer.* Clin Cancer Res, 2009. **15**(8): p. 2864-71.

77. Yao, J., et al., *Pleiotrophin expression in human pancreatic cancer and its correlation with clinicopathological features, perineural invasion, and prognosis.* Dig Dis Sci, 2009. **54**(4): p. 895-901.

78. Kurtz, K.A., et al., *Perineural and vascular invasion in oral cavity squamous carcinoma: increased incidence on re-review of slides and by using immunohistochemical enhancement.* Arch Pathol Lab Med, 2005. **129**(3): p. 354-9.

79. Liebig, C., et al., *Perineural invasion is an independent predictor of outcome in colorectal cancer.* J Clin Oncol, 2009. **27**(31): p. 5131-7.

80. Marchesi, F., et al., *The chemokine receptor CX3CR1 is involved in the neural tropism and malignant behavior of pancreatic ductal adenocarcinoma.* Cancer Res, 2008. **68**(21): p. 9060-9.

81. Ceyhan, G.O., et al., *Pancreatic neuropathy and neuropathic pain--a comprehensive pathomorphological study of 546 cases.* Gastroenterology, 2009. **136**(1): p. 177-186 e1.

82. Ceyhan, G.O., et al., *The severity of neural invasion is a crucial prognostic factor in rectal cancer independent of neoadjuvant radiochemotherapy.* Ann Surg, 2010. **252**(5): p. 797-804.

83. Bockman, D.E., M. Buchler, and H.G. Beger, *Interaction of pancreatic ductal carcinoma with nerves leads to nerve damage.* Gastroenterology, 1994. **107**(1): p. 219-30.

84. Dang, C., et al., *Ultrastructural study of the mechanism of perineural extension in pancreatic cancer.* Medical Electron Microscopy, 1998. **31**(1): p. 31-37.

85. Maxwell, P., P.W. Hamilton, and J.M. Sloan, *Three-dimensional reconstruction of perineural invasion in carcinoma of the extrahepatic bile ducts.* J Pathol, 1996. **180**(2): p. 142-5.

86. Noto, M., et al., *Pancreas head carcinoma: frequency of invasion to soft tissue adherent to the superior mesenteric artery.* Am J Surg Pathol, 2005. **29**(8): p. 1056-61.

87. Kayahara, M., et al., *Surgical strategy for carcinoma of the pancreas head area based on clinicopathologic analysis of nodal involvement and plexus invasion.* Surgery, 1995. **117**(6): p. 616-23.

88. Ohigashi, H., et al., *K-ras point mutation in the nerve plexuses around the superior mesenteric artery in resectable adenocarcinoma of the pancreatic head: distribution pattern and related factors.* Arch Surg, 2000. **135**(12): p. 1450-5.

89. Nakai, T., et al., *Importance of microperineural invasion as a prognostic factor in ampullary carcinoma.* Br J Surg, 1997. **84**(10): p. 1399-401.

90. Bellis, D., V. Marci, and G. Monga, *Light microscopic and immunohistochemical evaluation of vascular and neural invasion in colorectal cancer.* Pathol Res Pract, 1993. **189**(4): p. 443-7.

91. Pour, P.M., R.H. Bell, and S.K. Batra, *Neural invasion in the staging of pancreatic cancer.* Pancreas, 2003. **26**(4): p. 322-5.

92. Kimura, W., et al., *Histologic and biologic patterns of microscopic pancreatic ductal adenocarcinomas detected incidentally at autopsy.* Cancer, 1998. **82**(10): p. 1839-49.

93. Tezel, E., et al., *Clinical significance of intraportal endovascular ultrasonography for the diagnosis of extrapancreatic nerve plexus invasion by pancreatic carcinoma.* Pancreatology, 2004. **4**(2): p. 76-81.

94. Garcea, G., et al., *Tumour characteristics predictive of survival following resection for ductal adenocarcinoma of the head of pancreas.* Eur J Surg Oncol, 2007. **33**(7): p. 892-7.

95. Matsuno, S., S. Egawa, and M. Unno, *R0 resection for ductal pancreatic cancer - Japanese experience.* American Journal of Surgery, 2007. **194**(4A): p. S110-S114.

96. Kayahara, M., et al., *An evaluation of radical resection for pancreatic cancer based on the mode of recurrence as determined by autopsy and diagnostic imaging.* Cancer, 1993. **72**(7): p. 2118-23.

97. Griffin, J.F., et al., *Patterns of failure after curative resection of pancreatic carcinoma.* Cancer, 1990. **66**(1): p. 56-61.

98. Kelsen, D.P., et al., *Pain as a predictor of outcome in patients with operable pancreatic carcinoma.* Surgery, 1997. **122**(1): p. 53-9.

99. di Mola, F.F. and P. di Sebastiano, *Pain and pain generation in pancreatic cancer.* Langenbecks Arch Surg, 2008. **393**(6): p. 919-22.

100. van Roest, M.H., et al., *Results of pancreaticoduodenectomy in patients with periampullary adenocarcinoma: perineural growth more important prognostic factor than tumor localization.* Ann Surg, 2008. **248**(1): p. 97-103.

101. Lindsay, T.H., et al., *Pancreatic cancer pain and its correlation with changes in tumor vasculature, macrophage infiltration, neuronal innervation, body weight and disease progression.* Pain, 2005. **119**(1-3): p. 233-46.

102. Ceyhan, G.O., et al., *Pancreatic pain.* Best Pract Res Clin Gastroenterol, 2008. **22**(1): p. 31-44.

103. Demir, I.E., et al., *Perineural mast cells are specifically enriched in pancreatic neuritis and neuropathic pain in pancreatic cancer and chronic pancreatitis.* PLoS One, 2013. **8**(3): p. e60529.

104. Ceyhan, G.O., et al., *Pancreatic neuropathy results in "neural remodeling" and altered pancreatic innervation in chronic pancreatitis and pancreatic cancer.* Am J Gastroenterol, 2009. **104**(10): p. 2555-65.

105. Hartel, M., et al., *Vanilloids in pancreatic cancer: potential for chemotherapy and pain management.* Gut, 2006. **55**(4): p. 519-28.

106. Zhu, Y., et al., *Nerve growth factor modulates TRPV1 expression and function and mediates pain in chronic pancreatitis.* Gastroenterology, 2011. **141**(1): p. 370-7.

107. Wild, K.D., et al., *Antibodies to nerve growth factor reverse established tactile allodynia in rodent models of neuropathic pain without tolerance.* J Pharmacol Exp Ther, 2007. **322**(1): p. 282-7.

108. Sanga, P., et al., *Efficacy, safety, and tolerability of fulranumab, an anti-nerve growth factor antibody, in the treatment of patients with moderate to severe osteoarthritis pain.* Pain, 2013.

109. Ugolini, G., et al., *The function neutralizing anti-TrkA antibody MNAC13 reduces inflammatory and neuropathic pain.* Proc Natl Acad Sci U S A, 2007. **104**(8): p. 2985-90.

110. Cernea, C.R., et al., *Perineural invasion in aggressive skin carcinomas of the head and neck. Potentially dangerous but frequently overlooked.* ORL J Otorhinolaryngol Relat Spec, 2009. **71**(1): p. 21-6.

111. Terhaard, C.H., et al., *Salivary gland carcinoma: independent prognostic factors for locoregional control, distant metastases, and overall survival: results of the Dutch head and neck oncology cooperative group.* Head Neck, 2004. **26**(8): p. 681-92; discussion 692-3.

112. Lee, J.T., et al., *Prediction of perineural invasion and its prognostic value in patients with prostate cancer.* Korean J Urol, 2010. **51**(11): p. 745-51.

113. Bilici, A., et al., *Prognostic significance of perineural invasion in patients with gastric cancer who underwent curative resection.* Ann Surg Oncol, 2010. **17**(8): p. 2037-44.

114. Studer, U.E. and L. Collette, *What can be concluded from the ERSPC and PLCO trial data?* Urol Oncol, 2010. **28**(6): p. 668-9.

115. Sokoloff, M.H. and C.B. Brendler, *Indications and contraindications for nerve-sparing radical prostatectomy.* Urol Clin North Am, 2001. **28**(3): p. 535-43.

116. DeLancey, J.O., et al., *Evidence of perineural invasion on prostate biopsy specimen and survival after radical prostatectomy.* Urology, 2013. **81**(2): p. 354-7.

117. Feng, F.Y., et al., *Perineural invasion predicts increased recurrence, metastasis, and death from prostate cancer following treatment with dose-escalated radiation therapy.* Int J Radiat Oncol Biol Phys, 2011. **81**(4): p. e361-7.

118. Yu, H.H., et al., *Perineural invasion affects biochemical recurrence-free survival in patients with prostate cancer treated with definitive external beam radiotherapy.* Urology, 2007. **70**(1): p. 111-6.

119. Masieri, L., et al., *Prognostic role of perineural invasion in 239 consecutive patients with pathologically organ-confined prostate cancer.* Urol Int, 2010. **85**(4): p. 396-400.

120. Ng, J.C., et al., *Perineural invasion in radical prostatectomy specimens: lack of prognostic significance.* J Urol, 2004. **172**(6 Pt 1): p. 2249-51.

121. Jeon, H.G., et al., *Perineural invasion is a prognostic factor for biochemical failure after radical prostatectomy.* Int J Urol, 2009. **16**(8): p. 682-6.

122. de la Taille, A., et al., *Perineural invasion on prostate needle biopsy: an independent predictor of final pathologic stage.* Urology, 1999. **54**(6): p. 1039-43.

123. Beard, C., et al., *Perineural invasion associated with increased cancer-specific mortality after external beam radiation therapy for men with low- and intermediate-risk prostate cancer.* Int J Radiat Oncol Biol Phys, 2006. **66**(2): p. 403-7.

124. Cozzi, G., et al., *Perineural invasion as a predictor of extraprostatic extension of prostate cancer: A systematic review and meta-analysis.* Scand J Urol, 2013.

125. Harnden, P., et al., *The prognostic significance of perineural invasion in prostatic cancer biopsies: a systematic review.* Cancer, 2007. **109**(1): p. 13-24.

126. Poeschl, E.M., et al., *Perineural invasion: correlation with aggressive phenotype and independent prognostic variable in both colon and rectum cancer.* J Clin Oncol, 2010. **28**(21): p. e358-60; author reply e361-2.

127. Bognel, C., et al., *Prognostic value of neural invasion in rectal carcinoma: a multivariate analysis on 339 patients with curative resection.* Eur J Cancer, 1995. **31A**(6): p. 894-8.

128. Liebl, F., et al., *The severity of neural invasion is associated with shortened survival in colon cancer.* Clin Cancer Res, 2013. **19**(1): p. 50-61.

129. Peng, J., et al., *Perineural invasion in pT3N0 rectal cancer: the incidence and its prognostic effect.* Cancer, 2011. **117**(7): p. 1415-21.

130. Huh, J.W., H.R. Kim, and Y.J. Kim, *Prognostic value of perineural invasion in patients with stage II colorectal cancer.* Ann Surg Oncol, 2010. **17**(8): p. 2066-72.

131. Santos, C., et al., *Clinicopathological risk factors of Stage II colon cancer: results of a prospective study.* Colorectal Dis, 2013. **15**(4): p. 414-22.

132. Desolneux, G., et al., *Prognostic factors in node-negative colorectal cancer: a retrospective study from a prospective database.* Int J Colorectal Dis, 2010. **25**(7): p. 829-34.

133. Chou, H.H., et al., *Clinicopathologic study of node-negative advanced gastric cancer and analysis of factors predicting its recurrence and prognosis.* Am J Surg, 2013. **205**(6): p. 623-30.

134. Tianhang, L., et al., *The effect of perineural invasion on overall survival in patients with gastric carcinoma.* J Gastrointest Surg, 2008. **12**(7): p. 1263-7.

135. Selcukbiricik, F., et al., *Perineural invasion independent prognostic factors in patients with gastric cancer undergoing curative resection.* Asian Pac J Cancer Prev, 2012. **13**(7): p. 3149-52.

136. Du, C., et al., *Defining a high-risk subgroup of pathological T2N0 gastric cancer by prognostic risk stratification for adjuvant therapy.* J Gastrointest Surg, 2011. **15**(12): p. 2153-8.

137. Hamada, T., et al., *The effect of denervation on liver regeneration in partially hepatectomized rats.* J Surg Res, 2007. **142**(1): p. 170-4.

138. Plank, J.L., et al., *Influence and timing of arrival of murine neural crest on pancreatic beta cell development and maturation.* Dev Biol, 2011. **349**(2): p. 321-30.

139. Diaz, R., et al., *Histological modifications of the rat prostate following transection of somatic and autonomic nerves.* An Acad Bras Cienc, 2010. **82**(2): p. 397-404.

140. Dai, H., et al., *Enhanced survival in perineural invasion of pancreatic cancer: an in vitro approach.* Hum Pathol, 2007. **38**(2): p. 299-307.

141. Albo, D., et al., *Neurogenesis in colorectal cancer is a marker of aggressive tumor behavior and poor outcomes.* Cancer, 2011.

142. Ayala, G.E., et al., *Cancer-related axonogenesis and neurogenesis in prostate cancer.* Clin Cancer Res, 2008. **14**(23): p. 7593-603.

143. Larson, D.L., et al., *Perineural lymphatics: myth or fact.* Am J Surg, 1966. **112**(4): p. 488-92.

144. Ayala, G.E., et al., *Growth and survival mechanisms associated with perineural invasion in prostate cancer.* Cancer Res, 2004. **64**(17): p. 6082-90.

145. Ayala, G.E., et al., *Stromal antiapoptotic paracrine loop in perineural invasion of prostatic carcinoma.* Cancer Res, 2006. **66**(10): p. 5159-64.

146. Yang, G., et al., *Perineural invasion of prostate carcinoma cells is associated with reduced apoptotic index.* Cancer, 1996. **78**(6): p. 1267-71.

147. Ayala, G.E., et al., *In vitro dorsal root ganglia and human prostate cell line interaction: redefining perineural invasion in prostate cancer.* Prostate, 2001. **49**(3): p. 213-23.

148. Cornell, R.J., et al., *Neuroepithelial interactions in prostate cancer are enhanced in the presence ofprostatic stroma.* Urology, 2003. **61**(4): p. 870-5.

149. Ceyhan, G.O., et al., *Neural invasion in pancreatic cancer: a mutual tropism between neurons and cancer cells.* Biochem Biophys Res Commun, 2008. **374**(3): p. 442-7.

150. Bapat, A.A., et al., *Perineural invasion and associated pain in pancreatic cancer.* Nat Rev Cancer, 2011. **11**(10): p. 695-707.

151. Nakagawara, A., *Trk receptor tyrosine kinases: a bridge between cancer and neural development.* Cancer Lett, 2001. **169**(2): p. 107-14.

152. Chao, M.V., R. Rajagopal, and F.S. Lee, *Neurotrophin signalling in health and disease.* Clin Sci (Lond), 2006. **110**(2): p. 167-73.

153. Teng, K.K. and B.L. Hempstead, *Neurotrophins and their receptors: signaling trios in complex biological systems.* Cell Mol Life Sci, 2004. **61**(1): p. 35-48.

154. Sakamoto, Y., et al., *Expression of Trk tyrosine kinase receptor is a biologic marker for cell proliferation and perineural invasion of human pancreatic ductal adenocarcinoma.* Oncol Rep, 2001. **8**(3): p. 477-84.

155. Zhu, Z., et al., *Nerve growth factor and enhancement of proliferation, invasion, and tumorigenicity of pancreatic cancer cells.* Mol Carcinog, 2002. **35**(3): p. 138-47.

156. Geldof, A.A., et al., *Nerve growth factor stimulates in vitro invasive capacity of DU145 human prostatic cancer cells.* J Cancer Res Clin Oncol, 1997. **123**(2): p. 107-12.

157. Okada, Y., et al., *Nerve growth factor stimulates MMP-2 expression and activity and increases invasion by human pancreatic cancer cells.* Clin Exp Metastasis, 2004. **21**(4): p. 285-92.

158. Ketterer, K., et al., *Reverse transcription-PCR analysis of laser-captured cells points to potential paracrine and autocrine actions of neurotrophins in pancreatic cancer.* Clin Cancer Res, 2003. **9**(14): p. 5127-36.

159. Miknyoczki, S.J., et al., *Neurotrophins and Trk receptors in human pancreatic ductal adenocarcinoma: expression patterns and effects on in vitro invasive behavior.* Int J Cancer, 1999. **81**(3): p. 417-27.

160. Zhu, Z.W., et al., *Nerve growth factor exerts differential effects on the growth of human pancreatic cancer cells.* Clin Cancer Res, 2001. **7**(1): p. 105-12.

161. Schneider, M.B., et al., *Expression of nerve growth factors in pancreatic neural tissue and pancreatic cancer.* J Histochem Cytochem, 2001. **49**(10): p. 1205-10.

162. Airaksinen, M.S. and M. Saarma, *The GDNF family: signalling, biological functions and therapeutic value.* Nat Rev Neurosci, 2002. **3**(5): p. 383-94.

163. Takahashi, M., *The GDNF/RET signaling pathway and human diseases.* Cytokine Growth Factor Rev, 2001. **12**(4): p. 361-73.

164. Okada, Y., et al., *Experimental implication of celiac ganglionotropic invasion of pancreatic-cancer cells bearing c-ret proto-oncogene with reference to glial-cell-line-derived neurotrophic factor (GDNF).* Int J Cancer, 1999. **81**(1): p. 67-73.

165. Zeng, Q., et al., *The relationship between overexpression of glial cell-derived neurotrophic factor and its RET receptor with progression and prognosis of human pancreatic cancer.* J Int Med Res, 2008. **36**(4): p. 656-64.

166. Ito, Y., et al., *Expression of glial cell line-derived neurotrophic factor family members and their receptors in pancreatic cancers.* Surgery, 2005. **138**(4): p. 788-94.

167. Iwahashi, N., et al., *Expression of glial cell line-derived neurotrophic factor correlates with perineural invasion of bile duct carcinoma.* Cancer, 2002. **94**(1): p. 167-74.

168. Okada, Y., et al., *Glial cell-derived neurotrophic factor upregulates the expression and activation of matrix metalloproteinase-9 in human pancreatic cancer.* Surgery, 2003. **134**(2): p. 293-9.

169. Veit, C., et al., *Activation of phosphatidylinositol 3-kinase and extracellular signal-regulated kinase is required for glial cell line-derived neurotrophic factor-induced migration and invasion of pancreatic carcinoma cells.* Cancer Res, 2004. **64**(15): p. 5291-300.

170. Gil, Z., et al., *Paracrine regulation of pancreatic cancer cell invasion by peripheral nerves.* J Natl Cancer Inst, 2010. **102**(2): p. 107-18.

171. Cavel, O., et al., *Endoneurial macrophages induce perineural invasion of pancreatic cancer cells by secretion of GDNF and activation of RET tyrosine kinase receptor.* Cancer Res, 2012. **72**(22): p. 5733-43.

172. Ceyhan, G.O., et al., *The neurotrophic factor artemin promotes pancreatic cancer invasion.* Ann Surg, 2006. **244**(2): p. 274-81.

173. Kameda, K., et al., *Expression of highly polysialylated neural cell adhesion molecule in pancreatic cancer neural invasive lesion.* Cancer Lett, 1999. **137**(2): p. 201-7.

174. Vural, E., et al., *Correlation of neural cell adhesion molecules with perineural spread of squamous cell carcinoma of the head and neck.* Otolaryngol Head Neck Surg, 2000. **122**(5): p. 717-20.

175. Li, R., et al., *Neural cell adhesion molecule is upregulated in nerves with prostate cancer invasion.* Hum Pathol, 2003. **34**(5): p. 457-61.

176. Tezel, E., et al., *Expression of neural cell adhesion molecule in pancreatic cancer.* Pancreas, 2001. **22**(2): p. 122-5.

177. Solares, C.A., et al., *Neural cell adhesion molecule expression: no correlation with perineural invasion in cutaneous squamous cell carcinoma of the head and neck.* Head Neck, 2009. **31**(6): p. 802-6.

178. Hutcheson, J.A., et al., *Neural cell adhesion molecule expression in adenoid cystic carcinoma of the head and neck.* Laryngoscope, 2000. **110**(6): p. 946-8.

179. Chen, W., et al., *Inhibition of CD146 gene expression via RNA interference reduces in vitro perineural invasion on ACC-M cell.* J Oral Pathol Med, 2009. **38**(2): p. 198-205.

180. Zhang, S., et al., *Chemokine CXCL12 and its receptor CXCR4 expression are associated with perineural invasion of prostate cancer.* J Exp Clin Cancer Res, 2008. **27**: p. 62.

181. Antoni, M.H., et al., *The influence of bio-behavioural factors on tumour biology: pathways and mechanisms.* Nat Rev Cancer, 2006. **6**(3): p. 240-8.

182. Barron, T.I., et al., *Beta blockers and breast cancer mortality: a population- based study.* J Clin Oncol, 2011. **29**(19): p. 2635-44.

183. Magnon, C., et al., *Autonomic nerve development contributes to prostate cancer progression.* Science, 2013. **341**(6142): p. 1236361.

184. Guo, K., et al., *Norepinephrine-induced invasion by pancreatic cancer cells is inhibited by propranolol.* Oncol Rep, 2009. **22**(4): p. 825-30.

185. Guo, K., et al., *Interaction of the sympathetic nerve with pancreatic cancer cells promotes perineural invasion through the activation of STAT3 signaling.* Mol Cancer Ther, 2013. **12**(3): p. 264-73.

186. Zhang, D., et al., *beta2-adrenoceptor blockage induces G1/S phase arrest and apoptosis in pancreatic cancer cells via Ras/Akt/NFkappaB pathway.* Mol Cancer, 2011. **10**: p. 146.

187. Palm, D., et al., *The norepinephrine-driven metastasis development of PC-3 human prostate cancer cells in BALB/c nude mice is inhibited by beta-blockers.* Int J Cancer, 2006. **118**(11): p. 2744-9.

188. Li, X., et al., *Neurotransmitter substance P mediates pancreatic cancer perineural invasion via NK-1R in cancer cells.* Mol Cancer Res, 2013. **11**(3): p. 294-302.

189. Abiatari, I., et al., *Consensus transcriptome signature of perineural invasion in pancreatic carcinoma.* Mol Cancer Ther, 2009. **8**(6): p. 1494-504.

190. Abiatari, I., et al., *The microtubule-associated protein MAPRE2 is involved in perineural invasion of pancreatic cancer cells.* Int J Oncol, 2009. **35**(5): p. 1111-6.

191. Swanson, B.J., et al., *MUC1 is a counter-receptor for myelin-associated glycoprotein (Siglec-4a) and their interaction contributes to adhesion in pancreatic cancer perineural invasion.* Cancer Res, 2007. **67**(21): p. 10222-9.

192. Ryschich, E., et al., *Promotion of tumor cell migration by extracellular matrix proteins in human pancreatic cancer.* Pancreas, 2009. **38**(7): p. 804-10.

193. Sroka, I.C., et al., *The laminin binding integrin alpha6beta1 in prostate cancer perineural invasion.* J Cell Physiol, 2010. **224**(2): p. 283-8.

194. Mitsunaga, S., et al., *Nerve invasion distance is dependent on laminin gamma2 in tumors of pancreatic cancer.* Int J Cancer, 2010. **127**(4): p. 805-19.

195. Kawamoto, M., et al., *Nestin expression correlates with nerve and retroperitoneal tissue invasion in pancreatic cancer.* Hum Pathol, 2009. **40**(2): p. 189-98.

196. Prueitt, R.L., et al., *Expression of microRNAs and protein-coding genes associated with perineural invasion in prostate cancer.* Prostate, 2008. **68**(11): p. 1152-64.

197. Sahin, I.H., et al., *Association of diabetes and perineural invasion in pancreatic cancer.* Cancer Med, 2012. **1**(3): p. 357-62.

198. Li, J. and Q. Ma, *Hyperglycemia promotes the perineural invasion in pancreatic cancer.* Med Hypotheses, 2008. **71**(3): p. 386-9.

199. Ceyhan, G.O., et al., *Nerve growth factor and artemin are paracrine mediators of pancreatic neuropathy in pancreatic adenocarcinoma.* Ann Surg, 2010. **251**(5): p. 923-31.

200. Demir, I.E., et al., *The microenvironment in chronic pancreatitis and pancreatic cancer induces neuronal plasticity.* Neurogastroenterol Motil, 2010. **22**(4): p. 480-90, e112-3.

201. Yang, X., et al., *EMMPRIN silencing inhibits proliferation and perineural invasion of human salivary adenoid cystic carcinoma cells in vitro and in vivo.* Cancer Biol Ther, 2012. **13**(2): p. 85-91.

202. Capella, G., et al., *Orthotopic models of human pancreatic cancer.* Ann N Y Acad Sci, 1999. **880**: p. 103-9.

203. Eibl, G. and H.A. Reber, *A xenograft nude mouse model for perineural invasion and recurrence in pancreatic cancer.* Pancreas, 2005. **31**(3): p. 258-62.

204. Hingorani, S.R., et al., *Preinvasive and invasive ductal pancreatic cancer and its early detection in the mouse.* Cancer Cell, 2003. **4**(6): p. 437-50.

205. Moritz, R.L. and R.J. Simpson, *Application of capillary reversed-phase high-performance liquid chromatography to high-sensitivity protein sequence analysis.* J Chromatogr, 1992. **599**(1-2): p. 119-30.

206. Cox, J. and M. Mann, *MaxQuant enables high peptide identification rates, individualized p.p.b.-range mass accuracies and proteome-wide protein quantification.* Nat Biotechnol, 2008. **26**(12): p. 1367-72.

207. Tapley, P., F. Lamballe, and M. Barbacid, *K252a is a selective inhibitor of the tyrosine protein kinase activity of the trk family of oncogenes and neurotrophin receptors.* Oncogene, 1992. **7**(2): p. 371-81.

208. Katoh, H., et al., *Small GTPase RhoG is a key regulator for neurite outgrowth in PC12 cells.* Mol Cell Biol, 2000. **20**(19): p. 7378-87.

209. Vandesompele, J., et al., *Accurate normalization of real-time quantitative RT-PCR data by geometric averaging of multiple internal control genes.* Genome Biol, 2002. **3**(7): p. RESEARCH0034.

210. Liu, H., R.G. Sadygov, and J.R. Yates, 3rd, *A model for random sampling and estimation of relative protein abundance in shotgun proteomics.* Anal Chem, 2004. **76**(14): p. 4193-201.

211. Old, W.M., et al., *Comparison of label-free methods for quantifying human proteins by shotgun proteomics.* Mol Cell Proteomics, 2005. **4**(10): p. 1487-502.

212. Hendrickson, E.L., et al., *Comparison of spectral counting and metabolic stable isotope labeling for use with quantitative microbial proteomics.* Analyst, 2006. **131**(12): p. 1335-41.

213. Zhang, B., et al., *Detecting differential and correlated protein expression in label-free shotgun proteomics.* J Proteome Res, 2006. **5**(11): p. 2909-18.

214. Hood, B.L., et al., *Proteomic analysis of formalin-fixed prostate cancer tissue.* Mol Cell Proteomics, 2005. **4**(11): p. 1741-53.

215. Shi, S.R., et al., *Protein extraction from formalin-fixed, paraffin-embedded tissue sections: quality evaluation by mass spectrometry.* J Histochem Cytochem, 2006. **54**(6): p. 739-43.

216. Nirmalan, N.J., et al., *Initial development and validation of a novel extraction method for quantitative mining of the formalin-fixed, paraffin-*

embedded tissue proteome for biomarker investigations. J Proteome Res, 2011. **10**(2): p. 896-906.

217. Kim, K.K., et al., *Up regulation of GW112 Gene by NF kappaB promotes an antiapoptotic property in gastric cancer cells.* Mol Carcinog, 2010. **49**(3): p. 259-70.

218. Takadate, T., et al., *Novel prognostic protein markers of resectable pancreatic cancer identified by coupled shotgun and targeted proteomics using formalin-fixed paraffin-embedded tissues.* Int J Cancer, 2013. **132**(6): p. 1368-82.

219. Riedl, M.S., et al., *Proteomic analysis uncovers novel actions of the neurosecretory protein VGF in nociceptive processing.* J Neurosci, 2009. **29**(42): p. 13377-88.

220. Severini, C., et al., *TLQP-21, a neuroendocrine VGF-derived peptide, prevents cerebellar granule cells death induced by serum and potassium deprivation.* J Neurochem, 2008. **104**(2): p. 534-44.

221. Greene, L.A. and A.S. Tischler, *Establishment of a noradrenergic clonal line of rat adrenal pheochromocytoma cells which respond to nerve growth factor.* Proc Natl Acad Sci U S A, 1976. **73**(7): p. 2424-8.

222. Filogamo, G. and C. Cracco, *Models of neuronal plasticity and repair in the enteric nervous system: a review.* Ital J Anat Embryol, 1995. **100 Suppl 1**: p. 185-95.

223. Fiscus, R.R., *Involvement of cyclic GMP and protein kinase G in the regulation of apoptosis and survival in neural cells.* Neurosignals, 2002. **11**(4): p. 175-90.

224. Tabakman, R., et al., *Neuroprotection by NGF in the PC12 in vitro OGD model: involvement of mitogen-activated protein kinases and gene expression.* Ann N Y Acad Sci, 2005. **1053**: p. 84-96.

225. Greene, L.A., *Nerve growth factor prevents the death and stimulates the neuronal differentiation of clonal PC12 pheochromocytoma cells in serum-free medium.* J Cell Biol, 1978. **78**(3): p. 747-55.

226. Salton, S.R., D.J. Fischberg, and K.W. Dong, *Structure of the gene encoding VGF, a nervous system-specific mRNA that is rapidly and selectively induced by nerve growth factor in PC12 cells.* Mol Cell Biol, 1991. **11**(5): p. 2335-49.

227. Possenti, R., et al., *A protein induced by NGF in PC12 cells is stored in secretory vesicles and released through the regulated pathway.* EMBO J, 1989. **8**(8): p. 2217-23.

228. Lenz, J., et al., *Clinicopathological correlations of nestin expression in surgically resectable pancreatic cancer including an analysis of perineural invasion.* J Gastrointestin Liver Dis, 2011. **20**(4): p. 389-96.

229. Alder, J., et al., *Brain-derived neurotrophic factor-induced gene expression reveals novel actions of VGF in hippocampal synaptic plasticity.* J Neurosci, 2003. **23**(34): p. 10800-8.

230. Berg, D., et al., *Molecular profiling of signalling pathways in formalin-fixed and paraffin-embedded cancer tissues.* Eur J Cancer, 2010. **46**(1): p. 47-55.

231. Reimel, B.A., et al., *Proteomics on Fixed Tissue Specimens - A Review.* Curr Proteomics, 2009. **6**(1): p. 63-69.

232. Xiao, Z., et al., *Quantitative proteomic analysis of formalin-fixed and paraffin-embedded nasopharyngeal carcinoma using iTRAQ labeling, two-dimensional liquid chromatography, and tandem mass spectrometry.* J Histochem Cytochem, 2010. **58**(6): p. 517-27.

233. Perroud, B., et al., *Grade-dependent proteomics characterization of kidney cancer.* Mol Cell Proteomics, 2009. **8**(5): p. 971-85.

234. Nirmalan, N.J., et al., *Development and validation of a novel protein extraction methodology for quantitation of protein expression in formalin-fixed paraffin-embedded tissues using western blotting.* J Pathol, 2009. **217**(4): p. 497-506.

235. Grantzdorffer, I., et al., *Comparison of different tissue sampling methods for protein extraction from formalin-fixed and paraffin-embedded tissue specimens.* Exp Mol Pathol, 2010. **88**(1): p. 190-6.

236. Sprung, R.W., Jr., et al., *Equivalence of protein inventories obtained from formalin-fixed paraffin-embedded and frozen tissue in multidimensional liquid chromatography-tandem mass spectrometry shotgun proteomic analysis.* Mol Cell Proteomics, 2009. **8**(8): p. 1988-98.

237. Scicchitano, M.S., et al., *Protein extraction of formalin-fixed, paraffin-embedded tissue enables robust proteomic profiles by mass spectrometry.* J Histochem Cytochem, 2009. **57**(9): p. 849-60.

238. Becker, K.F., et al., *Quantitative protein analysis from formalin-fixed tissues: implications for translational clinical research and nanoscale molecular diagnosis.* J Pathol, 2007. **211**(3): p. 370-8.

239. Ostasiewicz, P., et al., *Proteome, phosphoproteome, and N-glycoproteome are quantitatively preserved in formalin-fixed paraffin-embedded tissue and analyzable by high-resolution mass spectrometry.* J Proteome Res, 2010. **9**(7): p. 3688-700.

240. Prieto, D.A., et al., *Liquid Tissue: proteomic profiling of formalin-fixed tissues.* Biotechniques, 2005. **Suppl**: p. 32-5.

241. Cheung, W., et al., *Application of a global proteomic approach to archival precursor lesions: deleted in malignant brain tumors 1 and*

tissue transglutaminase 2 are upregulated in pancreatic cancer precursors. Pancreatology, 2008. **8**(6): p. 608-16.

242. Kawamura, T., et al., *Proteomic analysis of laser-microdissected paraffin-embedded tissues: (1) Stage-related protein candidates upon non-metastatic lung adenocarcinoma.* J Proteomics, 2010. **73**(6): p. 1089-99.

243. Patel, V., et al., *Proteomic analysis of laser-captured paraffin-embedded tissues: a molecular portrait of head and neck cancer progression.* Clin Cancer Res, 2008. **14**(4): p. 1002-14.

244. Kojima, K., et al., *Validation of a robust proteomic analysis carried out on formalin-fixed paraffin-embedded tissues of the pancreas obtained from mouse and human.* Proteomics, 2012. **12**(22): p. 3393-402.

245. Issaq, H.J., et al., *Multidimensional separation of peptides for effective proteomic analysis.* J Chromatogr B Analyt Technol Biomed Life Sci, 2005. **817**(1): p. 35-47.

246. Motoyama, A. and J.R. Yates, 3rd, *Multidimensional LC separations in shotgun proteomics.* Anal Chem, 2008. **80**(19): p. 7187-93.

247. Gilar, M., et al., *Orthogonality of separation in two-dimensional liquid chromatography.* Anal Chem, 2005. **77**(19): p. 6426-34.

248. Sandra, K., et al., *Highly efficient peptide separations in proteomics. Part 2: bi- and multidimensional liquid-based separation techniques.* J Chromatogr B Analyt Technol Biomed Life Sci, 2009. **877**(11-12): p. 1019-39.

249. Gilar, M., et al., *Two-dimensional separation of peptides using RP-RP-HPLC system with different pH in first and second separation dimensions.* J Sep Sci, 2005. **28**(14): p. 1694-703.

250. Dwivedi, R.C., et al., *Practical implementation of 2D HPLC scheme with accurate peptide retention prediction in both dimensions for high-throughput bottom-up proteomics.* Anal Chem, 2008. **80**(18): p. 7036-42.

251. Callipo, L., et al., *Evaluation of different two-dimensional chromatographic techniques for proteomic analysis of mouse cardiac tissue.* Biomed Chromatogr, 2010. **25**(5): p. 594-9.

252. Dowell, J.A., et al., *Comparison of two-dimensional fractionation techniques for shotgun proteomics.* Anal Chem, 2008. **80**(17): p. 6715-23.

253. Wang, Y., et al., *Reversed-phase chromatography with multiple fraction concatenation strategy for proteome profiling of human MCF10A cells.* Proteomics, 2011. **11**(10): p. 2019-26.

254. Siu, S.O., et al., *Fully automatable two-dimensional reversed-phase capillary liquid chromatography with online tandem mass spectrometry for shotgun proteomics.* Proteomics, 2011. **11**(11): p. 2308-19.

255. Wisniewski, J.R., P. Ostasiewicz, and M. Mann, *High recovery FASP applied to the proteomic analysis of microdissected formalin fixed paraffin embedded cancer tissues retrieves known colon cancer markers.* J Proteome Res, 2011. **10**(7): p. 3040-9.

256. Wisniewski, J.R., et al., *Extensive quantitative remodeling of the proteome between normal colon tissue and adenocarcinoma.* Mol Syst Biol, 2012. **8**: p. 611.

257. Wisniewski, J.R., K. Dus, and M. Mann, *Proteomic workflow for analysis of archival formalin-fixed and paraffin-embedded clinical samples to a depth of 10 000 proteins.* Proteomics Clin Appl, 2013. **7**(3-4): p. 225-33.

258. Harrell, J.C., et al., *Contaminating cells alter gene signatures in whole organ versus laser capture microdissected tumors: a comparison of experimental breast cancers and their lymph node metastases.* Clin Exp Metastasis, 2008. **25**(1): p. 81-8.

259. Sugiyama, Y., et al., *Microdissection is essential for gene expression profiling of clinically resected cancer tissues.* Am J Clin Pathol, 2002. **117**(1): p. 109-16.

260. Ladanyi, A., et al., *Laser microdissection in translational and clinical research.* Cytometry A, 2006. **69**(9): p. 947-60.

261. Sanchez-Carbayo, M., et al., *Comparison of gene expression profiles in laser-microdissected, nonembedded, and OCT-embedded tumor samples by oligonucleotide microarray analysis.* Clin Chem, 2003. **49**(12): p. 2096-100.

262. Ostasiewicz, P., et al., *Proteome, Phosphoproteome, and N-Glycoproteome Are Quantitatively Preserved in Formalin-Fixed Paraffin-Embedded Tissue and Analyzable by High-Resolution Mass Spectrometry.* J Proteome Res. **9**(7): p. 3688-3700.

263. Banks, R.E., et al., *The potential use of laser capture microdissection to selectively obtain distinct populations of cells for proteomic analysis--preliminary findings.* Electrophoresis, 1999. **20**(4-5): p. 689-700.

264. Vogel, A., et al., *Mechanisms of laser-induced dissection and transport of histologic specimens.* Biophys J, 2007. **93**(12): p. 4481-500.

265. Kirana, C., et al., *Compatibility of toluidine blue with laser microdissection and saturation labeling DIGE.* Proteomics, 2009. **9**(2): p. 485-90.

266. Craven, R.A., et al., *Laser capture microdissection and two-dimensional polyacrylamide gel electrophoresis: evaluation of tissue preparation and sample limitations.* Am J Pathol, 2002. **160**(3): p. 815-22.

267. Sitek, B., et al., *Application of fluorescence difference gel electrophoresis saturation labelling for the analysis of microdissected precursor lesions of pancreatic ductal adenocarcinoma.* Proteomics, 2005. **5**(10): p. 2665-79.

268. Dalmas, D.A., et al., *Transcriptional profiling of laser capture microdissected rat arterial elements: fenoldopam-induced vascular toxicity as a model system.* Toxicol Pathol, 2008. **36**(3): p. 496-519.

269. Brown, A.L., et al., *Purity and enrichment of laser-microdissected midbrain dopamine neurons.* Biomed Res Int, 2013. **2013**: p. 747938.

270. Stingl, C., et al., *Reproducibility of protein identification of selected cell types in Barrett's esophagus analyzed by combining laser-capture microdissection and mass spectrometry.* J Proteome Res, 2011. **10**(1): p. 288-98.

271. Naidoo, K., et al., *Proteome of formalin-fixed paraffin-embedded pancreatic ductal adenocarcinoma and lymph node metastases.* J Pathol, 2012. **226**(5): p. 756-63.

272. Chen, G., et al., *Discordant protein and mRNA expression in lung adenocarcinomas.* Mol Cell Proteomics, 2002. **1**(4): p. 304-13.

273. Lomberk, G., *The extracellular matrix and cell migration.* Pancreatology, 2010. **10**(1): p. 4-5.

274. Farrow, B., D. Albo, and D.H. Berger, *The role of the tumor microenvironment in the progression of pancreatic cancer.* J Surg Res, 2008. **149**(2): p. 319-28.

275. Schneider, D., et al., *Induction and expression of betaig-h3 in pancreatic cancer cells.* Biochim Biophys Acta, 2002. **1588**(1): p. 1-6.

276. Thapa, N., B.H. Lee, and I.S. Kim, *TGFBIp/betaig-h3 protein: a versatile matrix molecule induced by TGF-beta.* Int J Biochem Cell Biol, 2007. **39**(12): p. 2183-94.

277. Ma, C., et al., *Extracellular matrix protein betaig-h3/TGFBI promotes metastasis of colon cancer by enhancing cell extravasation.* Genes Dev, 2008. **22**(3): p. 308-21.

278. Vaquero, E.C., et al., *Extracellular matrix proteins protect pancreatic cancer cells from death via mitochondrial and nonmitochondrial pathways.* Gastroenterology, 2003. **125**(4): p. 1188-202.

279. Powell, S.K. and H.K. Kleinman, *Neuronal laminins and their cellular receptors.* Int J Biochem Cell Biol, 1997. **29**(3): p. 401-14.

280. Plantman, S., et al., *Integrin-laminin interactions controlling neurite outgrowth from adult DRG neurons in vitro.* Mol Cell Neurosci, 2008. **39**(1): p. 50-62.

281. Chen, Z.L. and S. Strickland, *Laminin gamma1 is critical for Schwann cell differentiation, axon myelination, and regeneration in the peripheral nerve.* J Cell Biol, 2003. **163**(4): p. 889-99.

282. Chedotal, A., G. Kerjan, and C. Moreau-Fauvarque, *The brain within the tumor: new roles for axon guidance molecules in cancers.* Cell Death Differ, 2005. **12**(8): p. 1044-56.

283. Moyano, J.V., et al., *AlphaB-crystallin is a novel oncoprotein that predicts poor clinical outcome in breast cancer.* J Clin Invest, 2006. **116**(1): p. 261-70.

284. Ivanov, O., et al., *alphaB-crystallin is a novel predictor of resistance to neoadjuvant chemotherapy in breast cancer.* Breast Cancer Res Treat, 2008. **111**(3): p. 411-7.

285. Acunzo, J., M. Katsogiannou, and P. Rocchi, *Small heat shock proteins HSP27 (HspB1), alphaB-crystallin (HspB5) and HSP22 (HspB8) as regulators of cell death.* Int J Biochem Cell Biol, 2012. **44**(10): p. 1622-31.

286. Mao, Y.W., et al., *Human alphaA- and alphaB-crystallins bind to Bax and Bcl-X(S) to sequester their translocation during staurosporine-induced apoptosis.* Cell Death Differ, 2004. **11**(5): p. 512-26.

287. Ou, X.M., K. Chen, and J.C. Shih, *Monoamine oxidase A and repressor R1 are involved in apoptotic signaling pathway.* Proc Natl Acad Sci U S A, 2006. **103**(29): p. 10923-8.

288. Fitzgerald, J.C., et al., *Monoamine oxidase-A modulates apoptotic cell death induced by staurosporine in human neuroblastoma cells.* J Neurochem, 2007. **103**(6): p. 2189-99.

289. Herlin, G., et al., *11C-harmine as a potential PET tracer for ductal pancreas cancer: in vitro studies.* Eur Radiol, 2003. **13**(4): p. 729-33.

290. Grutzmann, R., et al., *Meta-analysis of microarray data on pancreatic cancer defines a set of commonly dysregulated genes.* Oncogene, 2005. **24**(32): p. 5079-88.

291. Grover, P.K., J.E. Hardingham, and A.G. Cummins, *Stem cell marker olfactomedin 4: critical appraisal of its characteristics and role in tumorigenesis.* Cancer Metastasis Rev, 2010. **29**(4): p. 761-75.

292. Chin, K.L., et al., *The regulation of OLFM4 expression in myeloid precursor cells relies on NF-kappaB transcription factor.* Br J Haematol, 2008. **143**(3): p. 421-32.

293. Zhang, X., et al., *GW112, a novel antiapoptotic protein that promotes tumor growth.* Cancer Res, 2004. **64**(7): p. 2474-81.

294. Kobayashi, D., et al., *Olfactomedin 4 promotes S-phase transition in proliferation of pancreatic cancer cells.* Cancer Sci, 2007. **98**(3): p. 334-40.

295. Liu, W., et al., *Expression of hGC-1 is correlated with differentiation of gastric carcinoma.* Histopathology, 2007. **51**(2): p. 157-65.

296. Luo, Z., et al., *OLFM4 is associated with lymph node metastasis and poor prognosis in patients with gastric cancer.* J Cancer Res Clin Oncol, 2011. **137**(11): p. 1713-20.

297. Besson, D., et al., *A quantitative proteomic approach of the different stages of colorectal cancer establishes OLFM4 as a new nonmetastatic tumor marker.* Mol Cell Proteomics, 2011. **10**(12): p. M111 009712.

298. Liu, W., et al., *Reduced hGC-1 protein expression is associated with malignant progression of colon carcinoma.* Clin Cancer Res, 2008. **14**(4): p. 1041-9.

299. Bouquet, C., et al., *Microtubule-associated protein 1B controls directionality of growth cone migration and axonal branching in regeneration of adult dorsal root ganglia neurons.* J Neurosci, 2004. **24**(32): p. 7204-13.

300. Dehmelt, L. and S. Halpain, *Actin and microtubules in neurite initiation: are MAPs the missing link?* J Neurobiol, 2004. **58**(1): p. 18-33.

301. Gonzalez-Billault, C., et al., *Microtubule-associated protein 1B is involved in the initial stages of axonogenesis in peripheral nervous system cultured neurons.* Brain Res, 2002. **943**(1): p. 56-67.

302. Jean, D.C., P.W. Baas, and M.M. Black, *A novel role for doublecortin and doublecortin-like kinase in regulating growth cone microtubules.* Hum Mol Genet, 2012. **21**(26): p. 5511-27.

303. Burgess, H.A. and O. Reiner, *Doublecortin-like kinase is associated with microtubules in neuronal growth cones.* Mol Cell Neurosci, 2000. **16**(5): p. 529-41.

304. Hong, N.A., et al., *Mice lacking Dad1, the defender against apoptotic death-1, express abnormal N-linked glycoproteins and undergo increased embryonic apoptosis.* Dev Biol, 2000. **220**(1): p. 76-84.

305. Gilyarov, A.V., *Nestin in central nervous system cells.* Neurosci Behav Physiol, 2008. **38**(2): p. 165-9.

306. Valder, C.R., et al., *Coupling gene chip analyses and rat genetic variances in identifying potential target genes that may contribute to*

neuropathic allodynia development. J Neurochem, 2003. **87**(3): p. 560-73.

307. Kim, D.S., et al., *Profiling of dynamically changed gene expression in dorsal root ganglia post peripheral nerve injury and a critical role of injury-induced glial fibrillary acidic protein in maintenance of pain behaviors [corrected].* Pain, 2009. **143**(1-2): p. 114-22.

308. Matsumura, S., et al., *Characterization of nestin expression in the spinal cord of GFP transgenic mice after peripheral nerve injury.* Neuroscience, 2010. **170**(3): p. 942-53.

309. Kutlu, O., et al., *Increased expression of nestin in the major pelvic ganglion following cavernous nerve injury.* Int J Impot Res, 2012. **24**(2): p. 84-90.

310. Takaoka, T., et al., *Neuronal re-juvenilization in the nucleus ambiguus after vagal nerve injury.* Neurosci Res, 2009. **65**(4): p. 353-9.

311. Demir, I.E., et al., *Neural plasticity in the gastrointestinal tract: chronic inflammation, neurotrophic signals, and hypersensitivity.* Acta Neuropathol, 2013. **125**(4): p. 491-509.

312. Mancino, M., et al., *The neuronal influence on tumor progression.* Biochim Biophys Acta, 2011. **1816**(2): p. 105-18.

313. Arafat, H., et al., *Tumor-specific expression and alternative splicing of the COL6A3 gene in pancreatic cancer.* Surgery, 2011. **150**(2): p. 306-15.

314. Kang, C.Y., et al., *Clinical Significance of Serum COL6A3 in Pancreatic Ductal Adenocarcinoma.* J Gastrointest Surg, 2013.

315. Cheng, I.H., et al., *Collagen VI protects against neuronal apoptosis elicited by ultraviolet irradiation via an Akt/phosphatidylinositol 3-kinase signaling pathway.* Neuroscience, 2011. **183**: p. 178-88.

316. Esposito, I., et al., *Tenascin C and annexin II expression in the process of pancreatic carcinogenesis.* J Pathol, 2006. **208**(5): p. 673-85.

317. Paron, I., et al., *Tenascin-C enhances pancreatic cancer cell growth and motility and affects cell adhesion through activation of the integrin pathway.* PLoS One, 2011. **6**(6): p. e21684.

318. Meiners, S., et al., *Tenascin-C contains domains that independently regulate neurite outgrowth and neurite guidance.* J Neurosci, 1999. **19**(19): p. 8443-53.

319. Chen, J., et al., *The extracellular matrix glycoprotein tenascin-C is beneficial for spinal cord regeneration.* Mol Ther, 2010. **18**(10): p. 1769-77.

320. Levi, A., J.D. Eldridge, and B.M. Paterson, *Molecular cloning of a gene sequence regulated by nerve growth factor.* Science, 1985. **229**(4711): p. 393-5.

321. Levi, A., et al., *Processing, distribution, and function of VGF, a neuronal and endocrine peptide precursor.* Cell Mol Neurobiol, 2004. **24**(4): p. 517-33.

322. Ferri, G.L., et al., *VGF: an inducible gene product, precursor of a diverse array of neuro-endocrine peptides and tissue-specific disease biomarkers.* J Chem Neuroanat, 2011. **42**(4): p. 249-61.

323. Mishiro-Sato, E., et al., *Distribution of neuroendocrine regulatory peptide-1 and -2, and proteolytic processing of their precursor VGF protein in the rat.* J Neurochem, 2010. **114**(4): p. 1097-106.

324. Salton, S.R., C. Volonte, and G. D'Arcangelo, *Stimulation of vgf gene expression by NGF is mediated through multiple signal transduction pathways involving protein phosphorylation.* FEBS Lett, 1995. **360**(2): p. 106-10.

325. Bozdagi, O., et al., *The neurotrophin-inducible gene Vgf regulates hippocampal function and behavior through a brain-derived neurotrophic factor-dependent mechanism.* J Neurosci, 2008. **28**(39): p. 9857-69.

326. Rukenstein, A., R.E. Rydel, and L.A. Greene, *Multiple agents rescue PC12 cells from serum-free cell death by translation- and transcription-independent mechanisms.* J Neurosci, 1991. **11**(8): p. 2552-63.

327. Ohta, T., et al., *Expression of basic fibroblast growth factor and its receptor in human pancreatic carcinomas.* Br J Cancer, 1995. **72**(4): p. 824-31.

328. Zhou, Y., Q. Zhou, and R. Chen, *Pancreatic stellate cells promotes the perineural invasion in pancreatic cancer.* Med Hypotheses, 2012. **78**(6): p. 811-3.

329. Rizzi, R., et al., *The VGF-derived peptide TLQP-21: a new modulatory peptide for inflammatory pain.* Neurosci Lett, 2008. **441**(1): p. 129-33.

330. Ji, R.R. and C.J. Woolf, *Neuronal plasticity and signal transduction in nociceptive neurons: implications for the initiation and maintenance of pathological pain.* Neurobiol Dis, 2001. **8**(1): p. 1-10.

331. Brancia, C., et al., *Differential expression and seasonal modulation of VGF peptides in sheep pituitary.* J Endocrinol, 2005. **186**(1): p. 97-107.

332. Brynczka, C., P. Labhart, and B.A. Merrick, *NGF-mediated transcriptional targets of p53 in PC12 neuronal differentiation.* BMC Genomics, 2007. **8**: p. 139.

333. Jia, L., et al., *PTEN suppression promotes neurite development exclusively in differentiating PC12 cells via PI3-kinase and MAP kinase signaling.* J Cell Biochem, 2010. **111**(6): p. 1390-400.

334. Wu, C.F. and B.D. Howard, *K252a-potentiation of EGF-induced neurite outgrowth from PC12 cells is not mimicked or blocked by other protein kinase activators or inhibitors.* Brain Res Dev Brain Res, 1995. **86**(1-2): p. 217-26.

335. Shimazawa, M., et al., *An inducer of VGF protects cells against ER stress-induced cell death and prolongs survival in the mutant SOD1 animal models of familial ALS.* PLoS One, 2010. **5**(12): p. e15307.

336. Moss, A., et al., *Origins, actions and dynamic expression patterns of the neuropeptide VGF in rat peripheral and central sensory neurones following peripheral nerve injury.* Mol Pain, 2008. **4**: p. 62.

337. Rindi, G., et al., *Peptide products of the neurotrophin-inducible gene vgf are produced in human neuroendocrine cells from early development and increase in hyperplasia and neoplasia.* J Clin Endocrinol Metab, 2007. **92**(7): p. 2811-5.

338. Santarpia, L., S.M. Lippman, and A.K. El-Naggar, *Targeting the MAPK-RAS-RAF signaling pathway in cancer therapy.* Expert Opin Ther Targets, 2012. **16**(1): p. 103-19.

339. Huang, X.Y., et al., *Norepinephrine stimulates pancreatic cancer cell proliferation, migration and invasion via beta-adrenergic receptor-dependent activation of P38/MAPK pathway.* Hepatogastroenterology, 2012. **59**(115): p. 889-93.

340. Hahm, S., et al., *Targeted deletion of the Vgf gene indicates that the encoded secretory peptide precursor plays a novel role in the regulation of energy balance.* Neuron, 1999. **23**(3): p. 537-48.

341. Sahlgren, C.M., et al., *A nestin scaffold links Cdk5/p35 signaling to oxidant-induced cell death.* EMBO J, 2006. **25**(20): p. 4808-19.

Appendices

Appendix table 1. List of proteins up-regulated in invaded nerves compared to non-invaded nerves. The mean of intensity values from five samples is shown. IN: invaded nerves, NIN: non-invaded nerves. FC: fold change

Protein ID	Gene Name	Protein name	IN	NIN	p value	FC
P51659	HSD17B4	Peroxisomal multifunctional enzyme type 2	2E+06	0	0.0000	
O00231	PSMD11	26S proteasome non-ATPase regulatory subunit 11	4E+06	0	0.0001	
P50440	GATM	Glycine amidinotransferase, mitochondrial	2E+06	0	0.0005	
P37802	TAGLN2	Transgelin-2	2E+08	1E+08	0.0008	1.63
Q14764	MVP	Major vault protein	5E+07	3E+07	0.0010	1.44
P04075	ALDOA	Fructose-bisphosphate aldolase A	2E+08	1E+08	0.0011	1.52
O95782	AP2A1	AP-2 complex subunit alpha-1	1E+07	9E+06	0.0016	1.34
P59768	GNG2	Guanine nucleotide-binding protein G subunit gamma-2	2E+07	7E+06	0.0017	2.27
P38646	HSPA9	Stress-70 protein, mitochondrial	4E+07	3E+07	0.0017	1.53
Q96FW1	OTUB1	Ubiquitin thioesterase OTUB1	1E+07	1E+07	0.0017	1.37
P26641	EEF1G	Elongation factor 1-gamma	2E+07	2E+07	0.0022	1.26
P19367	HK1	Hexokinase-1	5E+07	3E+07	0.0022	1.74
Q99798	ACO2	Aconitate hydratase, mitochondrial	5E+07	4E+07	0.0027	1.38
P07942	LAMB1	Laminin subunit beta-1	7E+08	4E+08	0.0031	1.60
P07339	CTSD	Cathepsin D	6E+07	3E+07	0.0037	2.03
Q9UHQ9	CYB5R1	NADH-cytochrome b5 reductase 1	2E+07	1E+07	0.0039	1.96
P14618	PKM2	Pyruvate kinase isozymes M1/M2	6E+08	4E+08	0.0040	1.44
Q8TAT6	NPLOC4	Nuclear protein localization protein 4 homolog	2E+07	2E+06	0.0040	8.12
P54577	YARS	Tyrosine--tRNA ligase, cytoplasmic	2E+06	3E+05	0.0040	7.57
P61158	ACTR3	Actin-related protein 3	3E+07	2E+07	0.0041	1.25
Q15233	NONO	Non-POU domain-containing octamer-binding protein	3E+07	2E+07	0.0044	1.27
P48681	NES	Nestin	4E+08	1E+08	0.0048	3.35
Q00839	HNRNPU	Heterogeneous nuclear ribonucleoprotein U	3E+07	3E+07	0.0050	1.20
P50479	PDLIM4	PDZ and LIM domain protein 4	4E+07	3E+07	0.0052	1.50
Q13200	PSMD2	26S proteasome non-ATPase regulatory subunit 2	8E+06	5E+06	0.0054	1.51
P51149	RAB7A	Ras-related protein Rab-7a	5E+07	4E+07	0.0056	1.23
P19971	TYMP	Thymidine phosphorylase	6E+07	2E+07	0.0064	2.42
P13521	SCG2	Secretogranin-2	3E+07	3E+06	0.0064	9.61
P24043	LAMA2	Laminin subunit alpha-2	5E+08	3E+08	0.0072	1.69
Q00325	SLC25A3	Phosphate carrier protein, mitochondrial	8E+06	2E+06	0.0072	3.36
Q96TA1	FAM129B	Niban-like protein 1	3E+07	1E+07	0.0074	1.81
P00403	MT-CO2	Cytochrome c oxidase subunit 2	3E+07	2E+07	0.0074	1.38
P49368	CCT3	T-complex protein 1 subunit gamma	3E+07	3E+07	0.0075	1.22
P63104	YWHAZ	14-3-3 protein zeta/delta	3E+08	2E+08	0.0077	1.44
P21796	VDAC1	Voltage-dependent anion-selective channel protein 1	1E+07	5E+06	0.0080	2.40

Appendix table 1 continued….

Protein ID	Gene Name	Protein name	IN	NIN	p value	FC
O15240	VGF	Neurosecretory protein VGF	1E+08	3E+07	0.0086	5.15
P24821	TNC	Tenascin	5E+07	2E+07	0.0088	2.57
P18085	ARF4	ADP-ribosylation factor 4	2E+07	1E+07	0.0091	1.31
Q01105	SET	Protein SET	2E+07	2E+07	0.0096	1.19
O75390	CS	Citrate synthase, mitochondrial	1E+07	1E+07	0.0102	1.32
P12111	COL6A3	Collagen alpha-3(VI) chain	4E+09	3E+09	0.0107	1.35
Q9HCJ6	VAT1L	Synaptic vesicle membrane protein VAT-1 homolog-like	2E+07	5E+06	0.0111	2.80
Q14204	DYNC1H1	Cytoplasmic dynein 1 heavy chain 1	3E+08	2E+08	0.0111	1.32
P31949	S100A11	Protein S100-A11	1E+07	7E+06	0.0112	1.94
O60831	PRAF2	PRA1 family protein 2	5E+06	3E+06	0.0114	1.88
P45880	VDAC2	Voltage-dependent anion-selective channel protein 2	1E+07	7E+06	0.0118	2.04
P52272	HNRNPM	Heterogeneous nuclear ribonucleoprotein M	3E+07	3E+07	0.0122	1.19
Q9UHG2	PCSK1N	ProSAAS;KEP	3E+07	6E+06	0.0123	4.69
P54920	NAPA	Alpha-soluble NSF attachment protein	5E+06	2E+06	0.0123	2.16
P11142	HSPA8	Heat shock cognate 71 kDa protein	3E+08	2E+08	0.0123	1.31
O60506	SYNCRIP	Heterogeneous nuclear ribonucleoprotein Q	2E+07	2E+07	0.0125	1.25
P40926	MDH2	Malate dehydrogenase, mitochondrial	4E+07	3E+07	0.0126	1.47
Q01484	ANK2	Ankyrin-2	5E+07	2E+07	0.0126	2.06
P02794	FTH1	Ferritin heavy chain	3E+07	2E+07	0.0131	1.60
P36543	ATP6V1E1	V-type proton ATPase subunit E 1	9E+06	4E+06	0.0133	2.27
P63010	AP2B1	AP-2 complex subunit beta	1E+07	9E+06	0.0141	1.39
O15075	DCLK1	Serine/threonine-protein kinase DCLK1	4E+06	9E+05	0.0142	4.26
Q9UI12	ATP6V1H	V-type proton ATPase subunit H	6E+06	3E+06	0.0154	2.24
P00338	LDHA	L-lactate dehydrogenase A chain	2E+08	2E+08	0.0158	1.24
P09104	ENO2	Gamma-enolase	2E+08	8E+07	0.0167	1.84
Q00610	CLTC	Clathrin heavy chain 1	2E+08	2E+08	0.0168	1.23
Q9NTK5	OLA1	Obg-like ATPase 1	3E+06	7E+05	0.0169	3.53
P49721	PSMB2	Proteasome subunit beta type-2	9E+06	5E+06	0.0171	1.60
O00429	DNM1L	Dynamin-1-like protein	1E+07	6E+06	0.0174	1.76
P19338	NCL	Nucleolin	4E+07	4E+07	0.0178	1.18
P43121	MCAM	Cell surface glycoprotein MUC18	9E+07	7E+07	0.0189	1.35
P61803	DAD1	Dolichyl-diphosphooligosaccharide--protein glycosyltransferase subunit DAD1	4E+06	1E+06	0.0190	3.76
Q15063	POSTN	Periostin	1E+08	4E+07	0.0201	3.54
P61981	YWHAG	14-3-3 protein gamma;	9E+07	5E+07	0.0209	1.60
P78559	MAP1A	Microtubule-associated protein 1A	9E+06	4E+06	0.0213	1.93
P61978	HNRNPK	Heterogeneous nuclear ribonucleoprotein K	1E+08	1E+08	0.0216	1.17
Q96QK1	VPS35	Vacuolar protein sorting-associated protein 35	2E+07	1E+07	0.0222	1.19
P17174	GOT1	Aspartate aminotransferase, cytoplasmic	2E+07	7E+06	0.0223	2.40
Q15121	PEA15	Astrocytic phosphoprotein PEA-15	2E+07	1E+07	0.0235	1.40
P27348	YWHAQ	14-3-3 protein theta	5E+07	3E+07	0.0239	1.37

Appendix table 1 continued….

Protein ID	Gene Name	Protein name	IN	NIN	p value	FC
P61160	ACTR2	Actin-related protein 2	2E+07	2E+07	0.0262	1.19
P12109	COL6A1	Collagen alpha-1(VI) chain	1E+09	8E+08	0.0268	1.26
P17096	HMGA1	High mobility group protein HMG-I/HMG-Y	3E+07	6E+06	0.0271	5.15
P13473	LAMP2	Lysosome-associated membrane glycoprotein 2	2E+07	1E+07	0.0275	1.58
P48163	ME1	NADP-dependent malic enzyme	2E+06	5E+05	0.0289	3.58
Q9BW30	TPPP3	Tubulin polymerization-promoting protein family member 3	5E+07	3E+07	0.0295	1.45
Q6PCE3	PGM2L1	Glucose 1,6-bisphosphate synthase	1E+07	8E+06	0.0299	1.85
P06753	TPM3	Tropomyosin alpha-3 chain	8E+07	6E+07	0.0302	1.30
P55072	VCP	Transitional endoplasmic reticulum ATPase	1E+08	9E+07	0.0302	1.28
P21281	ATP6V1B2	V-type proton ATPase subunit B, brain isoform	4E+07	2E+07	0.0306	1.61
Q16799	RTN1	Reticulon-1	1E+07	5E+06	0.0307	2.51
P62857	RPS28	40S ribosomal protein S28	1E+07	1E+07	0.0310	1.21
P17677	GAP43	Neuromodulin	2E+08	9E+07	0.0311	2.14
O75348	ATP6V1G1	V-type proton ATPase subunit G 1	9E+06	4E+06	0.0340	2.09
O00154	ACOT7	Cytosolic acyl coenzyme A thioester hydrolase	1E+07	4E+06	0.0342	2.75
Q99623	PHB2	Prohibitin-2	4E+07	3E+07	0.0350	1.27
Q9UJ70	NAGK	N-acetyl-D-glucosamine kinase	1E+07	9E+06	0.0355	1.23
P11047	LAMC1	Laminin subunit gamma-1	9E+08	7E+08	0.0356	1.32
P62318	SNRPD3	Small nuclear ribonucleoprotein Sm D3	1E+07	8E+06	0.0363	1.38
Q9NRW1	RAB6B	Ras-related protein Rab-6B	4E+07	2E+07	0.0365	1.84
P46821	MAP1B	Microtubule-associated protein 1B	4E+08	3E+08	0.0365	1.48
Q05193	DNM1	Dynamin-1	3E+07	2E+07	0.0368	1.70
Q15084	PDIA6	Protein disulfide-isomerase A6	4E+07	3E+07	0.0372	1.29
O60716	CTNND1	Catenin delta-1	3E+06	5E+05	0.0374	6.31
P12110	COL6A2	Collagen alpha-2(VI) chain	6E+08	5E+08	0.0374	1.30
Q1KMD3	HNRNPUL2	Heterogeneous nuclear ribonucleoprotein U-like protein 2	2E+06	4E+05	0.0377	4.18
P31948	STIP1	Stress-induced-phosphoprotein 1	1E+07	9E+06	0.0378	1.44
P49748	ACADVL	Very long-chain specific acyl-CoA dehydrogenase, mitochondrial	3E+07	2E+07	0.0379	1.25
P20591	MX1	Interferon-induced GTP-binding protein Mx1	8E+06	2E+06	0.0389	4.07
P38606	ATP6V1A	V-type proton ATPase catalytic subunit A	6E+07	3E+07	0.0390	1.59
P25789	PSMA4	Proteasome subunit alpha type-4	5E+06	4E+06	0.0397	1.51
Q14194	CRMP1	Dihydropyrimidinase-related protein 1	7E+06	4E+06	0.0400	1.88
P40121	CAPG	Macrophage-capping protein	1E+07	2E+06	0.0401	5.18
P50395	GDI2	Rab GDP dissociation inhibitor beta	1E+08	1E+08	0.0409	1.17
P14543	NID1	Nidogen-1	5E+08	3E+08	0.0410	1.44
Q86Y82	STX12	Syntaxin-12	1E+06	0	0.0420	
P62249	RPS16	40S ribosomal protein S16	8E+06	6E+06	0.0426	1.36
Q9P0J7	KCMF1	E3 ubiquitin-protein ligase KCMF1	335538	0	0.0426	
P59998	ARPC4	Actin-related protein 2/3 complex subunit 4	3E+07	2E+07	0.0427	1.17

Appendix table 1 continued….

Protein ID	Gene Name	Protein name	IN	NIN	p value	FC
Q02218	OGDH	2-oxoglutarate dehydrogenase, mitochondrial	7E+06	6E+06	0.0428	1.31
Q13509	TUBB3	Tubulin beta-3 chain	3E+09	2E+09	0.0444	1.31
P10809	HSPD1	60 kDa heat shock protein, mitochondrial	1E+08	8E+07	0.0445	1.21
Q08211	DHX9	ATP-dependent RNA helicase A	1E+07	9E+06	0.0449	1.27
P26373	RPL13	60S ribosomal protein L13	1E+07	1E+07	0.0452	1.34
P46940	IQGAP1	Ras GTPase-activating-like protein IQGAP1	7E+07	6E+07	0.0463	1.24
P62937	PPIA	Peptidyl-prolyl cis-trans isomerase A	3E+08	3E+08	0.0483	1.13
P07437	TUBB	Tubulin beta chain	4E+08	3E+08	0.0485	1.22
P10599	TXN	Thioredoxin	4E+07	4E+07	0.0489	1.14
P14314	PRKCSH	Glucosidase 2 subunit beta	3E+07	2E+07	0.0491	1.18
P18509	ADCYAP1	Pituitary adenylate cyclase-activating polypeptide	7E+06	0	0.0499	

Appendix table 2. List of proteins down-regulated in invaded nerves compared to non-invaded nerves. The mean of intensity values from five samples is shown. IN: invaded nerves, NIN: non-invaded nerves. FC: fold change

Protein ID	Gene name	Protein name	IN	NIN	p value	FC
P02647	APOA1	Apolipoprotein A-I	2E+08	6E+08	0.0010	0.37
P04040	CAT	Catalase	3E+07	6E+07	0.0012	0.42
P11166	SLC2A1	Solute carrier family 2	7E+06	5E+07	0.0036	0.16
P08294	SOD3	Extracellular superoxide dismutase [Cu-Zn]	3E+06	1E+07	0.0069	0.18
P30041	PRDX6	Peroxiredoxin-6	7E+07	9E+07	0.0074	0.81
P68871	HBB	Hemoglobin subunit beta;LVV-hemorphin-7	1E+09	8E+09	0.0078	0.19
P01857	IGHG1	Ig gamma-1 chain C region	1E+08	3E+08	0.0079	0.44
P02730	SLC4A1	Band 3 anion transport protein	6E+05	1E+07	0.0083	0.04
P11277	SPTB	Spectrin beta chain, erythrocyte	2E+05	2E+06	0.0098	0.08
O95865	DDAH2	N(G),N(G)-dimethylarginine dimethylaminohydrolase 2	2E+07	3E+07	0.0105	0.64
P30043	BLVRB	Flavin reductase (NADPH)	2E+07	4E+07	0.0118	0.62
P23229	ITGA6	Integrin alpha-6	9E+07	1E+08	0.0130	0.79
O00159	MYO1C	Unconventional myosin-Ic	4E+07	6E+07	0.0142	0.60
P06727	APOA4	Apolipoprotein A-IV	3E+07	7E+07	0.0150	0.47
P00918	CA2	Carbonic anhydrase 2	5E+05	7E+06	0.0155	0.07
P02042	HBD	Hemoglobin subunit delta	1E+07	1E+08	0.0155	0.10
O00339	MATN2	Matrilin-2	4E+07	5E+07	0.0157	0.76
P69905	HBA1	Hemoglobin subunit alpha	8E+08	4E+09	0.0179	0.19
P32119	PRDX2	Peroxiredoxin-2	5E+07	7E+07	0.0190	0.71
P01834	IGKC	Ig kappa chain C region	7E+07	2E+08	0.0202	0.38
P12429	ANXA3	Annexin A3	8E+06	1E+07	0.0231	0.56
P00915	CA1	Carbonic anhydrase 1	7E+06	4E+07	0.0232	0.17
P00450	CP	Ceruloplasmin	2E+07	5E+07	0.0240	0.44
P02790	HPX	Hemopexin	5E+07	9E+07	0.0266	0.50
Q15631	TSN	Translin	3E+06	7E+06	0.0287	0.45
Q9BZQ8	FAM129A	Protein Niban	4E+06	7E+06	0.0287	0.66
P02787	TF	Serotransferrin	1E+08	2E+08	0.0293	0.52
P08107	HSPA1A	Heat shock 70 kDa protein 1A/1B	1E+08	1E+08	0.0318	0.76
Q96AC1	FERMT2	Fermitin family homolog 2	1E+07	2E+07	0.0321	0.53
Q9NZN4	EHD2	EH domain-containing protein 2	7E+06	5E+07	0.0347	0.14
P00747	PLG	Plasminogen	7E+06	2E+07	0.0357	0.36
O43175	PHGDH	D-3-phosphoglycerate dehydrogenase	7E+06	1E+07	0.0357	0.65
P05156	CFI	Complement factor I	1E+06	7E+06	0.0368	0.16
Q14624	ITIH4	Inter-alpha-trypsin inhibitor heavy chain H4	2E+07	4E+07	0.0400	0.51
Q01118	SCN7A	Sodium channel protein type 7 subunit alpha	4E+06	2E+07	0.0408	0.23
P16144	ITGB4	Integrin beta-4	1E+08	1E+08	0.0422	0.76
P04271	S100B	Protein S100-B	1E+08	2E+08	0.0457	0.51

Appendix table 2 continued….

Protein ID	Gene name	Protein name	IN	NIN	p value	FC
P01008	SERPINC1	Antithrombin-III	1E+07	2E+07	0.0480	0.62
P11532	DMD	Dystrophin	4E+07	6E+07	0.0482	0.68
P13591	NCAM1	Neural cell adhesion molecule 1	4E+07	6E+07	0.0482	0.63
P01019	AGT	Angiotensinogen	5E+06	1E+07	0.0492	0.54
P05546	SERPIND1	Heparin cofactor 2	2E+06	7E+06	0.0493	0.30